EFFECT OF SILVER NANOPARTICLES ON PLANKTONIC AND BIOFILM CELL GROWTH

A Dissertation

presented to

the Faculty of the Graduate School

at the University of Missouri-Columbia

In Partial Fulfillment

of the Requirements for the Degree

Doctor of Philosophy

by

OKKYOUNG CHOI

Dr. Zhiqiang Hu, Dissertation Supervisor

DECEMBER 2009

The undersigned, appointed by the dean of the Graduate School, have examined the dissertation entitled

EFFECT OF SILVER NANOPARTICLES

ON PLANKTONIC AND BIOFILM CELL GROWTH

presented by Okkyoung Choi,

a candidate for the degree of doctor of philosophy,

and hereby certify that, in their opinion, it is worthy of acceptance.

Professor Zhiqiang Hu

Professor Matthew Bernards

Professor Baolin Deng

Professor Thomas E. Clevenger

Professor Rao Y. Surampalli

ACKNOWLEDGEMENTS

I would like to gratefully and sincerely thank Dr. Zhiqiang Hu for his guidance, understanding, and patience during my graduate studies at University of Missouri. He encouraged me to not only grow as an experimentalist and a science but also as an instructor and an independent thinker. I learn from him what good leadership is.

I would like to thank my committee members, Professor Baolin Deng, Thomas E. Clevenger, Matthew Bernards, and specially thank Dr. Rao Y. Surampalli drove to come from Kansas City for my committee. Their guidance and encouragement help me to successfully build whole researches.

I am thankful to Dr. Hu's research members; Zhihua Liang, Jia You, Yang Yu, Atreyee Das, Yanyan Zhang, Jia Guo, Qian Chen, Hilda F. Khoei, Shashikanth Gajaraj. Their co-works and discussion with them made many things I can not do by myself to be possible.

I am deeply grateful to my husband Eunsang. His support, encouragement, and love were undeniably the bedrock on my life. Also, I thank my daughter Je-In and her smiles always give me the energy to attain my study. I send love to my parents in Korea. I know I could not finish the study without their faithful prayers. Above all, I wholeheartedly thank my mighty God.

Table of Contents

LIST OF ILLUSTRATIONS

List of Tables

List of Figures

EFFECT OF SILVER NANOPARTICLES ON PLANKTONIC AND BIOFILM CELL GROWTH

Okkyoung Choi

Dr. Zhiqiang Hu, Dissertation Supervisor

ABSTRACT

Silver nanoparticles (Ag NPs) are one of the most widely used nanoparticles, most notably serving as an antimicrobial agent for sanitization and medical purposes. Despite of their widespread use, little was known about the environmental effect of silver nanoparticles. This research focused on the impact of AgNPs on planktonic (e.g., free swimming) and biofilm bacteria that are relevant to wastewater treatment and the natural environment. Nitrifying bacteria and *E. coli* were used as model microorganisms because they are essential in nitrification processes and a good water quality indicator in the environment, respectively. Ag NPs were prepared in the lab and fully characterized by analyzing their optical property, size distribution, and composition (Ag^+/Ag NPs). Several microbial toxicity tests (autotrophic respirometry, GFP-fluorescence microtiter assay, and oxygen based microrespirometry) were developed and applied individually depending on the microbial growth conditions. The research results demonstrated that the toxicity of Ag NPs was dependent on nanosilver particle sizes and related to of the concentration of intracellular reactive oxygen species (ROS). However, other metallic/oxide particles such as TiO_2 nanoparticles showed lower toxicity than Ag NPs to the microorganisms with higher ROS accumulation, indicating that ROS was not a good chemical marker to determine the toxicity of metallic nanoparticles. To control the toxicity by metallic nanoparticles such as Ag NPs, sulfide anion effectively reduced the

nanotoxicity because of the formation of stable Ag_xS_y complex as a result of nanosilver dissolution and silver-sulfide complexation.

E. coli biofilm cells were more resistance to the toxicity of Ag NPs than the planktonic cells. To determine the relationship between the toxicity and the fate of nanosilver in biofilms, the spatial distribution of Ag NPs in biofilms was analyzed using *E. coli* expressing green fluorescent protein (GFP) and the indigenous red fluorescence of aggregated silver particles. The results suggested that biofilms might confer resistance to nanosilver through particle aggregation and retarded Ag^+/Ag NPs diffusion.

1 Introduction

1.1 Silver Nanoparticles

Silver nanoparticles (nanosilver, nano-Ag, Ag NPs) are small-sized particles with at least one dimension less than 100 nm. Due to their small size, nanoparticles have large surface area with high-dense atoms. A 9-nm nanosilver contains about 24,000 silver atoms (Kulinowski, 2008). Nanoparticles are a bridge between bulk materials and atoms/molecules (Nel et al., 2006). Nanoparticles have size-dependent physicochemical properties while bulk material has generally constant property. Optical, electromagnetic and catalytic properties are also observed to increase in nanoparticles (Kelly et al., 2003; Wenseleers et al., 2002). Therefore, nanoparticles are used in many consumer products for commercial applications.

Silver nanoparticles have a broad range of applications in consumer products such as socks, wound dressing, toothpaste, air filters, food storage containers, and cosmetics because of their strong antimicrobial property (Maynard and Michelson, 2006). Silver nanoparticles are also used to kill bacteria in the clothes at low temperature in a so-called nanosilver washing machine (www.samsung.com). Nanosilver socks are claimed to remove odor by killing organic acid-producing bacteria. They are also applied in industry for selective coating for solar energy absorption (Cole and Halas, 2006; Rand et al., 2004), catalysis in chemical reactions (Zhai et al., 2006), surface-enhanced Raman scattering for imaging

(Yamamoto and Watarai, 2006), and antimicrobial sterilization (Pal et al., 2007; Sambhy et al., 2006; Savage and Diallo, 2005).

1.2 Toxicity of Silver nanoparticles

As nanotechnology enhanced products rapidly increase in the market, the risk of Ag NPs released into sewage systems and eventually to rivers, streams, and lakes is therefore of concern. Modeling results indicate that up to 15% of total silver in the form of Ag^+ ions or Ag NPs might be released from the nanosilver based biocidal plastic and textile into water (Blaser et al., 2008). Recent studies confirm that Ag NPs are easily released from nanosilver coated socks during the washing process (Benn and Westerhoff, 2008). If they are not well managed or disposed of appropriately, the increasing use of nanosilver products could affect wastewater operation because of the increased load of silver in wastewater.

The presence of different toxicants including nanoparticles may result in additive toxicity (sum of individual toxicity), synergistic toxicity (higher than simple sum of individual toxicity), and antagonistic toxicity (lower than sum of each toxicity) (Newman and Unger, 2003). Thus, the toxicity from a mixture of nanoparticles released from consumer products or industry also has to be considered to protect the environment. Evidence also shows that the toxicity of AgNPs is related to the release of silver ions or the nanoparticles themselves.

1.2.1 **Silver Ion**

Free silver ion (Ag^+) is highly toxic to a wide variety of organisms including bacteria. Metal toxicity to planktonic species such as algae (Lee et al., 2005) and bacteria (Hu et al., 2002; 2003) is often governed by the concentrations of aqueous free metal species (i.e., Ag^+). The inhibitory effect of Ag^+ is believed to be due to its sorption to the negatively charged bacterial cell wall, deactivating cellular enzymes, disrupting membrane permeability, and ultimately leading to cell lysis and death (Ratte, 1999; Sambhy et al., 2006). The aqueous concentrations of Ag^+ are typically low in wastewater treatment systems or in the natural environment because of its strong complexation with various ligands such as chloride ($K_{sp} = 10^{-9.75}$), sulfide ($K_{sp} = 10^{-49}$), thiosulfate, and dissolved organic carbon (Shafer et al., 1998; Wang, 2003). As a result, silver toxicity to microorganisms is generally not observed.

1.2.2 **Silver Nanoparticles**

While the fate and toxicity of silver ions are well studied, little is known about the adverse effects of Ag NPs on wastewater treatment and the environment. Unfortunately, the antimicrobial property of nanosilver does not kill only bad or infectious microorganisms. The nanoparticles released from various consumer products into the environment can be also highly toxic to benign microorganisms (Alvarez, 2006; Grassian et al., 2007; Hyung et al., 2007; Limbach et al., 2008). It is demonstrated that nanosilver has a potential to disrupt soil microbial communities (Noredal et al., 2007). Alsodifferent toxic effects of various

sized silver nanoparticles (Table 1) suggest that further studies on the environmental implications of nanoparticles are needed. Since nanoparticles have substantially different physiochemical properties from those of bulk materials of the same composition, different toxicity mechanisms of nanoparticles may apply to biological systems (Nel et al., 2006). More research is required to investigate nanoparticle properties such as size, shape, dissolution/aggregation, surface coating, and solubility that may affect the specific physicochemical and transport properties, which could exert significantly different impact on microbial growth (Nel et al., 2006).

Silver in the form of nanoparticles could be more reactive with its increased catalytic properties and become more toxic than the bulk counterpart. Furthermore, toxicity is presumed to be size- and shape dependent (Pal et al., 2007), because small size nanoparticles (e.g., < 10 nm) (Kloepfer et al., 2005; Morones et al., 2005) may pass through cell membranes and the accumulation of nanoparticles inside the cell can lead to cell malfunction and eventually death of the organism.

Table 1. The nanosilver inhibitory effect on different organisms.

Target cell	Average size	Toxicity	Investigated toxic mode
E.coli (Sondi and Salopek-Sondi, 2004)	12 nm	100 % inhibition at 50-60 mg/L Ag	Formation of pits in cell wall
E.coli (Morones et al., 2005)	1-10 nm	No growth at 75 mg/L Ag	Direct interaction of 1-10 nm nanosilver with the bacteria
E.coli (Cho et al., 2005)	10 nm	10 mg/L Ag MIC[1], 100 % inhibition at 100 mg/L Ag	Disrupted cell walls\
S. aureus (Cho et al., 2005)		5 mg/L Ag MIC[1], 100 % inhibition at 50 mg/L Ag	
E.coli (Lok et al., 2006)	9 nm	Bacterial proliferation inhibition at 0.4 nM	Envelope protein precursors accumulation Proton motive force dissipation Outer membrane destabilization Plasma membrane potential collapse Intracellular ATP deplete
E.coli (Pal et al., 2007)	39 nm	No growth at 0.5 mg/L Ag	Shape-dependent interaction
E.coli *St. aureus* yeast (Kim et al., 2007)	14 nm	3.3 nM MIC[1] 33 nM MIC[1] 6.6 nM MIC[1]	Free radical generation
HIV-1 virus (Elechiguerra et al., 2005)	1-10 nm	Binding with the gp120 subunit of the viral envelope glycoprotein at 100 mg/L Ag	Size dependent nanoparticles exclusively in the range of 1–10 nm attached to the virus
BRL 3A rat liver cells (Hussain et al., 2005)	15 nm 100 nm	Decrease mitochondrial function at 5-50 mg/L Ag.	LDH[3] leakage ROS[4] increase
Zebrafish (Lee et al., 2007)	5-16 nm	Deformed Zebrafish was maximized at 0.19 nM Ag (21 mg/L Ag)	Transported into and out through chorion pore canals

[1] Minimum Inhibitory Concentration
[2] 50% inhibition concentration
[3] Lactate Dehydrogenase
[4] Reactive Oxygen Species

1.3 Toxicological Methodology Used in This Study

Three methods were applied to analyze the toxicity of nanoparticles to planktonic and biofilms cells by comparing the bacterial growth rate between nanosilver treated samples and controls. The toxicity was inferred from the change of specific oxygen uptake rate of nitrifying bacteria (1.3.1), the activity of green protein fluorescence from gene-modified *E. coli* (gfp-tagged *E. coli*) (1.3.2), and relative oxygen consumption rate of *E. coli* (1.3.3).

1.3.1 Rate of Autotrophic Bacterial Growth Determined by Extant Respirometry

Autotrophic nitrifying microbial growth inferred from oxygen uptake rates due to ammonia oxidation was measured in duplicate using a batch extant respirometric assay (Hu et al., 2002). We chose nitrifying bacteria as a model organism for autotrophic bacteria because they play an important role in the nutrient removal from wastewater. Nitrification is often a rate-determining step because nitrifying bacteria are sensitive to environmental change such as pH, temperature, and DO concentration. Many toxic chemicals are reported to inhibit the growth of nitrifying bacteria (Blum and Speece, 1991).

Nitrification is oxidation process and nitrifying bacteria consume oxygen (equation 2). We monitored the change of dissolved oxygen (DO) concentration to evaluate autotrophic microbial activity of nanoparticles-amended culture.

$$NH_3 + O_2 \rightarrow 2H^+ + 2e^- + HNO_2 \qquad \text{Equation 1}$$

Aliquots (60 mL) of nitrifying bacteria were collected from the nitrifying reactor operated at a target solids retention time of 20 d and a hydraulic retention time of 1 d. MOPS [3-(N-morpholino) propanesulfonic acid, pH adjusted to 7.5] at a final concentration of 20 mM was added to maintain relatively constant pH of 7.5 during ammonium oxidation. The nitrifying bacterial suspensions were amended with nanoparticles or bulk materials of known concentration during the toxicity test. Each toxicity test at the known final nanoparticle concentration was conducted using respirometric bottles with no headspace. Every batch respirometric test was accompanied by a positive control (e.g., untreated nitrifying bacteria only) at room temperature (25 ± 2 °C). The nitrifying bacteria suspensions were aerated with pure oxygen gas before aliquots of NH_4^+-N (10 mg/L-N as NH_4NO_3) were injected. Magnetic stirring at ca. 100 rpm was provided in the bottles to ensure complete mixing. A decrease in the dissolved oxygen (DO) level in the respirometric vessel was measured by a DO probe (YSI model 5300A, Yellow Springs, OH) and continuously monitored at 4 Hz by an interfaced personal computer (Figure 2). The inhibition of autotrophic microbial growth was inferred from the difference between the measured specific oxygen uptake rate in the absence and presence of the Ag species like equation (3) (Hu et al., 2002).

$$Inhibtion,(\%) = \frac{OUR_{control} - OUR_{treated}}{OUR_{control}} \times 100 \qquad \text{Equation 2}$$

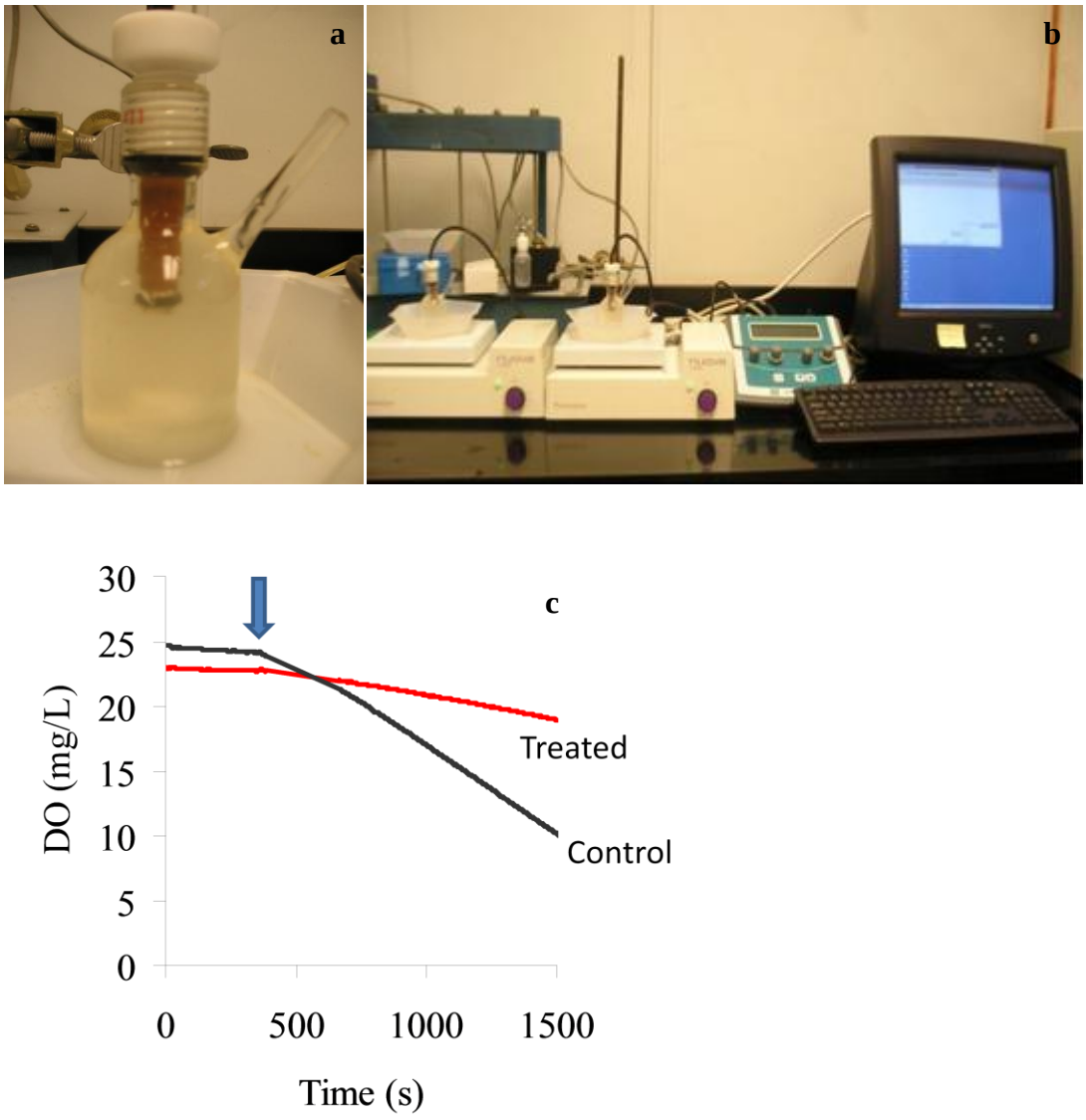

Figure 1. Respirometry assay to measure nitrification activity for nanotoxicity study.

(a) The respirometry bottle (b) DO concentration is measured by a DO probe in a closed respirometry bottle and recorded by interfaced PC. (c) The difference of oxygen uptake rate (the slope in the graph) between the control and the treated nitrifying culture indicates the inhibition of toxicants. The arrow pointed is the ammonium (10 mg-N/L) injection time through a sidestream injection port of the bottle using a microsyringe.

1.3.2 **Rate of Heterotrophic Growth Determined by Automated Microtiter Assay**

E. coli PHL628 was used as a model planktonic heterotroph in nanosilver toxicity study. This strain tagged with a green fluorescence protein (GFP) was a derivative of the *E. coli* K12 that forms biofilms as a consequence of the over-expression of curli (Junker et al., 2006). The test strain was grown overnight on a mechanical shaker (200 rpm) at room temperature in two different mediums, nutrient broth (BBL™, Diagnostic Systems, Framingham, MA) and LB (Luria-Bertani, Fisher Scientific, Pittsburgh, PA) medium, chosen depends on need of cell amounts. LB medium has rich nutrients (Table. 2), and the bacterial growth was faster with higher biomass concentrations compared to other growth media.

Table 2. Luria-Bertani v.s. Nutrient broth

	LB	Nutrient broth
Total carbohydrate (mg/L)	860	226
Planktonic cell concentration after 24 hrs (CFU/mL)	$1.3 (\pm 0.2) \times 10^{12}$	$8.7 (\pm 0.1) \times 10^{10}$
Biomass concentration after 24 hrs (CFU/peg*)	$3 (\pm 1) \times 10^{7}$	$3.6 (\pm 1.5) \times 10^{8}$

*in MBEC™ High-throughput (HTP) assay (MBEC BioProduct, Alberta, Canada)

To evaluate the inhibitory effects of Ag species on heterotrophic growth, *E. coli* PHL628-*gfp* was grown in nutrient broth (BBL) at room temperature overnight. For the microtiter fluorescence assay, aliquots of the fresh medium (190 μL) were pipetted into eight parallel wells of a 96-well microplate, and aliquots (10 μL) of overnight *E. coli* cells were

inoculated in each well. Aliquots of the Ag NP suspension, Ag^+ or AgCl colloidal solution were added individually to each well to reach predetermined Ag concentrations. The cells were exposed to ambient air and mixed intermittently to support their growth on the plate. A program was made to incubate the samples with vigorous mixing for 10 s per hour before the fluorescence intensities (535 nm) excited at 485 nm were recorded automatically every hour for 24 h. The plate was pre-equilibrated at room temperature (25 ± 2 °C) for 0.5 h and the fluorescence (in relative fluorescence unit, RFU) of microbial suspensions was measured with a fluorescence microreader (VICTOR^3, PerkinElmer, Shelton, CT).

The time-dependent microbial growth associated with organic substrate oxidation in the 96-microwells was simulated using an exponential growth model:

$$X = X_0 e^{\mu t} \qquad \text{Equation 3}$$

where X and X_0 are final and initial biomass concentrations, respectively, as reflected by the fluorescence intensity. The parameters of the specific microbial growth rate, μ, were determined via least-squares error (LSE) analysis using the SOLVER routine in Microsoft Excel.

1.3.3 **Rate of Bacterial Growth Inferred from Oxygen Based Microrespirometry**

This method based on the fact that oxygen quenches the fluorescence of the fluorophore like luminescent transition-metal complexes (e.g. Ru(II)-complexes) (Chan et al., 2000).

This phosphorescent oxygen-sensing probe can use to detect the change of dissolved oxygen concentration as a result of bacterial respiration so that the activity of aerobic bacteria is derived (O'Mahony et al., 2005; O'Mahony and Papkovsky, 2006). This simple method allows sensitive (down up to single cell) and fast measurement (within 5 hours in our results, Figure 4) of the total number of aerobic bacteria. Detail information is presented in the Chapter 6.

Figure 3 shows the reaction and kinetics between oxygen (quencher, Q) and fluorophore (dye, D). The fluorescence is increased as a result of oxygen consumption by aerobic bacteria. A calibration curve is established by recording the time to reach the maximum fluorescence (no oxygen) as a function of initial number of aerobic bacteria. Based on the calibration curve, we can induce the activity of bacteria in the sample.

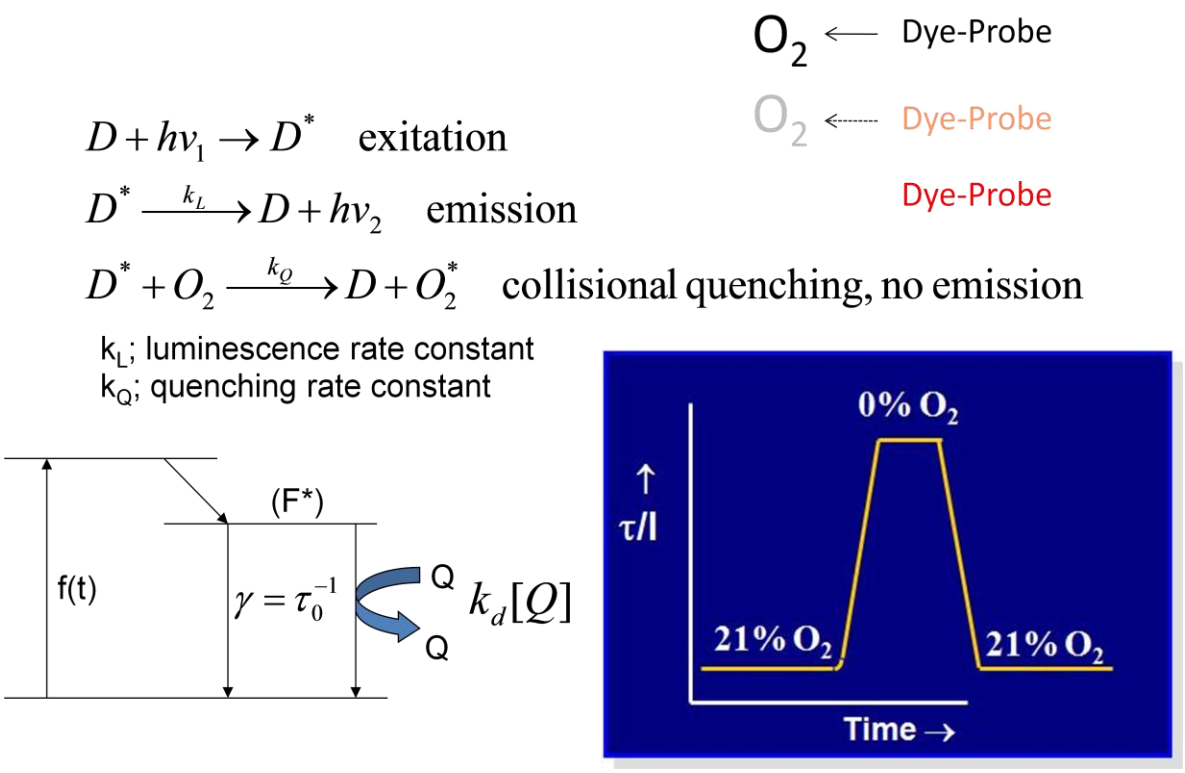

Figure 2. Reaction and kinetics between oxygen-sensing probes and oxygen in oxygen based microrespirometric assay.

After collision quenching, the fluorescence intensity is reduced. The rate of decrease is dependent on quencher (O_2) concentration.

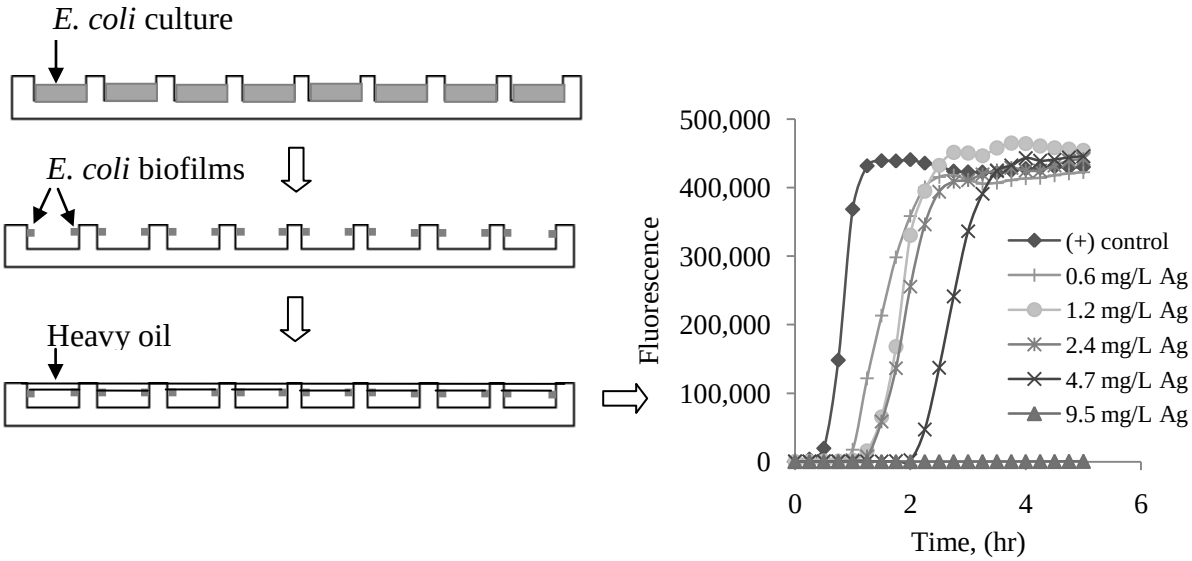

Figure 3. A schematic of microtiter based nanotoxicity study of biofilm resistance to nanosilver.

The microrespirometric assay is particularly useful in biofilm/nanotoxicity study. Biofilm was cultivated for one day on the barrier wall in 96-well microplates. After rinsing twice with fresh medium, each well was filled with fresh nutrient broth, oxygen probe, and nanosilver with a predetermined concentration. Heavy oil was used to cover the surface to prevent liquid evaporation or oxygen transfer. Fluorescence was measured automatically every 5 mins using a microreader. The time to reach the half of maximum fluorescence shows the abundance of active bacteria in the culture.

1.4 Mode of Antimicrobial Action of Silver Nanoparticles

The mechanisms by which silver nanoparticles kill microorganisms are largely unknown and the mode of antimicrobial action by nanosilver is still not fully understood. Possible mechanisms by which silver nanoparticles inhibit microbial growth include particle attachment to or penetration of the cell membranes accompanied with slow release of Ag^+, causing the changes of membrane permeability and redox cycle in the cytosol, intracellular radical accumulation, and dissipation of the proton motive force for ATP synthesis (Lok et al., 2006; Morones et al., 2005; Nel et al., 2006; Sondi and Salopek-Sondi, 2004). Recent studies suggested that ROS generation by Ag nanoparticles or Ag^+ ions is responsible for the strong bactericidal activity (Inoue et al., 2002; Kim et al., 2007), although a quantitative estimation was not carried out.

1.4.1 Silver Ion Release

Dissolution of nanosilver particles results in a slow and continuous release of silver ions. In one study, after one hour washing of nanosilver socks with ultrapure water, about 70 ~ 90 % of the total silver is released as silver ions (Benn and Westerhoff, 2008). Modeling study estimates 30 % of nanosilver consumer products could be released as silver ions (Mueller and Nowack, 2008). Several studies of nanosilver toxicity have been addressed because of the release of silver ions (Choi et al., 2008; Navarro et al., 2008).

The toxicitiy of heavy metals like silver ions are related to reactive oxygen species (ROS) (Jung et al., 2008; Yamanaka et al., 2005). The intracellular concentrations of reactive oxygen species such as singlet oxygen ($^1O_2$), superoxide (O_2^-), hydrogen peroxide (H_2O_2), and hydroxyl radical ($OH\cdot$) are generally very low in normal live organisms. Under oxidative stress conditions (e.g., exposure to hyperoxia or toxicants), the ROS are increased more than the cell recovery ability, causing lipid peroxidation (Sayes et al., 2005), cellular metabolic malfunction and cell membrane disruption (Limbach et al., 2007; Long et al., 2006; Wiesner et al., 2006).

The reactive oxygen species are generated constantly through *exogenous* (extracellular) and *endogenous* (intracellular) processes as part of aerobic life on the earth (Kohn and Nelson, 2007). While singlet oxygen is often generated following absorption of energy (light), other ROS are formed at the one-electron steps in oxygen reduction (Stumm and Morgan, 1996)

$$O_2 \xrightarrow{e^-} O_2^{-\cdot} \xrightarrow{e^- + 2H^+} H_2O_2 \xrightarrow{e^-} OH^- + OH^{\cdot} \xrightarrow{e^- + 2H^+} 2H_2O \qquad \text{Equation 4}$$

Exogenously, nanoparticles of TiO_2 and ZnO with large surface areas and highly reactive catalytic sites can produce photocatalytic ROS in the presence of near-UV light (Adams et al., 2006; Cho et al., 2004). Even without UV light irradiation, nanoparticles of transition metal oxides were capable of generating ROS monitored through fluorescence measurements (Limbach et al., 2007), and Ag nanoparticles were able to produce ROS detected by electron spin resonance spectroscopy (Kim et al., 2007).

Endogenous ROS are produced inside the cells. Normally cells are able to reduce oxygen to water through their electron transport chains and protect themselves from ROS damage through the use of enzymes such as superoxide dismutases (SOD, to convert superoxide to hydrogen peroxide) and catalases (to convert hydrogen peroxide to water and oxygen) (Farber, 1994; White, 2000). Under unfavorable environment such as hypoxia or in the presence of toxins, oxidation stress occurs and endogenous ROS accumulation can damage cellular constituents and disrupt cell functions.

1.4.2 **Cell Internalization of Nanoparticles**

Although the mechanisms of toxicity remain to be elucidated, nano-size particles can penetrate into the bacterial cells (Morones et al., 2005; Sondi and Salopek-Sondi, 2004). Evidence from scanning transmission electron microscopy also shows that smaller particles (< 10 nm) may enter the cell directly to inhibit microbial growth (Morones et al., 2005). Metallic/oxide nanoparticles has been proposed to efficiently enter the eukaryotic cells by a Trojan-horse type mechanism to provoke the transport of high levels of nanoparticles into the cells (Limbach et al., 2007). The nanoparticles rapidly enter the cells and successively dissolve, releasing damaging metal ions within the cell, which may react with enzymes or proteins in the cytoplasm to inactivate the cell metabolism (Moore, 2006).

Figure 1 shows different toxic mode of TiO_2 and Ag nanoparticles. Silver and titanium oxide are most used in consumer products. Silver nanoparticles release silver ions to induce

ROS or directly enter the cells if the particles size is small (dual mode). Cell-internalized particles may disrupt cell mechanism but how small nanoparticles inhibit in the metabolism of the cell is largely unknown. Semiconductor nanoparticles (e.g. TiO_2, ZnO) are activated by UVA emission, which induces extracellular reactive oxygen species (ROS) as found in toxicity caused by other heavy metal ions. We therefore would like to investigate how different nanoparticles with possibly different mode of action affect bacterial growth (Chapter 5).

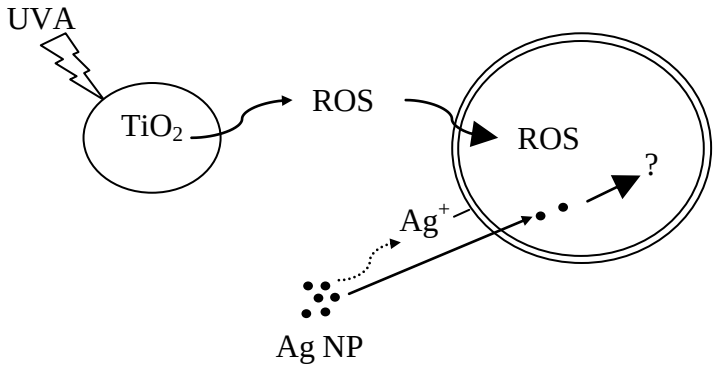

Figure 4. A schematic of the different mode of action of TiO_2 and Ag nanoparticles against microorganism.

The toxicity of nanoparticles is related to the physical and chemical characteristics of nanoparticles. Silver nanoparticles (Ag NPs) may provide dual modes of toxic action, i.e. by releaseing ionic Ag^+ and by penetrating of small size particles inside the cell. The semiconductor material, TiO_2 nanoparticles produce reactive oxygen speices (ROS) under the light (UVA).

1.5 Fate and Toxicity of Silver Nanoparticles in Wastewater Treatment

Nanosilver released in wastewater can be present as nanoparticles (Blaser et al., 2008), but it is likely dissolved and finally converted into Ag^+ ions (Benn and Westerhoff, 2008), complexed with ligands, agglomerated (Limbach et al., 2005; Zhang et al., 2008). While the fate of nanoparticles in water is largely unknown, studies indicated that metallic oxide nanoparticles such as TiO_2 and ZnO tend to be rapidly aggregated after discharged into water and remain stable for a long time (Zhang et al., 2008). The aggregation of nanoparticles is dependent upon the pH (affecting the point of zero charge (pH_{zpc}) of the nanoparticles), ionic strength, organic species, and natural porous surfaces (DunphyGuzman et al., 2006). It is reported that silver nanoparticles are easily accumulated in activated sludge (Benn and Westerhoff, 2008).

The fate of nanoparticles depends on particle properties and environmental conditions. Information on the composition and properties of engineered nanoparticles, such as size distribution, shape and particularly surface area, solubility, surface charge and other surface chemical properties, is essential to understand their potential ecotoxicological impact.

1.6 Fate and Toxicity of Silver Nanoparticles in Biofilms

Biofilms is commonly observed in the environment. Microbial cells in aquatic ecosystems often live in densely clustered and surface-attached communities known as biofilms to protect themselves from environmental changes (Harrison et al., 2007). Extracellular

polymeric substances (EPS) produced by the cells contribute to biofilm formation (Tsuneda et al., 2003). Biofilms are resistant to toxic chemicals such as heavy metals (Harrison et al., 2005; Harrison et al., 2005; Teitzel and Parsek, 2003) and antimicrobial agents (Elkins et al., 1999; Mah and O'Toole, 2001). The resistance can be explained by several mechanisms such as increased persister cells (Keren et al., 2004), quorum sensing systems (Miller and Bassler, 2001), biosorption (Qureshi et al., 2001), gene expression response (Lenz et al., 2008), and efflux systems (Teitzel and Parsek, 2003). Limited mass diffusive transport within biofilms also contributes to antimicrobial resistance of biofilms (Stewart and Franklin, 2008).

Whether biofilm is susceptible to inhibition by nanoparticles is largely unknown. The study of biofilm resistance to nanoparticles is important because their environmental impact is directly linked to the public health (e.g., biofilm associated infection and dental diseases) and the environment (e.g. wastewater treatment and ecosystem conservation). Nanoparticles tend to aggregate easily and, therefore, the transport of Ag NPs in biofilms may be restricted, thereby limiting their effectiveness as an antimicrobial agent. Physiological heterogeneity (Stewart and Franklin, 2008) in biofilms (oxygen, substrate, and by- product concentration gradient, pH range, EPS composition, etc.) may further influence aggregation, dissolution and diffusive transport of nanosilver.

As a part of this Ph.D research, we show how nanoparticles inhibit biofilm cell growth (nanoparticles action against microorganisms) and how the change of biological growth conditions affects the fate and toxicity of nanoparticles (microbial effect on nanoparticles).

To this end, we investigated the spatial distribution of nanoparticles in biofilms by taking adventage of the green fluorescence of GFP protein and the indigenous red florescence of aggregated nanosilver to know how deep nanoparticles penetrate inside the biofilms (Chapter 6).

1.7 Hypotheses and Research Overview

This Ph.D. thesis research focuses on the inhibitory effect of silver nanoparticles on planktonic (free swimming) and biofilm cells that are important in wastewater treatment plants. We chose nitrifying bacteria and *E. coli* as model organisms to examine the toxicity of nanoparticles to bacteria. We evaluated nano-toxicity to ammonium oxidation by nitrifying bacteria using extant respirometry. *E. coli* cells labeled with green fluorescence protein and oxygen based microrespirometry were also used for high throughput toxicity screen. This research aims to answer following questions:

a) *Is nanosilver toxic? Is it more toxic than silver ion?*
b) *Why is nanosilver toxic to bacteria?*
c) *Is the nanosilver toxicity related to reactive oxygen species (ROS) that can be used as a chemical marker for nanotoxicity?*
d) *Do different metal/metal oxide nanoparticles have different toxicity?*
e) *How to reduce or control the toxicity of nanosilver againt beneficial organisms?*
f) *What are the interactions between bacteria and nanoparticles?*

g) *What is the difference of nano-microbial interactions between planktonic and biofilm cells?*

To answer these questions, we have mainly five **hypotheses** in the following:

Hypothesis 1: Silver nanoparticles are toxic to planktonic and biofilm bacteria that is important to wastewater treatment.

Hypothesis 2: Small size nanoparticles are more toxic than large size nanoparticles.

Hypothesis 3: Reactive oxygen species generated extracellularly or intracellularly are related to nano-toxicity.

Hypothesis 4: Metal/metal oxide nanoparticles have different inhibitory mechanisms which depend on the chemical (e.g. microbial affinity, chemical coating) and physical (e.g. size, semi conductivity) properties.

Hypothesis 5: Biofilm cells are more resistant than planktonic cells to nanosilver. The retardation of transport limits nanoparticles to transport inside the biofilm.

In chapter 2, the toxicity of silver nanoparticles was tested using nitrifying bacteria as autotrophs and *E. coli* as a model heterotrophic organism. Chapter 3 demonstrates that nanosilver toxicity is dependent on its size and related to reactive oxygen species (ROS) accumulation in the cells. The toxicity of nanosilver can be remediated by chemical complexation, especially with sulfide salts as described in chapter 4. In chapter 5, compared

with different metal oxide nanoparticles, a dual modes (ionic Ag^{+} and penetration of small nanoparticles inside the cell) of antimicrobial action is proposed, which helps answer the question: Is ROS a good biomarker to show nano-toxicity? Finally, we compared the toxicity of silver nanoparticles between planktonic and biofilm cells and examined the microbial interaction with nanoparticles in chapter 6.

2 The Inhibitory Effects of Silver Nanoparticles, Silver Ions, and Silver Chloride Colloids on Microbial Growth[1]

2.1 Abstract

Emerging nanomaterials are of great concern to wastewater treatment utilities and the environment. The inhibitory effects of silver nanoparticles (Ag NPs) and other important Ag species on microbial growth were evaluated using extant respirometry and an automatic microtiter fluorescence assay. Using autotrophic nitrifying organisms from a well-controlled continuously operated bioreactor, the inhibitions by Ag NPs (average size = 14 $\pm$ 6 nm), Ag^+ ions ($AgNO_3$) and AgCl colloids (average size = 0.25 μm) at 1 mg/L Ag were 86 $\pm$ 3%, 42 $\pm$ 7%, and 46 $\pm$ 4%, respectively, whereas the inhibition on heterotrophic growth followed the order: Ag^+ > AgCl colloid > Ag NP at 0.5 mg/L Ag. No compromise on cell membrane integrity was observed under the treatment of test Ag species by using a LIVE/DEAD Baclight™ bacterial viability assay. However, electron micrographs demonstrated that Ag NPs attached to the microbial cells, probably causing cell wall pitting. The results suggest that nitrifying bacteria are especially susceptible to inhibition by Ag NPs, and the accumulation of Ag NPs could have detrimental effects on the microorganisms in wastewater treatment.

[1] *Water Research*, **2008**, *42*, 3066-3074.

2.2 Objectives

Little work has been done to evaluate the inhibition of microbial growth by different Ag species, especially Ag NPs in wastewater treatment systems where such information is valuable for operation planning and control. Both autotrophic and heterotrophic microorganisms are important in wastewater treatment. While heterotrophs are responsible for organic and nutrient removal, autotrophs are responsible for nitrification that is considered as the controlling step in biological nitrogen removal because of the slow growth rate of nitrifiers and their sensitivity to temperature, pH, dissolved oxygen concentration, and toxic chemicals (Blum and Speece, 1991; Hu et al., 2002). Consequently, the objective of this chapter was to evaluate the impact of Ag species such as Ag NPs, Ag^+ ions and AgCl colloids on heterotrophic and autotrophic growth.

In this research work, Ag NPs and AgCl colloids with larger sizes were synthesized in the laboratory and characterized by UV-vis spectroscopy and electron microscopy. The inhibitory effects on the autotrophic and heterotrophic growth were determined by a short-term extant respirometric assay and an automatic microtiter assay, respectively. Environmental scanning electron microscopy (ESEM) was applied as a complementary technique to examine the microbial/nanoparticle interactions. The mode of action of nanosilver toxicity was finally discussed based on the results of membrane integrity using a LIVE/DEAD Baclight™ bacterial viability kit.

2.3 Materials and Methods

Silver materials

Silver Nanoparticles

Silver nanoparticles (Figure 5) were synthesized by reducing silver nitrate with sodium borohydrate ($NaBH_4$, Sigma, St. Louis, MO) and adding polyvinyl alcohol (PVA, Sigma, St. Louis, MO) as the capping agent to control the growth of nanocrystals and agglomeration of nanoparticles. To dissolve polyvinyl alcohol, a solution containing 0.06% (wt) PVA was heated to 100 ℃ and cooled down to room temperature before use. Silver particles were prepared by rapidly injecting 0.5 mL of 10 mM $NaBH_4$ into the 20 mL PVA solution containing 0.25 mM silver nitrate at room temperature. After 5 minutes of stirring, the reaction mixture was stored at 4 ℃ before use.

Figure 5. Silver nanoparticles suspensions made from the reduction of silver ion by borohydride in polyvinyl alcohols.

Different colors of prepared nanosilver suspensions indicate various silver nanoparticle composition. Extra silver ions in suspension shows yellow color and the complete silver ion reduction results in the color change to brown. Dark brown color nanosilver suspension had relatively high toxicity due to its large portion of small sized particles (Chapter 3)

Silver Ions

A silver nitrate standard solution (14 mM, Fisher Scientific, Pittsburgh, PA) was used as a source of Ag^{+} ions. To reduce the complex with silver ion, we avoided the impurity of anion like chloride and sulfate.

Silver Chloride Colloids

Aliquots of 100 mg/L AgCl colloids were prepared freshly by vigorous mixing (700 rpm) 1 mL of 14 mM silver nitrate standard solution and 1mL of 28 mM sodium chloride with 18 mL of distilled water. Twice as much sodium chloride as silver nitrate was added to ensure

complete complexation with no residual Ag^+ ions in the colloidal solution (confirmed by Ag^+ measurements with an ion selective electrode).

Microbial cultures

Autotrophic Bacteria

The mixed and enriched nitrifying bacteria were cultivated in a continuously stirred tank reactor (14L, Figure 6) operated at solids retention time (SRT) of 20 d and hydraulic retention time (HRT) of 1 d using seed from a local nitrifying activated sludge plant in Missouri, USA. The reactor was fed with an inorganic medium containing ammonium (8.3 mM, NH_4NO_3) as the sole energy source and requisite macro- and micronutrients (Table 3). Low concentrations of anions such as chloride and sulfate were present in the reactor to minimize their complexation potential with Ag^+ ions. Sodium carbonate (0.5 M) was intermittently added to maintain the reactor pH at 7.5 ± 0.1 and fulfilled both carbon and alkalinity requirements. The typical effluent concentrations of NH_4^+-N (< 1 mg/L), NO_2^--N (< 1 mg/L) and NO_3^--N (~ 440 mg/L) indicated complete nitrification (APPENDIX A). After a few months of operation, mixed liquor was periodically withdrawn from the nitrifying reactor for batch respirometric studies.

Table 3. Composition of the growth nutrients in reactor influent

Compound	Concentrations in reactor influent		
	mg/L	Cations (mM)	Anions (mM)
$Mg(NO_3)_2$	61	$0.41Mg^{2+}$	$0.82NO_3^-$
$Ca(NO_3)_2$	41	$0.25Ca^{2+}$	$0.25NO_3^-$
$NaNO_3$	879	$10.34Na^+$	$10.34NO_3^-$
NH_4NO_3	667	$8.33NH_4^{+a}$	$8.33NO_3^-$
K_2HPO_4	3.9	$0.04K^+$	$0.02HPO_4^-$
$FeCl_2 \cdot 4H_2O$	2	$0.01Fe^{2+}$	$0.02Cl^{-b}$
$MnSO_4 \cdot H_2O$	3.4	$0.02\ Mn^{2+}$	$0.02SO_4^{2-c}$
$(NH_4)_6Mo_7O_{24} \cdot 4H_2O$	1.2	$0.006NH_4^{+a}$	$0.001Mo_7O_{24}^{6-}$
$CuSO_4$	0.8	$0.01Cu^{2+}$	$0.01SO_4^{2-c}$
$Zn(NO_3)_2 \cdot 6H_2O$	1.8	$0.01Zn^{2+}$	$0.02NO_3^-$
$Ni(NO_3)_2 \cdot 6H_2O$	0.3	$0.001Ni^{2+}$	$0.002NO_3^-$

[a] Total NH_4^+=8.336 mM. [b] Total Cl^-=0.02 mM. [c] Total SO_4^{2-}=0.03 mM.

Figure 6. The nitrifying bioreactor used to prepare autotrophic nitrifying bacteria.

The inorganic medium was fed to the reactor by pumping at a 4.8 mL/min flow rate. The solution pH was maintained at around 7.5 using a pH controller by adding 0.5 M $NaCO_3$ when the pH was below 7.3.

Heterotrophic Bacteria

The test heterotrophic bacterium was *Escherichia coli* PHL628-gfp, a gift from Dr. Anthony Hay at Cornell University. This strain tagged with a green fluorescence protein (GFP) was a derivative of the *Escherichia coli* K12 that forms biofilms as a consequence of the over-expression of curli (Junker et al., 2006). The test strain was grown overnight on a mechanical shaker (200 rpm) at room temperature in a nutrient rich medium (BBL™ containing 5g/L Gelysate™ peptone and 3g/L beef extract, pH 6.9 ± 0.2).

Measurement of Silver Toxicity

The nitrifying bacterial suspensions were amended with Ag NPs, Ag^+ ions and AgCl colloids individually at the final concentration range of 0.1-1 mg /L Ag. We measured oxygen uptake rate (OUR) of nitrifying bacterial culture amended with each concentration of silver and calculated inhibition as percentage according to equation (1). See detail information in 1.3.1.

Silver Species Characterization

Aliquots of the prepared Ag NP suspensions were periodically scanned from 250 to 700 nm to obtain absorption spectra using a UV-vis spectrophotometer (Cary 50, Varian, CA). Additional aliquots were used to determine the stability of the Ag NPs by measuring the

concentrations of Ag^{+} ions in the Ag NP suspensions on a regular basis using a silver ion/sulfide selective electrode (Denver instrument, Denver, CO).

The sizes of Ag NPs and AgCl colloids were characterized by a FEI Quanta 600F environmental scanning electron microscope (resolution: 3 nm at 30 kv, FEI Company, OR) equipped with a Scanning Transmission Electron Microscopy (STEM) detector. The Ag NP suspension was added to standard carbon-coated TEM grid. Images of the samples were taken at an accelerating voltage of 30 keV.

Microbial/Nanoparticle Interaction

The microbial/nanoparticle interaction was visualized using the FEI Quanta 600F SEM in the environmental (ESEM) mode that allows organic samples to be examined without applying a conductive coating prior to imaging. The enriched nitrifying culture amended with commercially available Ag NPs (advertised particle size = 10 nm, Nanostructured & Amorphous Materials, Inc.**,** Houston, TX) was placed in an Al cup on a cold stage (10 ℃) and imaged at about 7 Torr and 80% relative humidity. In order to obtain higher resolution images, bacteria amended with our own Ag NPs were examined under high-vacuum conditions utilizing a back-scattered electron (BSE) detector. The nanoparticle samples synthesized in our laboratory were prepared using a standard protocol described above, critically point dried and coated with ~10 nm of Pt.

Live/Dead Bacterial Viability Assays

Experiments were carried out in the presence and absence of nanoparticles to determine the cell viability of heterotrophic (*E. coli* PHL628 without GFP tagged) and autotrophic cultures by using a LIVE/DEAD Baclight™ bacterial viability kit (Molecular Probes, Eugene, OR) (Hu et al., 2003). Viable and dead cells were detected by differential staining with a mixture of a green fluorochrome, SYTO 9 (stains all cells, live or dead), and a red fluorochrome, propidium iodide (stains only bacteria with damaged membranes). A reduction in the SYTO 9 fluorescent emission results when both dyes are present in the cell. Dead cells subject to 75% ethanol killing for 1 h were provided as a positive control. To reduce background fluorescence, the microbial suspension was washed with 0.85% $NaNO_3$ after centrifuging at 10,000 g for 15min. After aliquots of microbial suspensions and stain solution were added to each well of a 96-well microplate, the plate was incubated at room temperature in the dark for 15 min, and the relative fluorescence intensity was measured by the VICTOR fluorescence microreader. Enumeration of stained cells was facilitated by excitation at 485 nm and detection at 642 nm (red) and 535 nm (green), for propidium iodide and SYTO 9, respectively.

2.4 Results and Discussion

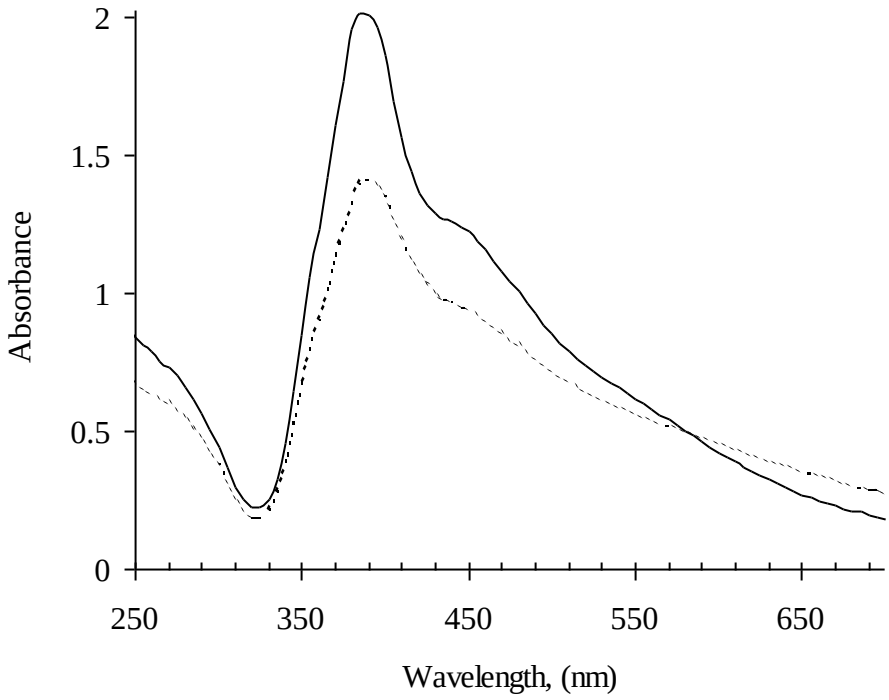

Figure 7. UV–vis absorption spectra of an Ag NP suspension.

Absorbance was recorded immediately after chemical reduction (solid line) and after 1 week storage (dash line) at room temperature.

Characterization of Ag Nanoparticles and Agcl Colloids

The absorption spectrum (Figure 7) of dark brown Ag NPs prepared by chemical reduction showed a surface plasmon absorption band with a maximum of about 400 nm, a characteristic peak of Ag NPs (Kong and Jang, 2006; Petit et al., 1993), indicating the presence of Ag NPs in the solution. Due to the excitation of plasma resonances or interband

transitions, some metallic nanoparticle dispersions exhibit unique bands/peaks (Creighton and Eadont, 1991). The broadness of the peak is a good indicator of the size of nanoparticles. As the particle size increases, the peak becomes narrower with a decreased bandwidth and an increased band intensity (Kong and Jang, 2006; Petit et al., 1993). Furthermore, there is an inverse linear relationship between the full width at half-maximum (FWHM) and the diameter of particles (Petit et al., 1993):

$$FWHM = 50 + \frac{230}{D} \qquad \text{Equation 5}$$

where both FWHM and the particle diameter (D) are in nanometers. The size of the Ag NPs was estimated as approximately 16 nm based on Equation 5. This result is consistent with the STEM results, which showed a size distribution between 10 and 40 nm (Figure 8) of the Ag NPs with an average of 14 ± 6 nm.

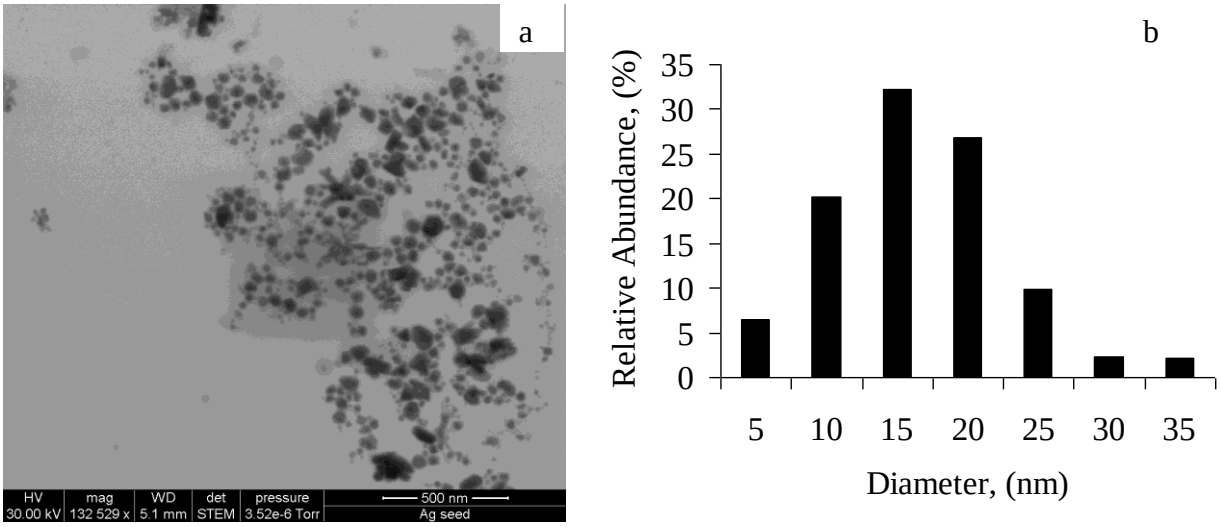

Figure 8. STEM image of Ag NPs and nanosilver particle size distribution.

The image of silver nanoparticles was taken by STEM (a) and their particle size distribution (b). The average particle size was 14nm. Bar size: 500nm.

A shoulder at approximately 425 nm was noticed in UV-vis absorption spectra, indicating a broad distribution of particle sizes and shapes in the solution because of crystallization, as was confirmed by STEM imaging. The position and the number of peaks in the absorption spectra are dependent on the shape of the particles: for an ellipsoidal particle there are two peaks whereas for spherical silver particles there is only one peak centered at about 400 nm (Creighton and Eadont, 1991; Petit et al., 1993).

The concentrations of Ag^+ ions were measured simultaneously to evaluate the stability of Ag NPs in the solution. The beginning Ag^+ concentration to make the Ag NP suspensions was 27 mg/L (0.25 mM). At the completion of the reaction, the residual Ag^+ concentration was measured at 0.6 ± 0.1 mg/L. The Ag^+ concentration remained largely unchanged at the

end of one day of resting at room temperature. Afterward, the Ag^+ concentrations increased gradually (data not shown), as also indicated from the changes of solution color.

During a week of Ag^+ monitoring at room temperature, the color of Ag NP suspensions changed from dark brown to yellow, presumably due to oxidative dissolution of the Ag NPs (Equation 6).

$$4Ag + O_2 + 2H_2O = 4Ag^+ + 4OH^- \qquad \text{Equation 6}$$

The color change associated with particle dissolution and the presence of multiple UV-vis absorption bands indicate the existence of Ag NPs of various shapes and sizes, as was confirmed by STEM imaging (Figure 8). To minimize the interference of dynamic changes of Ag NPs , we used the freshly prepared Ag NP suspensions that were stored shortly (a few days) at 4° C before use, during which no significant changes of Ag^+ concentrations were observed in the suspension (Figure 9).

Silver chloride colloids (100 mg /L Ag) were prepared with an average size of about 0.25 μm. The particle sizes ranged from 0.1 to 2 μm. A constant low Ag^+ concentration was detected because of the overdose of chloride. The fraction of Ag^+ was measured to be less than 0.1% of the total Ag in the AgCl colloidal solution.

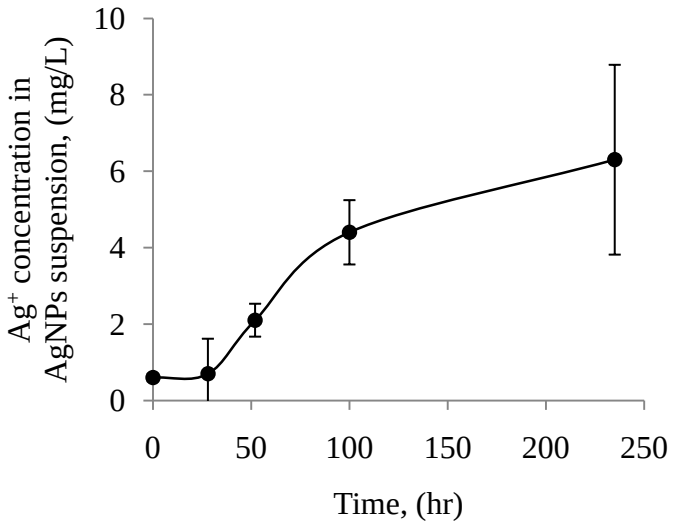

Figure 9. Silver ion release from silver nanoparticles.
Error bars indicate the range of duplicate data.

Effect of Ag Species on Autotrophic Growth

An extant respirometric technique was developed to determine biokinetic parameters from small pulses of substrate (e.g., NH_4^+) while minimizing changes in the microbial physiological state (Chandran and Smets, 2000; Hu et al., 2002). Figure 10 shows a representative respirograph of ammonia oxidation after an aliquot of ammonium was injected at ~100 s in the enriched nitrifying microbial suspension. The lack of change in dissolved oxygen illustrates nitrification inhibition in the presence of Ag NPs. There was no significant pH change before and after the test because of the addition of MOPS.

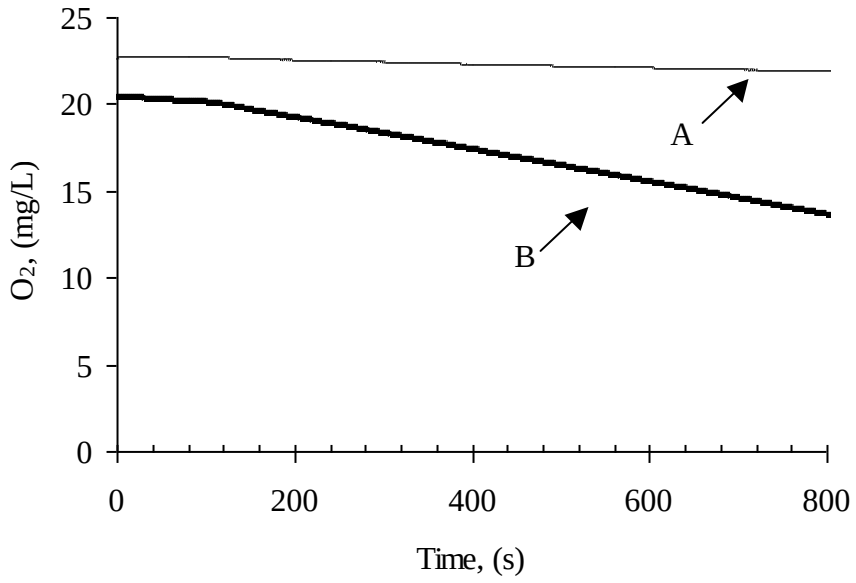

Figure 10. A respirometric test to determine the effect of silver nanoparticles on nitrification.

Nitrification inhibition inferred from the decrease of specific oxygen uptake rate (slope of curve A) in the presence of Ag NPs, as compared with control (curve B) after an aliquot of ammonium nitrate was injected individually at approximately 100 s.

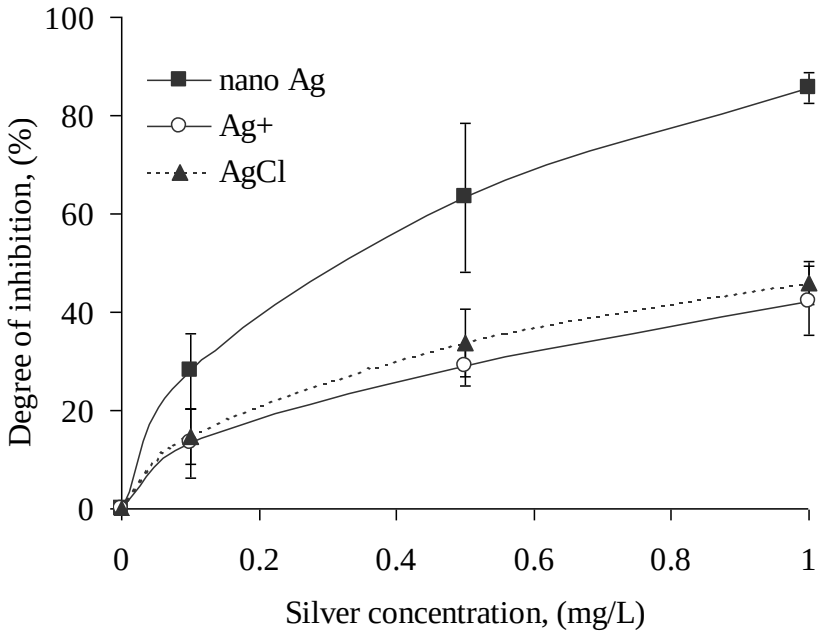

Figure 11. Inhibition of ammonium oxidation by different silver materials.

Inhibition of NH_4^+ oxidation as a function of the concentrations of silver in the form of silver nanoparticle, silver ion, and silver chloride. Error bars indicate one standard deviation.

As shown in Figure 11, at 1 mg/L Ag in the nitrifying suspension, the inhibitions by Ag NPs, Ag^+ ions, and AgCl colloids were 86 ± 3%, 42 ± 7%, and 46 ± 4%, respectively. Of all the Ag species tested, Ag NPs presented the highest inhibition on autotrophic growth. Interestingly, the freshly prepared AgCl colloids with an average size of 0.25 μm also inhibited nitrification. At the same level of Ag dose, there was no statistical difference ($p > 0.05$) of inhibition between AgCl colloids and Ag^+ ions. At this small size, silver chloride colloids appeared to reduce the bacterial growth as effectively as Ag^+.

Effect of Ag Species on Heterotrophic Growth

Consistent with the results from autotrophic growth study, silver nanoparticles inhibited *E. coli* growth. While no inhibition was observed at Ag NP concentrations below 1.0 μM (0.1 mg/L), the heterotrophic growth rate was reduced significantly by 55% as the Ag NP concentrations increased to 4.2 μM (0.6 mg/L) (Table 4). The IC50 of inhibition by the Ag NP suspension, or the half maximal inhibitory concentration, was estimated to be 4.0 μM (n = 8). Surprisingly, silver ion was the most toxic species to inhibit heterotrophic growth. At 4.2 μM Ag (~0.5 mg/L Ag), the inhibitions on the growth of *E. coli* PHL628-gfp were 55 ± 8%, 100%, and 66 ± 6% by Ag NPs, Ag^+ ions and AgCl colloids, respectively. *E. coli* treated with 1 mg/L Ag (or 9.3 μM) in the forms of Ag NPs, Ag^+ ions, or AgCl did not exhibit signs of growth (data not shown). The inhibition on heterotrophic growth appeared to be more severe from the long-term microtiter fluorescence assays, as we reported earlier that inhibition on microbial growth with longer period of metal exposure tends to be more significant (Cho et al., 2004).

Table 4. The specific growth rates and the degrees of inhibition by various silver species at different silver concentrations.

	Nano-Ag		Ag^+		AgCl colloid	
Concentration (μM)	μ (d^{-1})	Inhibition (%)	μ (d^{-1})	Inhibition (%)	μ (d^{-1})	Inhibition (%)
1.4	0.40(±0.03)	17(±5)	0.41(±0.02)	11(±4)	0.43(±0.01)	7(±4)
2.8	0.34(±0.03)	30(±6)	0.14(±0.03)	69(±6)	0.35(±0.02)	24(±5)
4.2	0.22(±0.04)	55(±8)	0	100	0.16(±0.03)	66(±6)

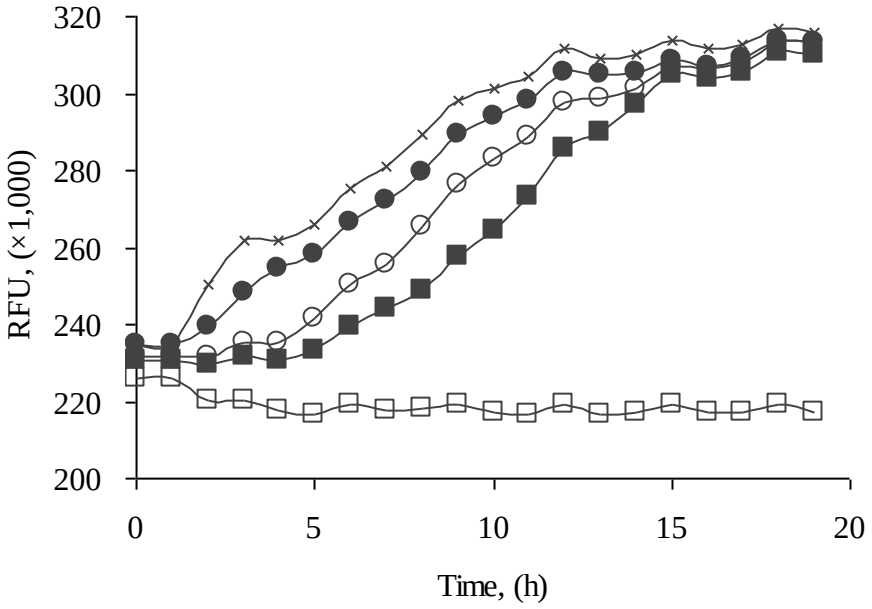

Figure 12.*E. coli* bacterial growth inhibition by nanosilver.

Effect of silver nanoparticle concentrations (×, 0 μM; ●, 1.4 μM; ○, 2.8 μM; ■, 4.2 μM; □, 9.3 μM) on the growth of *E. coli* PHL628-gfp as measured by relative fluorescence.

A slight lag phase of *E. coli* growth (~ 1.5 h) was observed during the automatic microtiter assays (Figure 12). Stationary phase was reached after incubation of the heterotrophic strain for approximately 12 h at room temperature (25 ± 2℃). Upon the addition of Ag NPs in the microbial suspension, a slight decrease of fluorescence efficiency (i.e., fluorescence quenching) with increasing Ag NP concentrations was observed. In the case of AgCl colloids, the quenching effect was less significant (data not shown). The results are consistent with the existing experimental data (Sabatini et al., 2007; Yamaguchi et al., 2007), indicating that the overlap between the GFP-tagged microbial fluorescence and the plasmon absorption of Ag nanoparticles may slightly cause the quenching of the excited-state of GFP molecules on the Ag nanoparticles.

Microscopic Observation of Microbial/Nanoparticle Interaction

The microbial-nanoparticle interaction was visualized by environmental scanning electron microscopy, a specialized technique capable of imaging hydrous samples without the need of pretreatment for conductive coating (Priester et al., 2007; Redwood et al., 2005). Commercially available Ag NPs (Nanostructured & Amorphous Materials, Inc., advertised powder size of 10 nm) aggregated in water and the nitrifying microbial suspension. It appeared that the particles were embedded in microbial extracellular polymeric substances (Figure 13). The true size (from 200 nm to a few μm) of Ag NPs in water suspension was

significantly different from the claimed size of commercial nanopowders, consistent with the results reported by others (Adams et al., 2006).

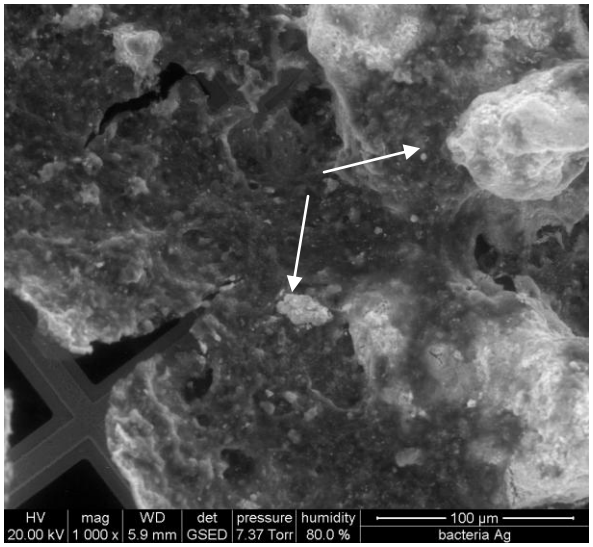

Figure 13. ESEM image of commercially available nanoparticles in the presence of nitrifying culture.

Silver nanoparticles adsorbed to the enriched nitrifying culture on a copper grid using ESEM. Arrows show aggregated Ag NPs that attached to microbial cells or embedded in microbial extracellular polymeric substances. Bar size: 100 μm.

Higher resolution electron micrographs were obtained using backscattered electron mode. After mixing a freshly prepared Ag NP suspension with the nitrifying cultures, it appeared that Ag NPs were adsorbed to the microbial surfaces, probably causing cell wall pitting (Figure 14). Additional work is underway to take higher resolution images in order to better understand the microbial-nanoparticle interactions.

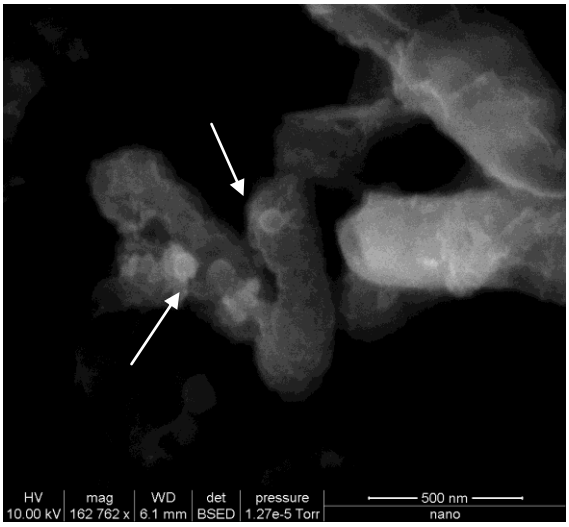

Figure 14. Silver nanoparticles attached to the cell membrane of nitrifying bacteria.

Silver nanoparticles adsorbed to the enriched nitrifying culture using a high-speed BSE detector. Arrows show spherical or hexagon types of Ag NPs that attached to the microbial cells, probably causing cell wall pitting. Bar size: 500 nm.

Cell Membrane Integrity Inferred from Live/Dead Assays

The fluorescence intensities of the stained microbial cells at 535 nm (green) and 642 nm (red) represent live and dead cells, respectively. The green/red fluorescence ratio, obtained by dividing the green and red intensities, was applied to compare the difference among various treatments by Ag species. At 1 mg/L Ag, the ratio obtained from the microbial suspensions treated with Ag NPs showed no significant difference compared to controls ($P > 0.05$), indicating that there is no evidence of cell membrane leakage caused by Ag NPs. Similar results were observed in samples treated with Ag^+ ions or AgCl colloids (Figure 15).

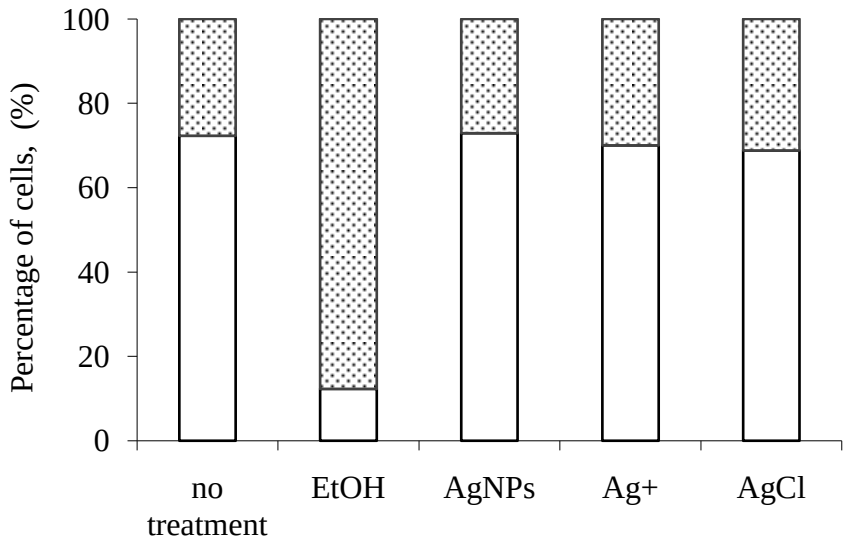

Figure 15. The percentage of cells with/without membrane damage after treatment with silver materials.

A positive control was treated with 70% ethanol. The blank bars indicate the percentage of live cells in the samples and the dotted bars show the percentage of membrane-damaged cells.

Inhibition Comparison and Mode of Antimicrobial Action

Among the Ag species tested, the freshly prepared Ag NPs presented the highest inhibition to autotrophic nitrifying microorganisms. In contrast, silver ion appeared to be the most toxic to heterotrophic growth. Different experimental assays chosen for the autotrophic nitrifying bacteria and heterotrophic *E. coli* cells made it difficult to compare the toxicity of Ag nanoparticles to the two bacterial species. The difference of toxicity may be attributed to different growth conditions and cell properties. Also we found in following works that silver nanoparticles aggregated in rich medium like nutrient broth and the toxicity of nanparticles may decrease due to its size-dependent toxicity.

The nitrifying bacteria were completely mixed in the respirometric bottles, aerated with pure oxygen and their activities were monitored by oxygen uptake rate measurements. Conversely, the *E. coli* cells were mixed intermittently in microwells, aerated with ambient air and their activities were inferred from fluorescence measured over a prolonged period of time (~1 d). Because they have a faster growth rate than nitrifying bacteria, *E. coli* cells may have stronger oxidizing/reducing power and interact with Ag species to form cell-particle aggregates (Kahraman et al., 2007; Sondi and Salopek-Sondi, 2004), as visible from Figure 13 and 14, or produce extracellular or intracellular Ag NPs (Efrima and Bronk, 1998), causing more complex growth problems. Nitrifying bacteria have remarkably complex internal membrane systems where ammonia monooxygenase (AMO, responsible for ammonia oxidation to produce hydroxylamine, NH_2OH) is located, whereas hydroxylamine oxidoreductase (HMO) is located in the periplasm (Madigan et al., 2000).

Therefore, we speculate that Ag NPs may have a direct impact on nitrifying cell membranes where key ammonia oxidation enzymes are located. The use of PVA during the synthesis of Ag NPs to control the nanoparticles size could affect the antibacterial activity by the coverage of PVA on Ag NPs to prevent the direct contact with bacteria. Due to the significant dilution (1:25 or higher) of the Ag NP suspension and solvent competition in cell cultures, the effect of PVA on nanosilver toxicity, however, would be minimal.

The mode of antimicrobial action by Ag NPs could be the inhibition of the microbial processes on the cell surface and in the cell. Previous research demonstrated that Ag NPs attach to the surface of cell membrane, causing the change of membrane permeability, dissipation of the ATP pool and proton motive force, and finally cell death (Lok et al., 2006; Morones et al., 2005; Sondi and Salopek-Sondi, 2004). The results from our bacterial viability tests indicated that there is no evidence of the cell membrane leakage caused by any Ag species at 1 mg/L Ag. The size of the Ag NPs used in this study was 14 ± 6 nm. These particles would be too large to diffuse into the cell, as only the smaller particles mainly in the range of 1–10 nm could enter the cell based on indirect microscopic evidences (Morones et al., 2005). Electrophoresis studies indicated no direct effect of Ag NPs on intracellular DNA or protein expression (Gogoi et al., 2006).

Bulk silver toxicity is generally governed by the total concentration of labile dissolved intracellular Ag species (Lee et al., 2005). In the cell, silver ions may deactivate cellular enzymes and DNA by reacting with electron-donating groups such as thiol (-SH) groups and generate reactive oxygen species (Matsumura et al., 2003; Sambhy et al., 2006).

Because of its cationic nature and its strong association with various ligands in natural waters, the toxicity of Ag^+ ions depends largely on the strength and amount of the ligands present (Ratte, 1999). The freshly prepared AgCl colloids can be viewed as one of the labile species with respect to their small size and low stability constant (log K_1= 3.3) in solution (Stumm and Morgan, 1996). Depending on their size and bioavailability, the inhibition caused by AgCl colloids can be as significant as that of Ag^+ ions.

Silver Nanoparticle Dissolution

The time-dependent increases of Ag^+ concentrations and associated color changes of the Ag NP suspension demonstrated the complexity of various processes such as oxidation, crystallization, dissolution and aggregation involved in microbial-nanoparticle interactions. Previous research showed that Ag NPs were susceptible to oxidation by oxygen, and the partially oxidized particles appeared more toxic than the freshly prepared nanoparticles (Lok et al., 2007). Others found, however, that the concentration of Ag^+ decreased by 80% after 24 hours, possibly due to Ag^o cluster formation (Morones et al., 2005). When the Ag NPs were added into a liquid medium, the antimicrobial effectiveness appeared to decrease when compared to that on the agar plates, presumably because of microbial-induced coagulation of nanoparticles (Sondi and Salopek-Sondi, 2004). Experiments involving synthetic zinc sulfide nanoparticles and representative amino acids also indicated a driving role of microbially derived extracellular proteins in rapid nanoparticle aggregation (Moreau et al., 2007).

Environmental Application and Implication

The numerous engineered nanomaterials with different sizes, shapes, compositions and coatings require high-throughput benchmarked protocols to screen for potential hazards in the environment (Maynard and Michelson, 2006). The developed extant respirometric assay and the automatic microtiter assay employed in this research are suitable for toxicity assessment of nanomanterials to microorganisms. The bacteria selected for each assay, however, are generally not exchangeable between the two assays. Because of the intrinsic slow growth of autotrophic nitrifying bacteria and their high oxygen uptake (4.3 mg O_2/mg of NH_4^+-N oxidized to nitrate) (Grady et al., 1999), the enriched nitrifying cultures are particularly useful in respirometric assays, but were not successful in the cell enumeration-based microtiter assay in this study. In contrast, *E. coli* cells were easily determined with the automatic microtiter assay because of their fast growth rate, but failed to produce meaningful oxygen profiles from the extant respiorometric assay because of the low biomass concentrations from overnight batch cultivation and their low oxygen uptake constants (~0.5 mg O_2/mg COD removed) (Grady et al., 1999).

The results of nanosilver toxicity to environmentally sensitive nitrifying microorganisms suggest that stringent regulations of Ag NPs entering wastewater treatment plants are necessary. Nitrifying microorganisms involved in nitrification are critical to biological nutrient removal in modern wastewater treatment. Research is underway to evaluate the fate and impact of Ag NPs in wastewater treatment systems.

3 Size and ROS-Dependent Nanosilver Toxicity to Nitrifying Bacteria[2]

3.1 Abstract

The intrinsic slow growth of nitrifying bacteria and their high sensitivity to environmental perturbations often result in bacterial growth inhibition by toxins. Emerging nanomaterials are of great concern to the environment. This work sought to provide insights in the mechanism of nitrification inhibition by Ag nanoparticles. Nanoparticles with an average size range of 9 to 21 nm were synthesized by varying the molar ratios of BH_4^- /Ag^+ in the solution. The resulting reactive oxygen species (ROS) generation was quantified in the presence and absence of the bacteria while the degree of nitrification inhibition was determined by extant respirometry. By examining the correlation between nanoparticle size distribution, photocatalytic ROS generation, intracellular ROS accumulation, and nitrification inhibition, we observed that inhibition by Ag nanoparticles correlated well with the intracellular ROS concentrations, but not the photocatalytic ROS fractions. Furthermore, the degree of inhibition correlated with the relative abundance of Ag nanoparticles smaller than 5 nm in the solution. It appeared that these size nanoparticles could be more toxic to bacteria than any other fractions of nanoparticles or their counterpart bulk species.

[2] *Environmental Science and Technology,* **2008**, *42*, 4583-4588.

3.2 Objectives

The objective of this chapter was to quantitatively determine the size and ROS dependent nanosilver toxicity to microorganisms. Ag nanoparticles of different sizes were synthesized to evaluate their size effect on microbial growth. We also measured the photocatalytic and intracellular ROS concentrations from silver exposure to determine their correlations with nanosilver toxicity. Nitrifying bacteria were chosen as model microbes because they are sensitive to a number of environmental conditions such as pH, dissolved oxygen concentration, and temperature, and are therefore susceptible to inhibition (Hu et al., 2003). A quantitative description of the nanoparticle sizes and ROS production that affect nanosilver toxicity will ultimately contribute to a mechanistic understanding of nanosilver toxicity for appropriate use and disposal of the nanotechnology-enhanced products in the environment.

3.3 Materials and Methods

General Experimental Design

Aliquots of nanosilver solutions of different sizes and concentrations were spiked in enriched nitrifying cultures for microbial growth inhibition tests. Aliquots of the same nanosilver samples were used for UV/Vis characterization and size distribution analysis by transmission electron microscopy. ROS formation following exposure to Ag nanoparticles was determined in the presence and absence of nitrifying cultures. For comparison purposes,

silver ions and AgCl colloids (average size = 0.25 μm) were used as reference materials. The results of nanoparticle sizes and ROS measurements were correlated with the degrees of inhibition by Ag nanoparticles, AgCl colloids, and Ag^+ ions.

Nitrifying Culture

Nitrification involving the oxidation of ammonium ions to nitrates by nitrifying bacteria is commonly observed in municipal wastewater treatment plants and ecosystems. Detailed information about the operation of the nitrifying reactor was presented in chapter 2. The cell suspensions were periodically withdrawn from the nitrifying reactor for ROS measurements and inhibition tests.

Silver Nanoparticles and Silver Bulk Species

Silver nanoparticles were made from 0.25 mM $AgNO_3$ (EM Science) by adding different concentrations (0.025, 0.05, 0.09, 0.15, 0.3 mM) of sodium borohydride ($NaBH_4$, Sigma) with polyvinyl alcohol (PVA) as a capping agent. Sodium borohydride was added into a 0.06% (wt) PVA solution, and silver nitrate was then rapidly injected at room temperature. The freshly prepared nanoparticle solutions were used for size characterization and growth inhibition studies.

Silver nitrate (Fisher Scientific) was used to provide free Ag^+ ions in the solution. Silver chloride colloids were prepared by vigorous mixing (700 rpm) 1 mL of a 14 mM silver nitrate standard solution and 1mL of a 28 mM sodium chloride solution with 18 mL of distilled water.

Nanoparticle Characterization

Aliquots of the prepared nanosilver solutions were periodically scanned from 250 to 700 nm to check the characteristic surface plasmon absorption band of Ag nanoparticles at approximately 400 nm using a UV-Vis spectrophotometer (Cary 50, Varian, CA). The concentrations of Ag nanoparticles in the solution were inferred from the difference between the measured concentrations of Ag^+ ions using a silver ion/sulfide selective electrode (Denver instrument, CO) and the total Ag^+ ions added initially. Transmission electron microscopy (TEM, JEOL 1400) was utilized to identify the nanoparticles and determine their size distribution. The nanosilver solution was added to a standard carbon-coated TEM grid and images of the samples were taken at an accelerating voltage of 100 keV. The histograms of nanosilver size distribution were generated from TEM images using ImageJ, a free, Java-based image processing package available at http://rsb.info.nih.gov/ij/.

Intracellular ROS Determination

Intracellular ROS concentrations were determined using an established fluorescence assay with modification (Limbach et al., 2007). Aliquots of nitrifying cultures were removed from the bioreactor and centrifuged at × 10,000 rpm for 15 min. The pellet was then resuspended in a loading buffer solution containing 10 μM H_2DCFDA (dichlorodihydrofluorescein diacetate, Invitrogen, OR, USA), 20 mM MOPS, 1 mM NH_4NO_3, trace metals, and 4 mg/L K_2HPO_4 to mimic normal growth and incubated at room temperature for 30 min. After the loading buffer solution containing H_2DCFDA was removed via centrifugation, the pellet cells were inoculated with prewarmed growth medium, amended with nanosilver (average size: 15 nm) or silver bulk species at predetermined concentrations, and plated into 96-well plates. The fluorescence of the cells from each well was measured using a microreader (VICTOR^3, PerkinElmer, CT, USA) with 485 nm excitation and 535 nm emission filter. Fluorescence data were taken automatically after 30 min incubation. Hydrogen peroxide (30%, Fisher Scientific) was used as a standard for ROS measurements (see Figure 16), and intracellular ROS concentrations due to silver exposure were determined in H_2O_2 unit.

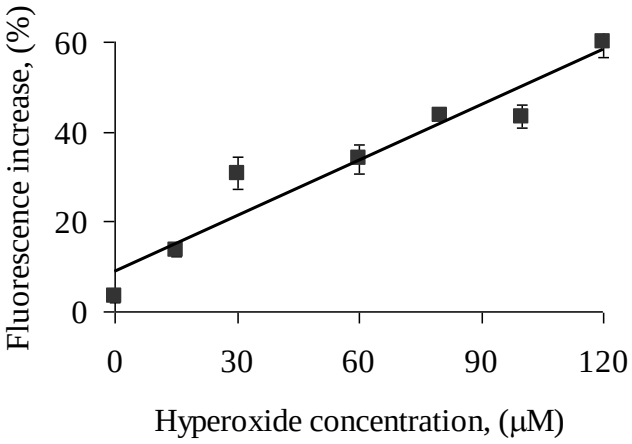

Figure 16. An intracellular ROS standard curve.

The percentage increase of fluorescence due to H_2DCFDA oxidation after 30 min exposure to hydrogen peroxide (H_2O_2) of various concentrations in the presence of nitrifying bacteria. The line of linear regression is also shown (R^2 = 0.92). Error bars indicate one standard deviation (n =8).

Photocatalytic ROS Determination

Photocatalytic ROS was measured using APF [3'-(p-aminophenyl) fluorescein], a new ROS indicator with greater specificity (mainly sensitive to OCl^- and OH^-) and higher resistance to light-induced oxidation than H_2DCFDA according to the vender's protocol (Invitrogen, OR, USA). The APF was added at a final concentration of 5 μM to a series of Ag nanoparticle (average size: 15 nm) or silver bulk solutions of various concentrations (C = 0.05 to 1 mg/L Ag) and plated into a 96-well plate. Initial fluorescence of the solution in each well was measured using the microreader with 485 nm excitation and 535 nm emission filter described above. The 96-well microplate was placed on the lab bench under

the room light for 30 min and the fluorescence was measured again. The percentage of fluorescence increase was calculated by comparing the fluorescence before and after light illumination as described previously (Wang and Joseph, 1999). Hypochlorite (6% $NaOCl^-$, Fisher Scientific) was used as a ROS standard for photocatalytic ROS measurements (Figure 17).

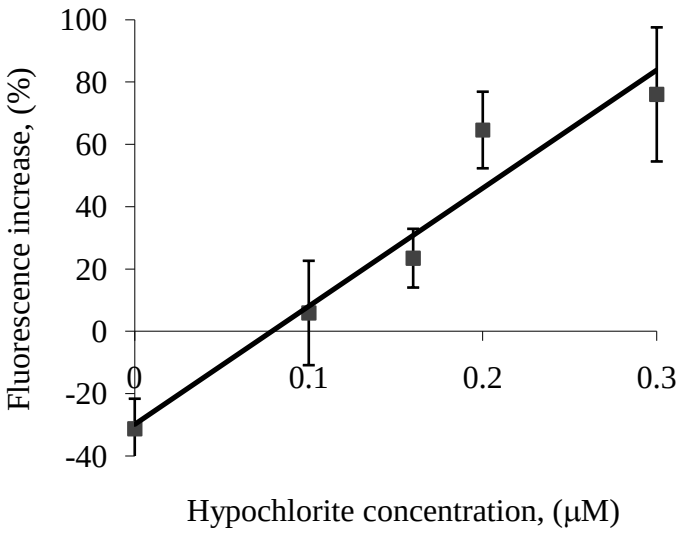

Figure 17. A photocatalytic ROS standard curve.

The percentage increase of fluorescence after 30 min exposure to hypochlorite (OCl^- as NaOCl) in DI water. The line of linear regression is also shown (R^2 = 0.94). Error bars indicate one standard deviation.

3.4 Results and Discussion

Size-Dependent Nanosilver Toxicity

Silver nanoparticles with an average size range of 9 to 21 nm were synthesized by varying the molar ratios (R) of BH_4^-/Ag^+ due to the changes of $NaBH_4$ concentrations (Table 5). The synthesized Ag nanoparticles had different average sizes (Figure 18a), size distributions (Figure 19), and UV-Visible spectra (Figure 18a). As the concentrations of $NaBH_4$ increased, the fraction of Ag nanoparticles of sizes less than 5 nm was reduced, reaching a minimum at R = 0.6 and became increased as more $NaBH_4$ was added (Figure 18A). At R = 0.1, the relative abundance of the nanoparticles less than 5 nm was the highest among the prepared nanosilver solutions while the concentration of Ag nanoparticles was low due to incomplete reaction. Because of excess of Ag^+ ions in the solution, red shifts in the maximum plasmon peak occurred (Henglein, 1998) when R was less than 0.2. Most added Ag^+ ions were reduced to Ag nanoparticles at R equal to 0.36 or above, possibly because PVA functioned both as a reducing agent and a capping agent (Porel et al., 2005).

Table 5. The properties of silver nanoparticles made by varying sodium borohydride concentrations and their corresponding toxicity to nitrifying bacteria

$NaBH_4$ (mM)	0.025	0.05	0.09	0.15	0.3
Molar ratio of BH_4^-/Ag^+ ($AgNO_3$, 0.25 mM)	0.1	0.2	0.36	0.6	1.2
Average particle size, (nm)	9 ± 5	15 ± 9	14 ± 6	12 ± 4	21 ± 14
Ag nanoparticle concentration (mg/L)	3 (± 2.4)	14 (± 0.6)	25 (± 2.3)	26 (± 0.3)	24 (± 2.1)
Surface plasmon peak (nm)	400	400	395	395	395
Degree of inhibition at 0.5 mg/L Ag	53 % (± 4.2)	63 % (± 8.6)	6 % (± 9.8)	17 % (± 5.2)	23 % (± 4.0)

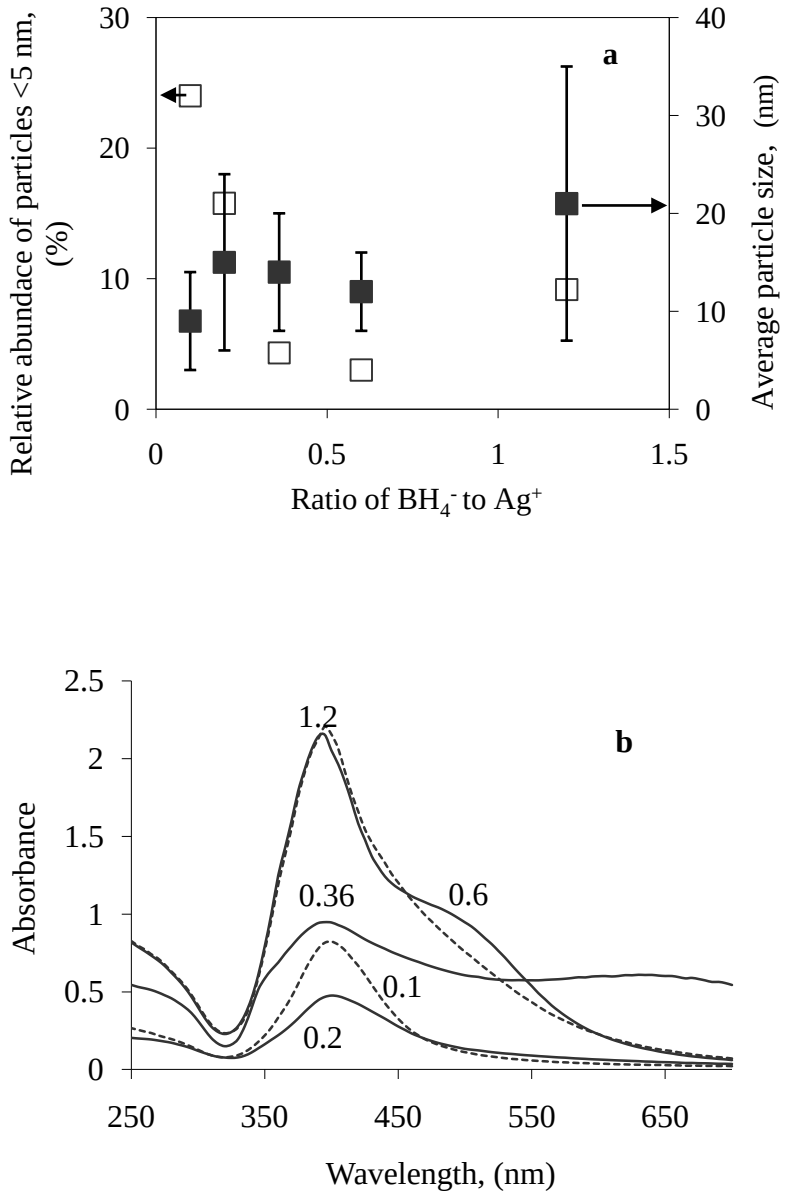

Figure 18. An average size and UV-visible spectra of nanopartiels made with various ratios of BH_4^-/Ag^+

(a) The change of average size (right arrow) and relative abundance of Ag nanoparticles (left arrow) by varying molar ratio of sodium borohydride to silver nitrate. (b) UV-visible spectra of silver nanoparticles solutions by varying molar ratios (see values on the figure) of sodium borohydride to silver nitrate.

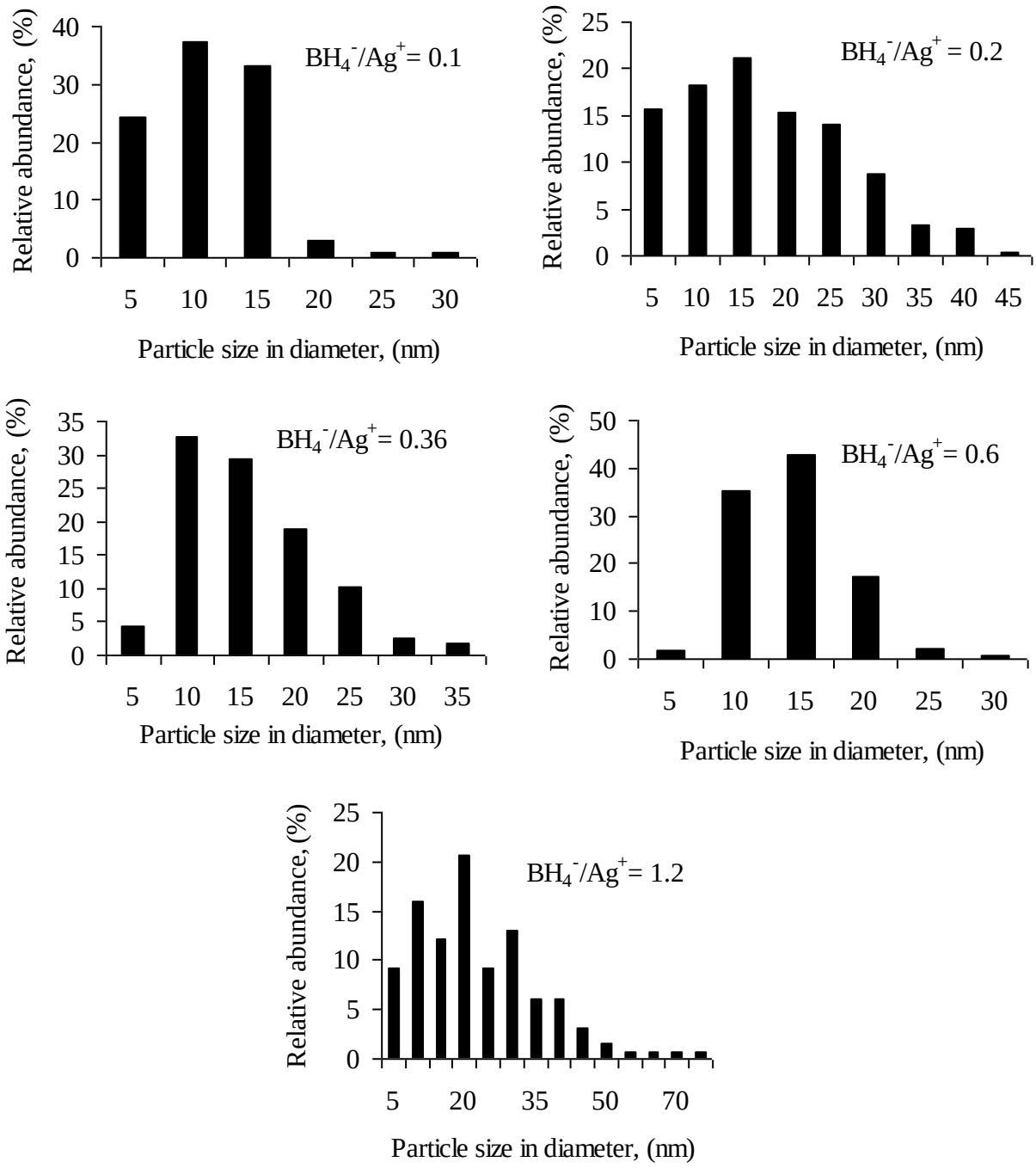

Figure 19. Size distribution of Ag nanoparticles made by varying molar ratio of sodium borohydride to silver nitrate.

A plot of the degree of nitrification inhibition as a function of the fraction of nanoparticles of defined sizes in the solution showed that the degree of inhibition correlated with the relative abundance of Ag nanoparticles smaller than 5 nm ($R^2 = 0.74$) (Figure 20). There was no correlation between the inhibition and the average nanoparticle size (Figure 21). Furthermore, there was poor relationship between the degrees of inhibition and the Ag^+ ion concentrations in the solution (Figure 22). Previously we demonstrated that Ag nanoparticles were more toxic to nitrifying bacteria than Ag^+ ions at constant concentrations (Chapter 2). Hence, the high degree of inhibition at low BH_4^-/Ag^+ ratios cannot be attributed to the presence of Ag^+ ions only. We suggested that the Ag nanoparticles of sizes less than 5 nm were responsible for inhibiting microbial growth and could be more toxic to bacteria than their counterpart species.

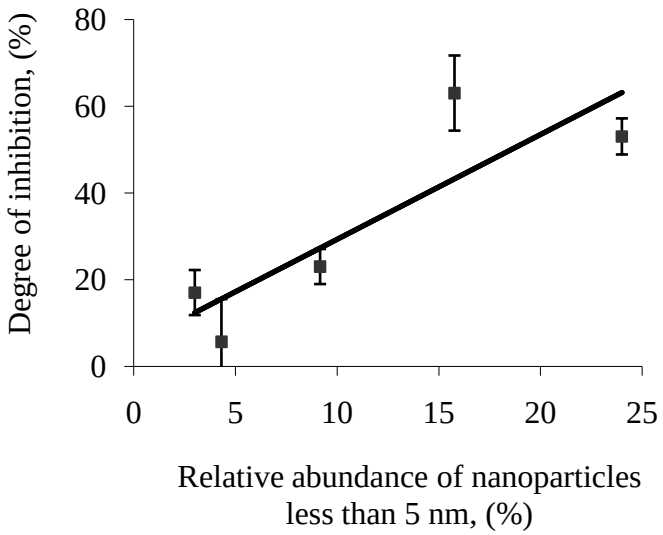

Figure 20. Relationship between the degree of inhibition and the percentage of Ag nanoparticles with sizes less than 5 nm.

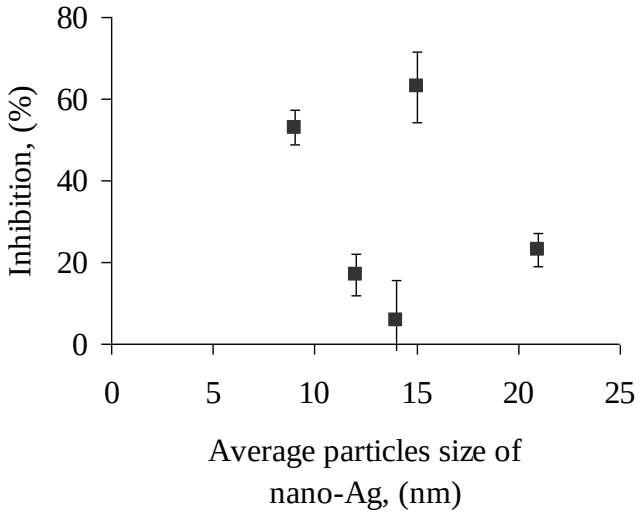

Figure 21. The degree of inhibition as function of average silver nanoparticles size.

Error bars indicate one standard deviation.

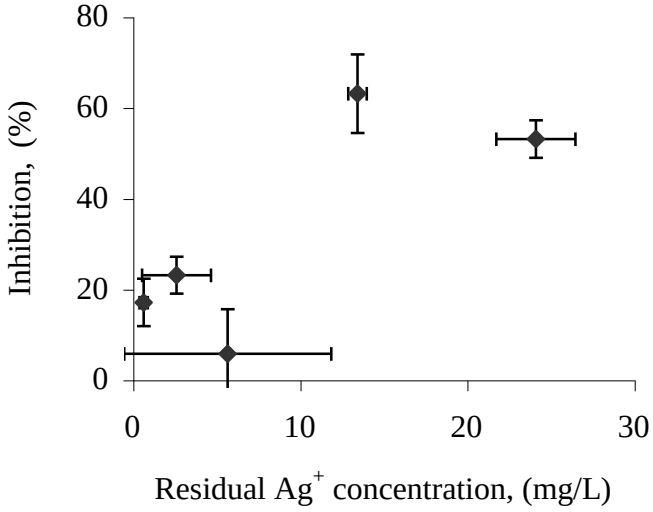

Figure 22. The relationship between inhibition and residual Ag^+ concentration present in the parent nanosilver suspensions.

Note that approximately 30-fold or more dilution was made to determine the inhibition in the biomass suspensions. Error bars indicate one standard deviation.

Toxicity Related to Intracellular ROS Concentration

Exposure of Ag nanoparticles of 15 nm average size at incremental concentrations onto preincubated nitrifying cultures resulted in an overall increase in intracellular ROS concentrations (Figure 23a). It appeared that at the same silver concentrations, AgCl colloids generated at least an equivalent amount of ROS compared to that by Ag nanoparticles. In contrast, Ag^+ ions generated less intracellular ROS than that by Ag nanoparticles (Figure 16a). The degree of inhibition by Ag nanoparticles was strongly correlated with intracellular ROS concentration ($R^2 = 0.86$) using a saturation type model (Figure 24). Similarly, the degrees of inhibition were correlated with intracellular ROS levels induced by Ag^+ ions or AgCl colloids ($R^2 = 0.70$-0.89). Taken all silver species together, however, there was a poor correlation between the degrees of nitrification inhibition and intracellular ROS concentrations ($R^2 = 0.54$) by a saturation-type model. It appeared that although there was correlation between the degrees of nitrification inhibition and the intracellular ROS concentrations induced by Ag nanoparticles or bulk species, the pattern of correlation was species specific.

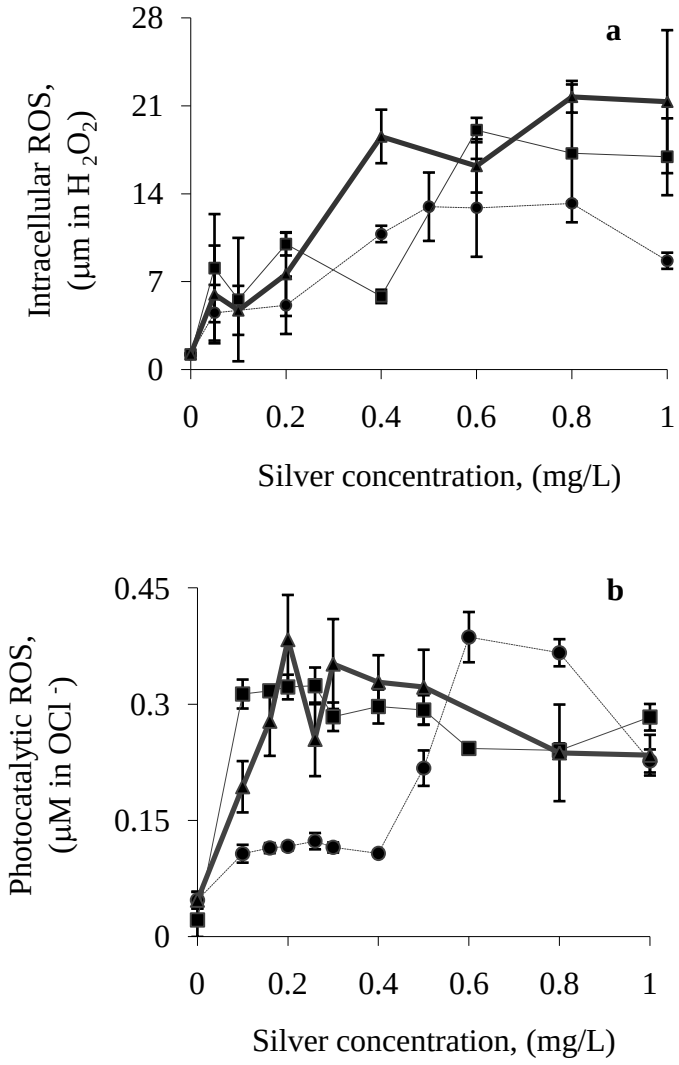

Figure 23. Increase of ROS concentrations caused by silver exposure.

The increase of intracellular ROS (a) and photocatalytic ROS concentrations (b) as function of the concentration of Ag nanoparticle (■), AgCl colloid (▲), and Ag^{+}(●).

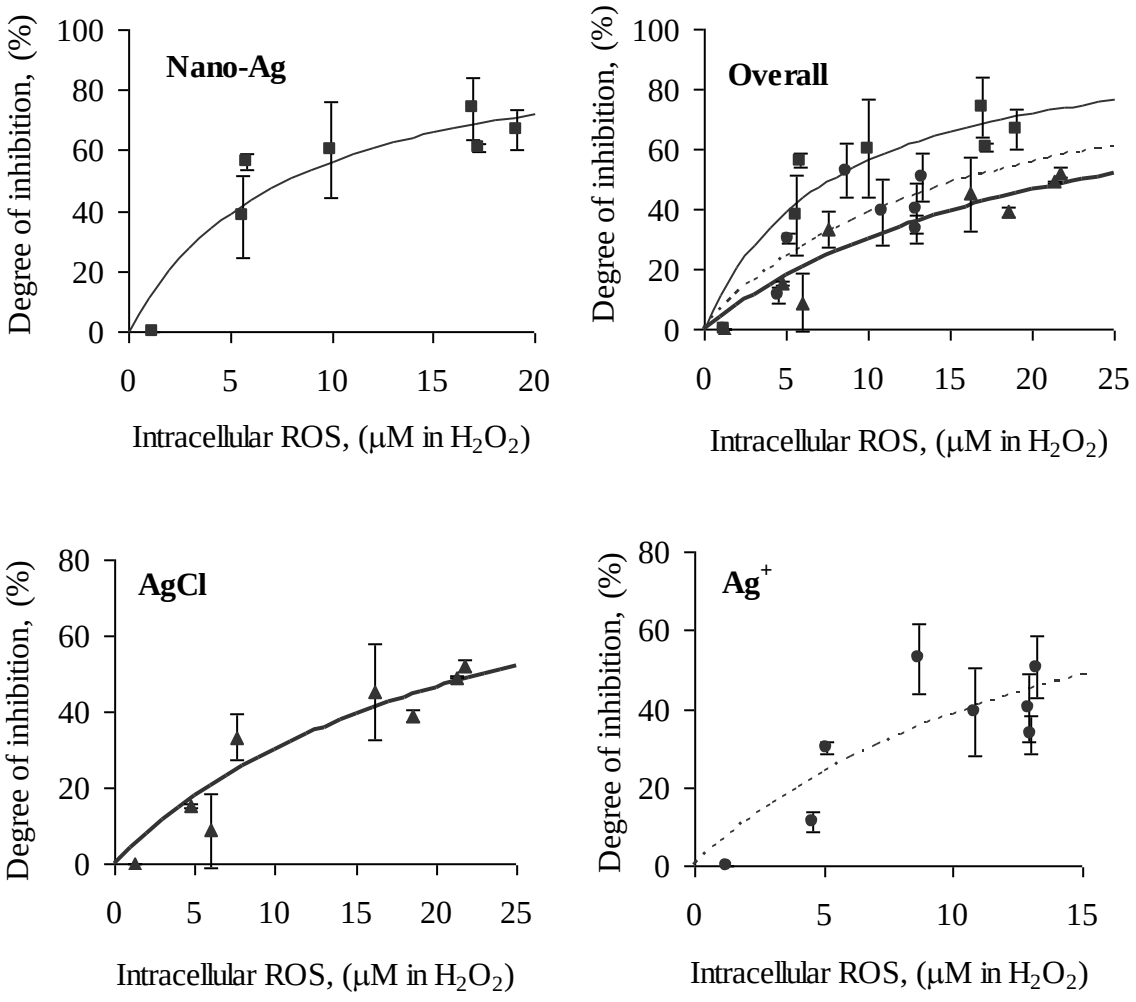

Figure 24. Silver toxicity as a function of intracellular ROS concentration.

The degree of nitrification inhibition as function of the intracellular ROS (in hydrogen peroxide unit) concentration after 30 min exposure of nitrifying bacteria to Ag nanoparticle (■), AgCl colloid (▲), and Ag^{+}(●). The best-fit lines are also shown using a saturation-type model.

Toxicity Related to Photocatalytic ROS Concentration

ROS generation in cells may proceed through *exogenous* (extracellular) and *endogenous* (intracellular) processes. We therefore measured the ROS concentrations induced by Ag nanoparticles, AgCl colloids, and Ag^+ ions in the absence of nitrifying cultures. Since without light there was no ROS generation in Ag nanoparticle solution or bulk solutions (data not shown), the concentrations of photocatalytic ROS was measured after 30 min natural light illumination in the lab. It appeared that photocatalytic ROS increased rapidly in the presence of 0.1 mg/L Ag but gradually decreased as the Ag nanoparticle concentrations increased (Figure 23b). A similar trend applied for AgCl colloids. The pattern of photocatalytic ROS generation by Ag^+ ions, however, appeared differently. ROS only increased significantly when silver concentrations were above 0.4 mg/L. Poor correlation (R^2 = 0.53-0.72) was noticed between the observed inhibition and the photocatalytic ROS concentrations by a saturation-type model (Figure 25). Therefore, photocatalytic ROS concentrations were not good predictors of the growth inhibition by Ag nanoparticles.

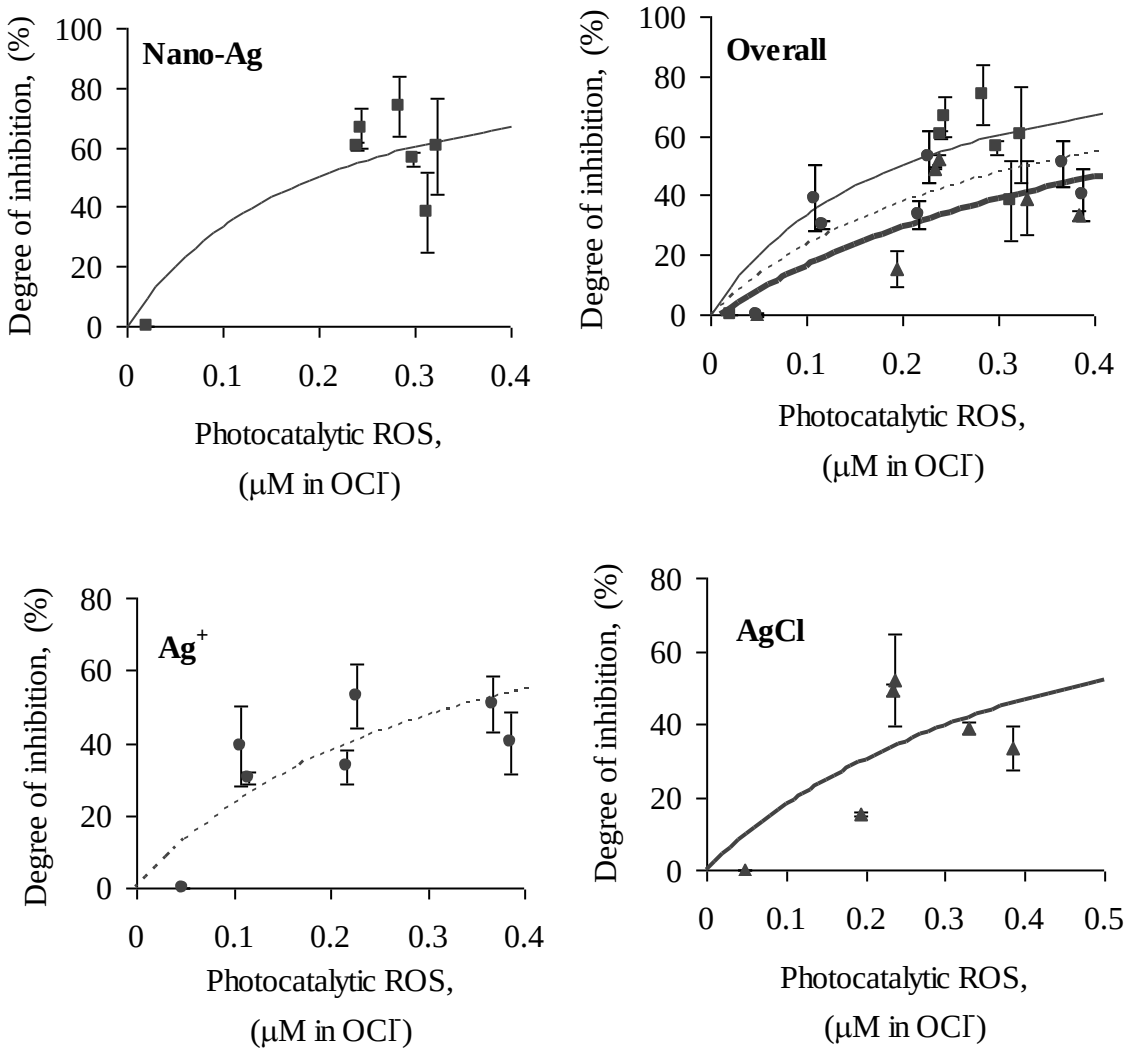

Figure 25. Silver toxicity as a function of photocatalytic ROS concentration.

The degree of nitrification inhibition as function of the photocatalytic ROS (in hypochlorite unit) concentration after 30 min exposure of Ag nanoparticle (■), Ag^+ (●), and AgCl colloid (▲) to nature light. Error bars indicate one standard deviation (n=8).

Discussion

The results of ROS measurements showed that Ag nanoparticles, AgCl colloids, and Ag^+ ions all induced intracellular ROS generation and accumulation, and the degrees of inhibition correlated well with their individual intracellular ROS concentrations. Previous studies in a variety of cell types suggested that ROS generation might damage cell DNA and induce apoptosis (programmed cell death) with no visible membrane damage (Farber, 1994; Inoue et al., 2002; Polyak et al., 1997). Our results from bacterial live/dead assays indicated that no cell membrane integrity was compromised at 1 mg Ag/L for all of the silver species tested. This suggested that the toxicity of Ag nanoparticles could be partially related to intracellular ROS mediated cell death process. At the same level of intracellular ROS, however, silver nanoparticles appeared to be more toxic than Ag^+ ions (Figure 24), suggesting their modes of antimicrobial action might be different as described earlier.

The results also demonstrated that there was poor correlation between the observed inhibition and photocatalytic ROS concentrations induced by Ag nanoparticles or Ag bulk species. According to some, photocatalytic ROS generated by light can induce intracellular ROS in the cell: the photocatalytic ROS generation by TiO_2 nanoparticles under sunlight illumination was positively correlated with antibacterial activity (Cho et al., 2004; Wei et al., 1994). Nanoparticles such as TiO_2, SiO_2, and ZnO are photo-sensitive to promote ROS generation (Adams et al., 2006). Because of their transition metal characteristics, they can be catalytically so active (Limbach et al., 2007) that under dark condition microbial inhibition was observed (Adams et al., 2006). Our study, however, showed that Ag nanoparticles did not generate ROS in the absence of light.

Silver nanoparticles produced photocatalytic ROS under natural light, but the photocatalytic ROS generation had no relationship (or more precisely negative correlation) with the intracellular ROS concentrations. Therefore, there was no direct correlation of photocatalytic ROS with nitrification inhibition.

Both Ag nanoparticles and AgCl colloids generated almost the same amount of photocatalytic and intracelluar ROS at the same silver concentrations (Figure 23). However, inhibition results showed that Ag nanoparticles were more toxic than AgCl colloids (Figure 11). Sizes of the particles therefore may play an important role in silver toxicity. Smaller size nanoparticles with higher surface areas could interference cell membrane function by directly reacting with cell membrane to allow a large portion of silver atoms to attack or enter into the cells (Elechiguerra et al., 2005; Nel et al., 2006). Our results demonstrated that the degree of inhibition correlated well with the relative abundance of Ag nanoparticles smaller than 5 nm, but not with the other particle size fractions (e.g., 10, 15, 20 nm, R^2 = 0.04 –0.39), suggesting that these smaller size nanoparticles could be more toxic to bacteria than any other fractions of the nanoparticles. This result is consistent with recent findings that Ag nanoparticles of 1-10 nm sizes interacted strongly with HIV-1 after attached to the virus (Elechiguerra et al., 2005; Nel et al., 2006), and the average size of Ag nanoparticles penetrating into an *E. coli* membrane was 5(± 2) nm even though the average particles size of added nanoparticles was 21(± 18) nm (Elechiguerra et al., 2005). Particles must be sufficiently small to pass through transmembrane porins (typical internal pore size in nm) for transport across cell membranes (Madigan et al., 2005) to damage cellular constituents and metabolism.

Hence, the results confirmed that the antimicrobial effect of nanosilver is size dependent.

4 Role of Sulfide and Ligand Strength in Controlling Nanosilver Toxicity[3]

4.1 Abstract

Nanosilver has been used broadly in nanotechnology enhanced consumer products because of its strong antimicrobial properties. Silver nanoparticles (AgNPs) released from these products will likely enter wastewater collection and treatment systems. This research evaluated the role of sulfide and ligand strength in controlling nanosilver toxicity to nitrifying bacteria that are important in wastewater treatment. The nanosilver toxicity in the absence and presence of ligands (SO_4^{2-}, S^{2-}, Cl^-, PO_4^{3-}, and $EDTA^-$) commonly present in wastewater was determined from the oxygen uptake rate measurements. Sulfide appeared to be the only ligand to effectively reduce nanosilver toxicity. By adding a small aliquot of sulfide that was stoichiometrically complexed with AgNPs, the nanosilver toxicity to nitrifying organisms was reduced by 80%. Scanning electron microscopy coupled with energy dispersive X-ray analysis indicated that AgNPs were highly reactive with sulfide to form new Ag_xS_y complexes or precipitates. These complexes were not oxidized after a prolonged period of aeration (18 hrs). This information is useful for wastewater treatment design and operation to reduce nanosilver toxicity via sulfide complexation. While the biotic ligand model was successful in predicting the toxicity of Ag^+ ions, it could not accurately predict the toxicity of AgNPs. Nevertheless, it could be one of the many tools useful in predicting and controlling nanosilver toxicity to wastewater microorganisms.

[3] *Water Research.* **2009**, *43*, 1879-1886.

4.2 Objectives

Figure 26 presents a scheme of proposed fate of silver nanoparticles in wastewater and wastewater treatment plants (WWTPs). Silver nanoparticles may continuously change their forms/sizes in the sewer pipe and the WWTPs through oxidative, dissolution and chemical complexation. Sulfide concentrations as high as 6 mg/L in free ion form may be present in the sewer pipe (Nielsen et al., 2008). Nanosilver and its dissolved ions may complex with sulfide in the pipe to reduce its toxicity. The main objective of this research work is to study the impact of ligands and ligand strength on nanosilver toxicity to nitrifying bacteria, which are critical to nutrient removal from wastewater.

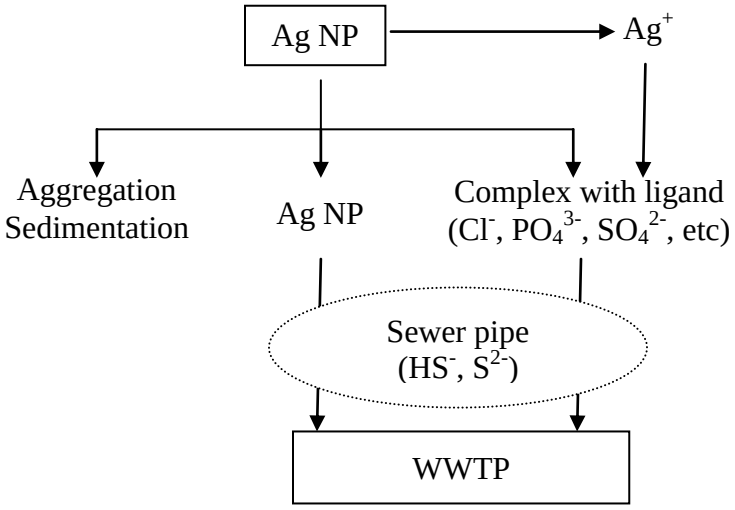

Figure 26. An environmental fate model of silver nanoparticles in wastewater treatment.

Nanoparticles tend to aggregate and settle before entering WWTP. When nanosilver enters a wastewater treatment system, it may be oxidized to silver ion (Ag^+) that may further complex with various ligands (anions) presented in wastewater.

The two-step nitrification process consists of ammonia oxidation to nitrite ($NH_4^+ \rightarrow NH_2OH \rightarrow NO_2^-$) by ammonia oxidizing bacteria (AOB) and nitrite oxidation to nitrate ($NO_2^- \rightarrow NO_3^-$) by nitrite oxidizing bacteria (NOB). AOB are especially sensitive to toxicants (Radniecki et al., 2008; Radniecki and Ely, 2008) and may therefore serve as a good indicator of toxicity or normal operation in wastewater treatment. The stability of silver sulfide complexes made from Ag NPs was evaluated by extant respirometry, and detailed compositions of the complexes were determined by Scanning Electron Microscopy/Energy Dispersive Spectroscopy (SEM-EDS). These new findings may help better understand the nano-bio interactions between bacteria and Ag NPs, and provide new information on how to control and/or eliminate nanosilver toxicity in wastewater treatment plants.

4.3 Materials and methods

Inhibition of Enzymatic Activity Involved in Nitrification by Silver Nanoparticles

There are at least three critical enzymes involved in nitrification processes: ammonia monooxygenase (AMO), hydroxylamine oxidoreductase (HAO), and nitrite oxidoreductase (NOR). To differentiate the degree of inhibition on these enzymes, aliquots of ammonium (NH_4NO_3), hydroxylamine ($NH_2OH \cdot H_2SO_4$), and nitrite ($NaNO_2$), each at a final concentration of 10 mg/L N (0.7 mM), were added to the individual respirometric bottles at around 300 s after initiation of data acquisition. Due to nitrification a decrease in the dissolved oxygen (DO) level in the closed respirometric vessel was measured by a DO probe (stability: ±1% of full scale, YSI model 5300A,

Yellow Springs, OH) and continuously monitored at 4 Hz by an interfaced personal computer. The oxygen uptake rate was calculated based on a linear aggression analysis because a zero-order reaction was observed for a long time at 10 mg/L N in the closed respirometric bottles. The inhibition was calculated by relative oxygen uptake rate (OUR) as described in equation (1) explicitly for AMO, HAO and NOR involved in reduced nitrogen oxidation. Every batch of respirometric test was accompanied by a positive control (e.g., untreated nitrifying biomass only) and experiments were performed in duplicate.

Effect of Ligands on Nanosilver Toxicity

The experiments of ligand impact on silver toxicity were performed in two different methods, i.e., via a one-time addition of the freshly prepared Ag-ligand complexes and via sequential addition of a specific ligand followed by Ag NPs to the enriched nitrifying culture. Since no difference on nanosilver toxicity measurements was found between the two methods, the result of the later method was reported. Briefly, each ligand (anion) such as Cl^-, SO_4^{2-}, PO_4^{3-}, $EDTA^{4-}$, and S^{2-} in sodium form was added at a final concentration of 10 μM to the 60 mL nitrifying culture followed by the addition of 9 μM Ag NPs in final concentration to ensure complete complexation. After the nitrifying culture amended with Ag NPs and/or ligands were transferred to the respirometric vessels, the extant respirometric assay was performed as described above to determine the nanotoxicity in the presence and absence of ligands. For major ligands, such as Cl^- and PO_4^{3-}, present in wastewater (Burks and Minnis, 1994), the nanosilver toxicity was

determined at several predetermined concentrations (0-100 mg/L or 2.8 mM Cl; 0-10 mg/L or 0.3 mM P) to reflect their concentrations in typical wastewater.

Effect of Sulfide on Nanosilver Toxicity and Nitrification Inhibition

To determine the effect of sulfide on silver toxicity, the toxicity of Ag NPs and Ag^{+} ions (9 μM Ag) was measured at predetermined sulfide concentrations (0, 0.15, 0.25, 0.5, 1, 1.5, 2 mg/L or 0-62 μM) using extant respirometry. Since sulfide (true species including H_2S/HS^- at neutral pH) oxidation ($S^{2-} \rightarrow SO_4^{2-}$) consumes oxygen, ammonium (10 mg/L N) was injected after the completion of sulfide oxidation as evidence of very slow oxygen decrease due to endogenous respiration. To delineate the inhibition by sulfide itself (Joye and Hollibaugh, 1995), a broader range of sulfide concentrations (0-15 mg/L or 0-0.5 mM) was evaluated.

Stability of Silver Sulfide Complexes under Prolonged Aeration

Sulfide is a prevalent anion under anaerobic conditions, but it can be oxidized to sulfate under aerobic conditions (Janssen et al., 1998). This raises a question, "Will Ag_xS_y (e.g., AgS^-, AgHS, $AgHS_2^{2-}$, $AgH_2S_2^-$, Ag_2S) made from Ag NPs and sulfide be oxidized in aerobic wastewater treatment?" To evaluate the stability of the Ag_xS_y complexes under aerobic conditions, an aliquot of freshly prepared Ag_xS_y or, for comparison, Na_2S was added to nitrifying cultures in respirometric bottles at a final concentration of 0.6 mM sulfide. Silver sulfide was made from Ag NPs of average size of 15 nm by adding a

stoichiometric amount of sulfide. The DO concentrations in respirometric vessels were automatically recorded as described earlier for 8 or 18 hours.

Silver/Nanosilver Toxicity Predicted from Biotic Ligand Model

MINEQL+4.6 software (Schecher and McAvoy, 2001), a chemical equilibrium modeling system, was employed to calculate concentrations of silver species at pH 7.5. Before simulation, the cell concentrations in chemical oxygen demand (1.42 g COD/g VSS) were converted into mole units ($C_5H_7O_2N$, 113 g/mol). The Ag-cell binding constant was obtained from the best fit to the experimental data of nanosilver toxicity in the presence of sulfide. It was assumed that S represents about 1% of cell dry weight (Tchobanoglous et al., 2003) and the ratio of concentration of Ag^+ ions to sulfide functional groups of the cell is 1:1 to form {Ag-SH}, which is positively correlated with inhibition.

SEM-EDS

To locate Ag NPs attached to nitrifying cells and determine the possible formation of Ag_xS_y complexes in the presence of sulfide, the nitrifying culture amended with 1 mg/L (9 μM) Ag NPs in the absence and presence of sulfide (10 μM). Treated bacterial samples were dropped onto a specimen stub, air-dried and coated with carbon. Images of the samples were taken at an accelerating voltage of between 7 and 10 kV under a high vacuum mode. To locate Ag NPs or Ag_xS_y complexes, a back-scattered electron (BSE) detector coupled with a secondary electron (SE) detector were applied. Energy dispersive X-ray spectroscopy (EDS), an integrated feature of SEM, was performed to identify the

elemental composition of the specimen. The NORAN System Six (Thermo Scientific, Waltham, MA) was used for X-ray microanalysis of the collected EDS data.

4.4 Results

Nanosilver toxicity to enzymes involved in nitrification

Three critical enzymes (AMO, HAO, NOR) involved in nitrification showed different responses to Ag NPs and Ag^+ ions (Figure 27). Ammonia monooxygenase was most sensitive to silver regardless of Ag NPs or Ag^+ ions (AMO>NOR>HAO). For that reason, we used ammonium as a substrate in the rest of inhibitory tests. 'Inhibition' is derived from the change of AMO-related oxygen uptake rates before and after exposure to toxicants.

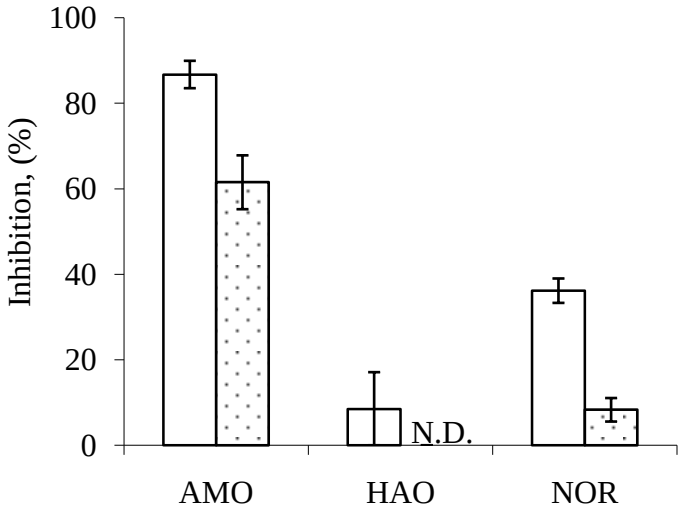

Figure 27. The toxicity of Ag NPs to enzymes related to nitrification.

Sensitivity of enzymes exposed to 1 mg/L (9 μM) Ag in the form of Ag NPs (open column) and Ag^+ ions (dotted column) at a nitrifying biomass concentration of 540 mg/L (3.3 mM) COD. Error bars indicate data ranges of duplicate or triplicate samples. These enzymes include ammonia monooxygenase (AMO), hydroxylamine oxidoreductase (HAO) involved in ammonia oxidation and nitrite oxidoreductase (NOR) involved in nitrite oxidation. (N.D = not detected. HAO was not inhibited by Ag^+ ions at 1 mg/L).

Effect of Ligands on Nanosilver Toxicity

In this study, at 1 mg/L (9 μM) Ag, nanosilver inhibited nitrification by 100 % while silver ions decreased microbial activity by 83(±1) % at a nitrifying biomass concentration of 1.3 mM or 210 mg/L COD (Figure 28). The results are consistent with our previous findings that Ag NPs can be more toxic than the bulk forms of silver.

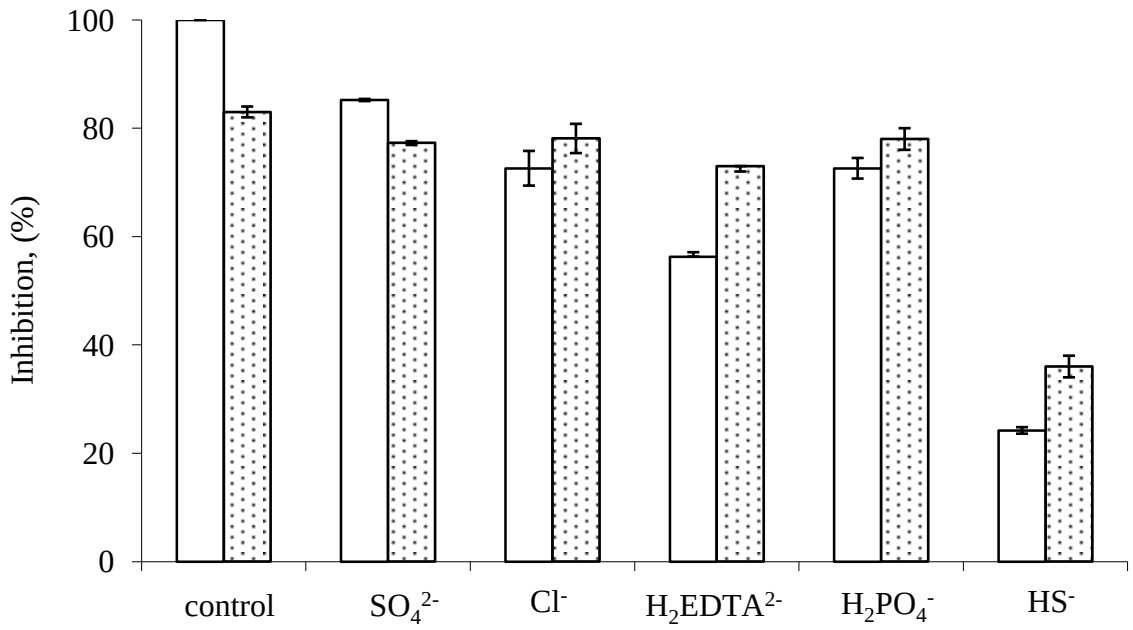

Figure 28. The reduced toxicity of silver nanoparticles in the presence of various ligands.

The effect of various ligands on reducing inhibition caused by Ag NPs (open column) and Ag^+ ions (dotted column) at 1 mg/L (9 μM) Ag at a nitrifying biomass concentration

of 210 mg/L (1.3 mM) COD. Error bars indicate data ranges of duplicate or triplicate samples. Each ligand was added at a final concentration of 10 μM.

With the addition of ligands at a final concentration of 10 μM, the toxicity decreased regardless of the forms of silver (Ag NPs or Ag^+ ions). Sulfide was the only ligand to effectively reduce nanosilver toxicity (by approximately 80%), knowing that sulfide has the highest stability constant (Table 6) to form Ag-ligand complexes. Except for the weak ligand like SO_4^{2-}, it appeared that ligands such as Cl^-, PO_4^{3-}, EDTA, and S^{2-} reduced silver toxicity more effectively in the nitrifying cultures exposed to Ag NPs than if the cultures were exposed to Ag^+ ions (ANOVA, P = 0.006 at 95 % confidence level) (Figure 28).

Table 6. Comparison of silver toxicity between the experimental results and the predicted values using the BLM model.

Silver-ligand complex	Stability constant, log K*	Experimental data of toxicity, (%)	Toxicity estimated by the BLM model (%)
Ag_2SO_4	4.8	76.9 ~ 77.6	83
AgCl (s)	9.8	75.4 ~ 80.8	83
Ag{EDTA}	8.1	72 ~ 73	83
Ag_3PO_4	17.6	76 ~ 80	83
Ag_2S	50.1	34 ~ 38	35

*(Schecher and McAvoy, 2001; Stumm and Morgan, 1996)

The biotic ligand model (BLM) was applied to estimate the binding constant for Ag-SH complexes between Ag^+ and cellular S-containing functional groups (e.g, -SH), {Ag-SH}, by best fitting to experimental toxicity data in the presence of sulfide. The binding constant (log K) for {Ag-SH} was estimated to be 26.5 using MINEQL+4.6 and the following simulation information: 9 μM total silver, 10 μM total sulfide, 1.3 mM total cell, and pH 7.5. Similar Ag-BLM based studies have been reported using fish (Bertram and Playle, 2005; Janes and Playle, 1995; Zhou et al., 2005) and daphnids (Bianchini et al., 2005; Bury et al., 2002). Currently we are not aware of any bacteria-based Ag-BLM. The predicted toxicity values by Ag^+ ions were close to the observed ones in the presence of SO_4^{2-}, Cl^-, PO_4^{3-}, and EDTA (Table 6).

To evaluate the effect of ligand concentrations on nanosilver toxicity, chloride and phosphate concentrations were changed from 0 to 100 mg/L (2.8 mM) Cl^- and from 0 to 10 mg/L (0.3 mM) P, respectively, to reflect their concentrations in real wastewater. These phosphate concentrations appeared to have little impact on silver toxicity (Figure 29a). However, increasing Cl^- concentrations slightly reduce nanosilver toxicity (up to 20%) and decrease the toxicity caused by Ag^+ ions by up to 63% (Figure 29b).

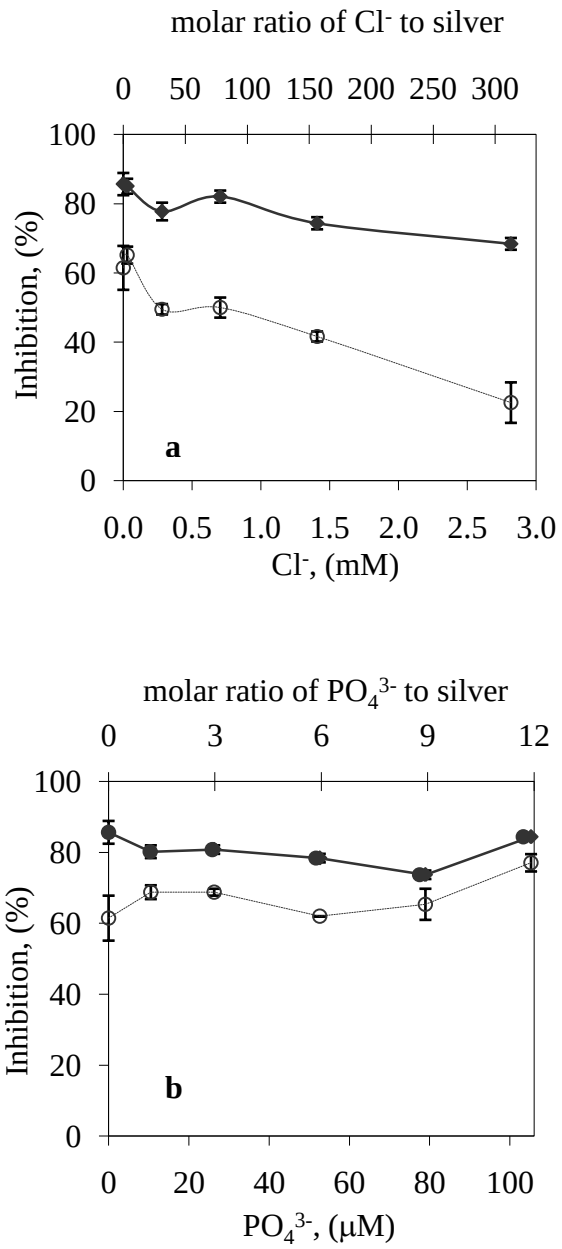

Figure 29. Effect of chloride and phosphate concentrations on nanosilver toxicity.

Effect of chloride (a) and phosphate (b) concentrations on inhibition caused by Ag NPs (filled circles) or Ag^{+} ions (open circles) at 1 mg/L Ag and a nitrifying biomass concentration of 540 mg/L COD. Error bars indicate data ranges of duplicate or triplicate samples. Where no error bars are shown, these were within the dimensions of the symbols.

Role of sulfide in controlling nanosilver toxicity

Addition of a small aliquot of sulfide (at a final concentration of 0.15 mg/L (5 μM) S^{2-}) reduced nanosilver toxicity dramatically (Figure 30). Nanosilver toxicity was reduced from 86 (± 3) % to 15 (± 4) % in the presence of 0.5 mg/L (15 μM) sulfide. Further increase of sulfide concentrations tended to increase the toxicity gradually (Figure 30). Such increases became remarkable at sulfide concentrations above 1 mg/L and were attributed to free available sulfide (H_2S/HS^-) to inhibit bacterial activities (Figure 30). The effective concentrations of sulfide causing 50% inhibition (EC_{50}) were estimated to be 2.0 mg/L (62 μM).

For comparison, the toxicity by silver ions was decreased from 62 (± 6) % to 15 (± 3) % in the presence of 0.5 mg/L sulfide. However, if more than 0.5 mg/L sulfide was added, the inhibition increased rapidly (Figure 30), indicating that there is a very narrow window to reduce toxicity caused by bulk silver species.

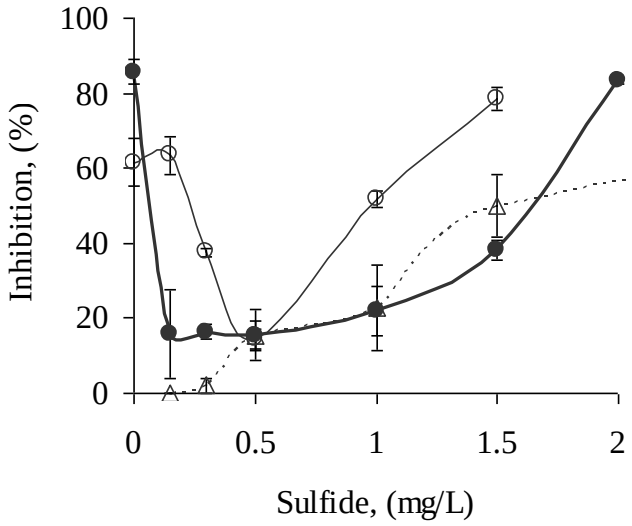

Figure 30. Effect of sulfide concentrations on nanosilver toxicity.

Effect of sulfide concentration on inhibition caused by Ag NPs (line with filled circles) or by Ag^{+} ions (line with open circles). Inhibition by sulfide itself was also shown (dotted line with open triangular). Error bars indicate data ranges of duplicate or triplicate samples.

Stability of silver sulfide complexes

There was little decrease of oxygen at the beginning of respirometric measurements due to lack of substrate (ammonium) oxidation and low endogenous respiration (Figure 31). After injection of sodium sulfide in the respriometric vessel, oxygen concentrations decreased immediately due to sulfide oxidation followed by prolonged slow decrease. When the freshly prepared Ag_xS_y complexes were injected in the respirometric vessel, however, very little decrease in oxygen concentrations, likely due to microbial endogenous respiration, were observed in 8 hours (Figure 31), indicating that silver sulfide was stable under aerobic conditions and would unlikely be oxidized in activated sludge wastewater treatment processes. An extended respirometric measurement to last more than 18 hours was conducted and similar results were observed (data not shown).

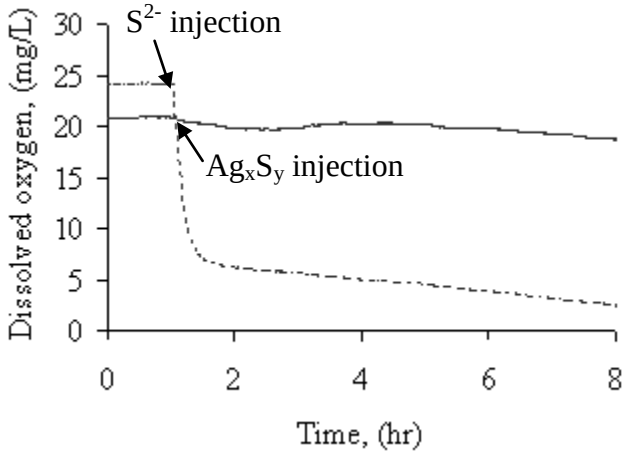

Figure 31**.** Stability of silver sulfide complexes inferred from respirometric measurements. Sodium sulfide and the freshly made silver sulfide complexes from Ag NPs were injected individually at a final concentration of 0.6 mM at approximately 1 hr after the initiation of data acquisition. Oxygen concentrations decreased rapidly after sodium sulfide injection followed by a slow decrease that was attributed to microbial endogenous respiration.

Location and identification of nanosilver by SEM-EDS

Scanning electron microscopy (SEM) coupled with energy dispersive spectroscopy (EDS) was effective in locating and identifying Ag NPs and Ag_xS_y complexes adsorbed to nitrifying cultures. In the presence of Ag NPs only, the bright spots showed that nanoparticles were embedded in nitrifying cell flocs (Figure 32). EDS elemental analysis confirmed further that these bright spots were Ag NPs. When sulfide was added to the same nitrifying cultures prior to nanosilver exposure, however, these bright spots largely disappeared. The combined uses of secondary electron detector and back-scattered electron detector allowed us to locate the formation of new Ag_xS_y complexes or precipitates (Figure 33), the elemental composition of which was validated by EDS showing high S peaks and multiple Ag peaks.

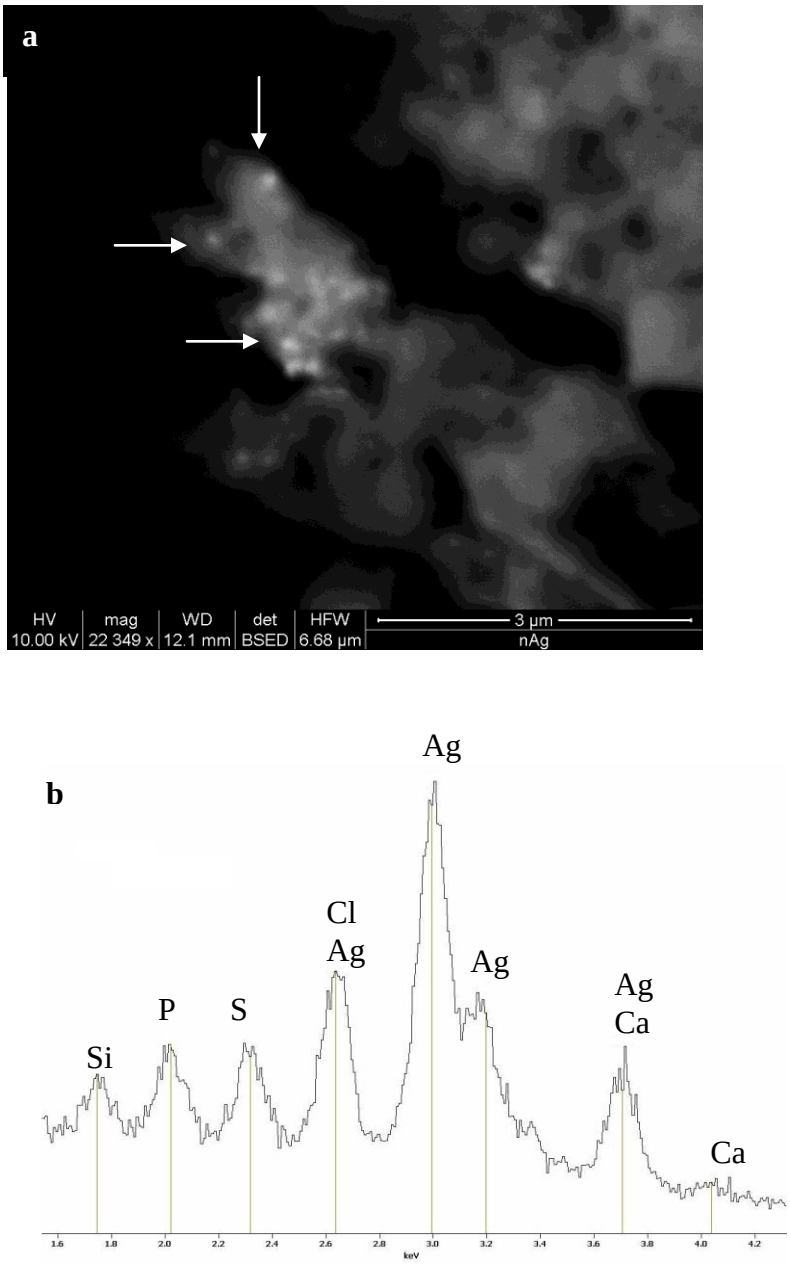

Figure 32. SEM-EDS analysis of silver nanoparticles in the presence of a nitrifying culture.

SEM image of Ag NPs (arrow-pointed bright spots) embedded in nitrifying bacterial flocs using back-scattered electron microscopy (a). The EDS analysis showed detailed elemental compositions to confirm that the particles (arrow-pointing) were silver-rich (b).

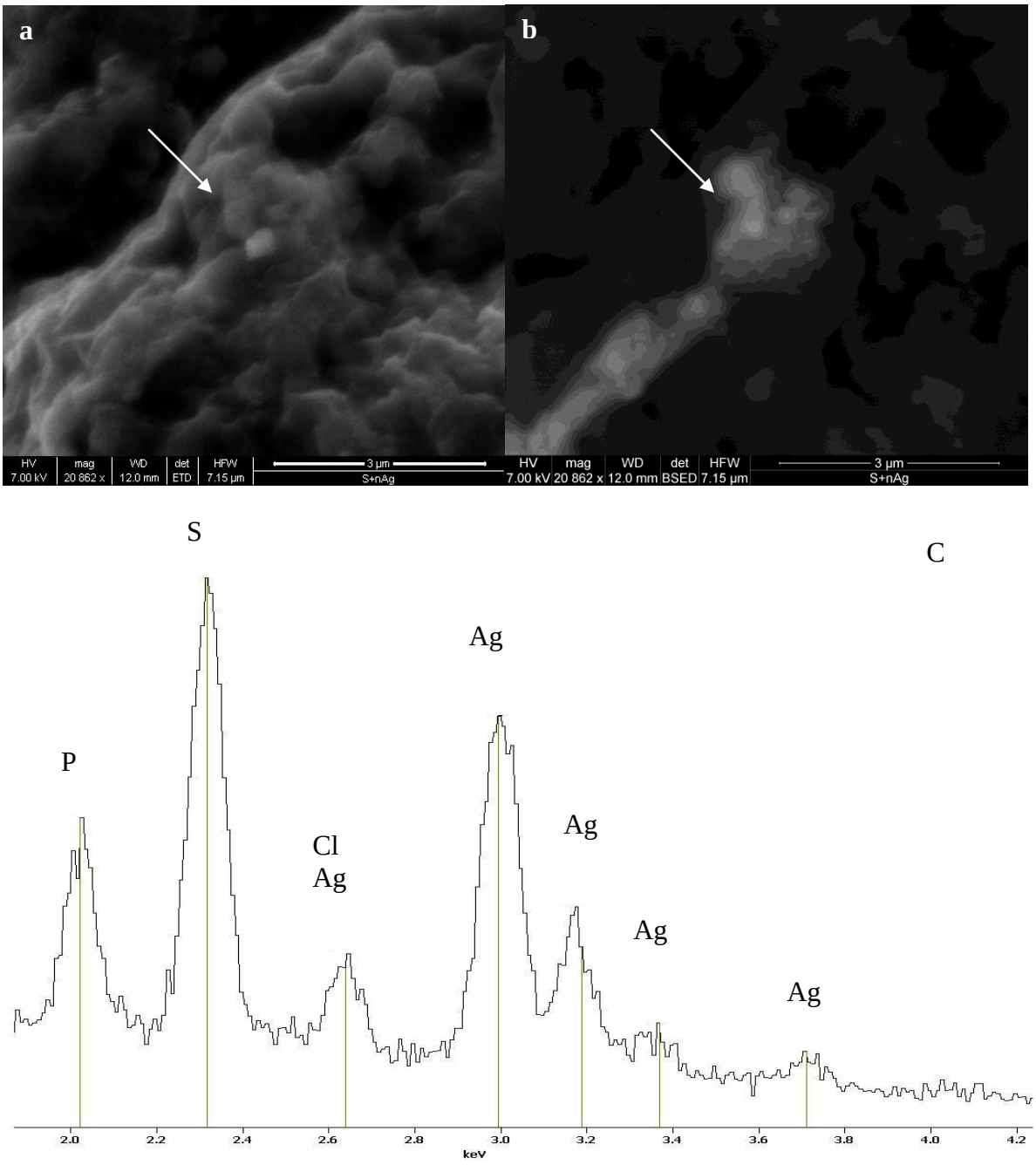

Figure 33. SEM-EDS results of silver nanoparticles in sulfide-amended nitrifying culture.

SEM image of silver sulfide complexes attached to nitrifying bacteria using a secondary electron detector (a) and a back-scattered electron detector (b). EDS analysis of elemental compositions indicated the region (arrow pointing) with a high sulfide peak likely due to the formation of new silver sulfide complexes/precipitates after the sequential addition of sulfide and Ag NPs at a final concentration of 10 μM S^{2-} and 9 μM Ag NPs, respectively (c).

4.5 Discussion

We presented, for the first time, quantitative respirometric data to determine the role of sulfide in controlling nanosilver toxicity. By adding a small aliquot of sulfide that forms complexes with Ag NPs, the nanosilver toxicity to nitrifying organisms was reduced dramatically (Figure 30). Scanning electron microscopy coupled with EDS analysis indicated that Ag NPs were highly reactive with sulfide to form new Ag_xS_y complexes (Figure 31). This further indicates that the surface of Ag NPs (oxidized to Ag^+) has reacted rapidly with sulfide ions producing Ag_xS_y species on the nanoparticles thereby preventing or greatly slowing down further AgNP oxidation (and toxicity).

The sulfide complexes appeared to be stable under aerobic conditions (Figure 31), indicating that silver complexes may undergo rapid exchange with other ligands, but with S-ligands as a final thermodynamic sink. Metal sulfide complexes are resistant to oxidation and dissociation, as reported before (Rozan et al., 2000). Thus, the negative impact of Ag NPs on beneficial microorganisms in wastewater treatment may be minimized by sulfide complexation. The concentrations of sulfide in a sewer line could reach up to 6 mg/L (0.2 mM) (Nielsen et al., 2008). Nanosilver present in wastewater could therefore react with sulfide, as the reaction is thermodynamically favorable from equation 7 (Stumm and Morgan, 1996).

$$2Ag + S^{2-} \rightarrow Ag_2S + 2e^-,\ \Delta G^0 = -126.5\ kJ/mol \qquad \text{Equation 7}$$

A caution should be made that free S^{2-} would not be readily available in wastewater. It's more likely that metal ions including Ag^+ would sorb to sulfide-containing particles in

wastewater (Shafer et al., 1998; Wang, 2003). Based on sulfide concentrations in sewage, engineers and wastewater operators may consider a new pretreatment module/method involving sulfide compounds in front of wastewater facilities to retain toxic metallic nanomaterials such as Ag NPs.

Other common ligands present in wastewater such as SO_4^{2-}, Cl^-, PO_4^{3-}, and EDTA were less effective than sulfide in controlling or reducing nanosilver toxicity, largely because of their lower stability constants to form Ag-ligand complexes or precipitates (Table 6). Interestingly, chloride appeared to be less effective in reducing nanosilver toxicity, but it was capable of reducing the toxicity by Ag^+ ions (Figure 29, again indicating that the surface of Ag NPs reacted rapidly with chloride ions producing $AgCl_y$ species on the nanoparticles, thereby slowing down further AgNP oxidation and toxicity. Remedial strategies to remove nanosilver toxicity should therefore be handed differently than when we deal with the toxicity from bulk silver species.

While there is continuous debate on the mechanism of AgNP toxicity to bacteria, possible mechanisms of microbial growth inhibition by Ag NPs include particle attachment to cell membranes or directly entering the cell (Morones et al., 2005), causing the changes of membrane permeability and redox cycle in the cytosol, interference with the cellular S-containing compounds, intracellular radical accumulation, and dissipation of the proton motive force for ATP synthesis (Nel et al., 2006; Sondi and Salopek-Sondi, 2004). For comparison, the inhibitory effect of Ag^+ is believed to be due to its sorption to the negatively charged bacterial cell wall, deactivating cellular enzymes, disrupting membrane permeability, and ultimately leading to cell lysis and death (Ratte, 1999; Sambhy et al., 2006). The mechanism of toxicity alleviation by ligands upon directly

interacting with Ag NPs is more complex. It may include, but not limited to, (1) dissolution and oxidation of Ag NPs to Ag^+ ions, followed by ligand complexation; (2) particle surface modification or coating; and (3) particle aggregation.

The biotic ligand model was successfully applied to calculate the binding constant between Ag^+ ions and nitrifying cells. The predicted silver toxicity values in the presence of various ligands were close to the experimental data (Table 6). However, the BLM model could not help explain why Ag NPs were more toxic than Ag^+ ions, while the addition of ligands such as S^{2-}, Cl^-, PO_4^{3-} and EDTA appeared to reduce toxicity by Ag NPs more effectively than by Ag^+ ions (Figure 28). For that reason, the binding constant between Ag NPs and bacterial S-containing functional groups was not calculated using the BLM model. Nevertheless, the similarity of toxicity data and their attenuation trends between Ag NPs and Ag^+ ions suggested that the BLM and other factors should be considered to predict and control nanosilver toxicity.

The results showed that ammonia monooxygenase was the most sensitive enzyme subjected to silver poisoning (Figure 27). Knowing that AMO is a membrane-bounded enzyme (Chain et al., 2003) and HAO is located in periplasm, we speculated that uncharged Ag NPs of smaller size (e.g., < 5 nm) might enter the cells (Sondi and Salopek-Sondi, 2004; Verma et al., 2008) to generate more reactive oxygen species (ROS) than Ag^+ ions or interfere with the cellular S-containing compounds in the respiratory path (Holt and Bard, 2005), thus rendering higher toxicity to nitrifying organisms.

5 Role of Reactive Oxygen Species in Determining Nitrification Inhibition by Metallic/Oxide Nanoparticles[4]

5.1 Abstract

The toxicity of several metallic/oxide nanoparticles (TiO_2, CuO, ZnO and Ag) to nitrifying bacteria was evaluated individually or in combination in batch studies. The mixture inhibition of nanoparticles was the sum of individual inhibition with no synergistic or antagonistic interaction observed among the nanoparticles studied. Although there was no inhibitory effect of TiO_2 nanoparticles under ambient light or dark conditions, nitrification inhibition was significantly increased when TiO_2 nanoparticles were exposed to ultraviolet (UV) for 30 minutes. Under UV exposure, both TiO_2 nanoparticles and bulk TiO_2 generated the same amount of reactive oxygen species (ROS) in the cell although TiO_2 nanoparticles were more toxic than the bulk counterpart. While the inhibition was well correlated to intracellular ROS concentration, the ROS correlations were different for the different forms of TiO_2 or for the different nanoparticles (e.g., Ag vs. TiO_2). ROS is therefore not a good chemical marker to indicate the toxicity of nanoparticles.

[4] *Journal of Environmental Engineering,* **2009**, *in press.*

5.2 Objectives

Among the metallic/oxide nanomaterials, titanium dioxide (TiO_2) nanoparticles are one of the most used nanoparticles in consumer products such as cosmetics or paints (Mueller and Nowack, 2008). A recent modeling study proposed the higher risk quotients of the nano-TiO_2 than nano-Ag or carbon nanotubes (Mueller and Nowack, 2008). TiO_2 is a photocatalyst and semiconductor having an energy band gap of 3.2 eV (365 nm) (Kormann et al., 1988). While there are three crystal forms of titanium dioxide (anatase, rutile, and brookite), anatase-TiO_2 is more efficient than rutile-TiO_2 to serve as a photocatalyst although rutile is more stable. This photocatalytic property makes TiO_2 wildly used for water disinfection (McCullagh et al., 2007), organic pollutant removal (Karunakaran and Dhanalakshmi, 2008), and solar cell manufacturing (Chou et al., 2008). With their particularly small size, TiO_2 nanoparticles have improved electrochemical properties compared to bulk TiO_2 (Jang et al., 2006; Wang et al., 2008).

Nano-TiO_2 was reported to be less toxic than other semiconductors, such as nano-ZnO and nano-CuO, to aquatic organisms (Adams et al., 2006; Heinlaan et al., 2008). However, after sunlight exposure, the toxicity of nano-TiO_2 increased by more than two-fold, presumably due to its role in promoting reactive oxygen species (ROS) generation (Adams et al., 2006). Indeed, a ultraviolet (UV) A (315 nm ~ 400 nm) irradiation system combined with TiO_2 could efficiently inactivate microorganisms due to ROS generation (Hamamoto et al., 2007). This raises an important question, "Can ROS be a potentially predictive chemical marker of nanotoxicity?"

The main objective of this work was to evaluate the role of ROS in determining nanotoxicity. In this study, we tested nitrification inhibition by several metallic/oxide nanoparticles (Ag, CuO, ZnO, and TiO_2) to evaluate whether the measured intracellular ROS can be served as a predictive indicator of toxicity. Nitrification involving ammonia oxidation by nitrifying bacteria is sensitive to a number of environmental factors such as pH, dissolved oxygen concentration, and temperature, and is therefore susceptible to inhibition in wastewater treatment (Hu et al., 2002). Furthermore, we measured the toxicity of a mixture of these nanoparticles to nitrifying bacteria to examine any synergistic interactions of selected nanoparticles and to indicate whether each nanomaterial has the same mode of antimicrobial action. The results underscore the need for further research on oxidative stress via ROS formation, the role of nanomaterials in cell membrane disruption, and cytotoxicity mechanisms of metallic/oxide nanoparticles.

5.3 Materials and Methods

Nanoparticles

All metal oxide nanoparticles with purity of more than 99% (Nanostructured & Amorphous Materials Inc, Los Alamos, NM) were purchased in powder form and used without further modification. Detailed particle size information is listed in Table 7. Anatase type TiO_2 was used because of its high photocatalytic efficiency (Bojinova et al., 2007). For comparison, a bulk TiO_2 crystal (Fisher Scientific, anhydrous amorphous powder) with an average particle size above 0.5 μm (obtained from Stokes' Law) was also used. All suspensions of the commercial nanoparticles were sonicated (Fisher

Scientific, Model 100 Sonic Dismembrator) in the deionized water (conductivity, 18Ω) for ca. 25 minutes before the analysis of real particle size distribution or the batch microbial-based respirometric test was initiated. A suspension of silver nanoparticle with an average size of 15 nm was prepared in the lab following a previous work, which was freshly made before every test. For particle characterization, Transmission Electron Microscopy (TEM, JEOL 1400) was applied under an acceleration voltage of 100 keV for real particle size distribution measurement. The nanoparticle suspension was added to a standard carbon-coated TEM grid for imaging and the size analysis was performed using ImageJ, a free, Java-based image-processing package available at http://rsb.info.nih.gov/ij/.

Table 7. Selected metallic/oxide nanoparticles used in nitrification inhibition study

Nanoparticles	Source	Advertised particle size (nm)	Average size in water and size range (nm)	Band gap energy (eV)
TiO_2 (anatase)	Nanostructured & Amorphous Materials Inc.	5	370 (150 ~ 2,600)	3.2 (Kormann et al., 1988)
Ag	Lab-synthesized	N/A	15 (2~45)	N/A
CuO	Nanostructured & Amorphous Materials Inc.	30-55	1500 (250 ~ 4,200)	1.5 (Ghijsen et al., 1988)
ZnO	Nanostructured & Amorphous Materials Inc.	20	1600 (40 ~ 10,000)	3.3 (Srikant and Clarke, 1998)

T-RFLP Analysis of Nitrifying Bacterial Community

Molecular studies in the lab using terminal restriction fragment length polymorphism (T-RFLP) indicate that the enriched nitrifying bacteria mainly consist of *Nitrosospira* (ammonia-oxidizing bacteria, AOB), *Nitrobacter* (nitrite-oxidizing bacteria, NOB), *Nitrospira* (NOB) (see final fragments in APPENDIX B). Regular measurement of NH_4^+, NO_2^--N, NO_3^--N, and COD (chemical oxygen demand) from the effluent indicated complete nitrification with typical effluent concentrations of NH_4^+-N and NO_2^--N less than 1 mg/L and NO_3^--N around 380 mg/L. The nitrifying cultures were periodically withdrawn from the reactor for ROS measurements and inhibition tests.

We used 3 mL of the nitrifying bacteria culture to isolated DNA using Ultraclean soil DNA isolation kit (MoBio Laboratories, Carlsbad, CA), following the manufacturer's protocol. We eluted DNA from the kits column membrane with 50 μL DNA grade water (Fisher Scientific, Fairlawn, NJ). We confirmed the intact DNA on 1% agarose gel electrophoresis.

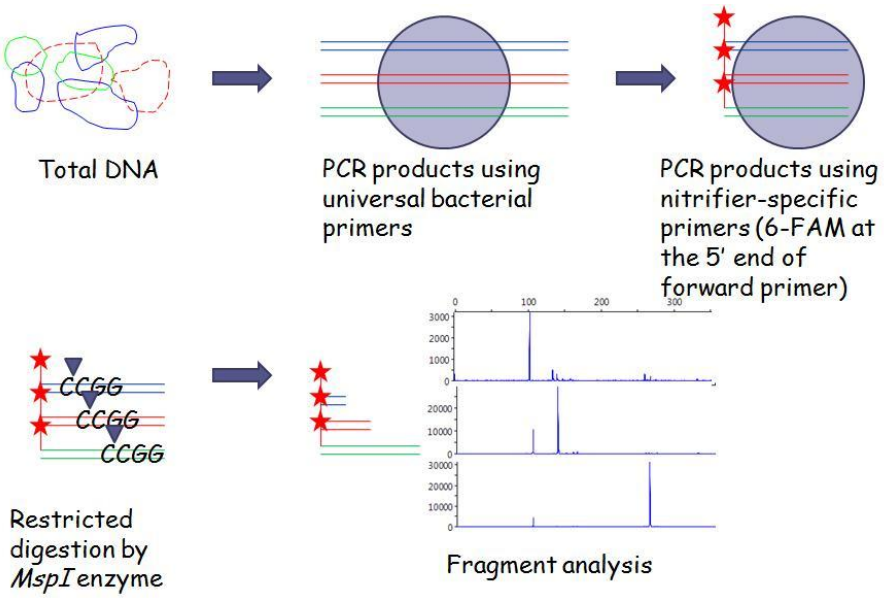

Figure 34**.** A schematic diagram of terminal restriction fragment length polymorphism (T-RFLP) to analyze nitrifying bacterial community structure.

Extracted DNAs are amplified by PCR using nitrifier-specific primers labeled with a dye (6-FAM). PCR products were digested using restriction enzyme (*MspI*) and each final fragment indicates each species.

We applied T-RFLP (Figure 34) targeting 16S rRNA genes for AOB and NOB. We used nested PCR using universal primers 11f and 1492r to amplify initial DNA stocks, because a low initial concentration of DNA from nitrifiers could result in a poor T-RFLP electropherograms (Siripong and Rittmann, 2007). Table 8 summarized the primers we used in amplifying the 16S rRNA gene, their sequences, and their specificities. All primers (Table 8) were systhesized by Interated DNA technologies (IDT, Skokie, IL) and Eub338f included phophoramidite dye 6-FAM at the 5’ end.

Table 8. PCR primes for T-RFLP analysis of nitrifying bacterial community structure

Primer	Sequence (5′–3′)	Specificity
11f	GTTTGATCCTGGCTCAG	Bacteria 16S rRNA gene
1492r	TACCTTGTTACGACT T	Bacteria 16S rRNA gene
Eub338f*	ACTCCTACGGGAGGCAGC	Bacteria 16S rRNA gene
Nso1225r	CGCCATTGTATTACGTGTGA	*β-Proteobacteria* AOB 16S rRNA gene
NIT3r	CCTGTGCTCCATGCTCCG	*Nitrobacter* 16S rRNA gene
Ntspa685r	CGGGAATTCCGCGCTC	*Nitrospira* 16S rRNA gene

Using a DNA thermocycles (Effendorf, Westbury, NJ), we amplified environmental DNA based on the 16S rRNA using a total volume of 50 μL in 0.2-ml Eppendorf tubes. The reaction solution contained Taq 2× PCR master mix (Qiagen, Valencia, CA), 20 pmol of each primer, and 1 μL of template extracted DNA (universal amplification product for the nitrifier-specific amplification). After the first round of universal amplification of the 16S rRNA gene, we purified PCR products using the QIAquick® purification kit (Qiagen, Valencia, CA) to eliminate the universal primers so that they would not interfere with the next round of amplification. The thermal profile used for the universal amplification was: 5 min at 95 ℃; 35 cycles of 30 s at 95 ℃, 30 s at 55 ℃, and 45 s at 72 ℃; and a final elongation for 10 min at 72 ℃. The thermal profile used for the nitrifier-specific amplification was: 5 min at 95 ℃; 35 cycles of 90 s at 95 ℃, 30 s at 60 ℃, and 90 s at 72 ℃; and a final elongation for 10 min at 72 ℃. Finally, we purified PCR products and digested 16S rRNA-gene amplicons with *Msp*I restriction endonuclease (Promega, Madison, WI) at 37 ℃ for 3 h.

Digested PCR products, along with Genescan 600 LIZ size standard (Applied Biosystems, Foster City, CA), were run through an ABI 3730 DNA Analyzer (Applied Biosystems,

Foster City, CA) in the DNA core at the University of Missouri. We analyzed the peak results using Peak Scanner Software v1.0 (Applied Biosystems, Foster City, CA) and compared fragment sizes to expected fragment sizes (Table 9).

Table 9. Expected terminal fragment (TF) sizes and their corresponding AOB and NOB groups.

Nitrifier group	**TF size (bp)**
Group 1 *Nitrosomonas europaea/eutropha* lineage	164–166, 276
Group 2 *Nitrosomonas oligotropha* lineage	276
Group 3 *Nitrosomonas cryotolerans* lineage	276
Group 4 *Nitrosomonas marina* lineage	166
Group 5 *Nitrosomonas communis* lineage	276
Group 6 *Nitrosospira* lineage	105–107
Nitrobacter species	141
Nitrospira species	265–267, 277 (134, 194, 333)

Acute UVA Exposure

To evaluate the toxicity of metallic/oxide nanoparticles under ultraviolet exposure, an ultraviolet A (UVA) lamp (Blak-Ray Lamp Model UVL-56, 365 nm, 750 $\mu W/cm^2$ at 15cm) was used as the light source. Before transferring the nitrifying bacterial suspension (with or without treatment of nanoparticles) to respirometric bottles, the enriched bacterial culture was exposed to UVA light at fixed distance (i.e., 15 cm) for a predetermined period of time. Figure 1 shows that nitrification inhibition increased linearly as the UV exposure time increased. The rest of experiments were therefore conducted at a fixed exposure time of 30 minutes, at which the value of half maximal inhibitory concentration (IC_{50}) is roughly located (Figure 35). The culture was treated

with Ag nanoparticles, TiO_2 nanoparticles or TiO_2 bulk materials and then exposed to UVA for 30 mins before the inhibition tests or ROS measurements were performed.

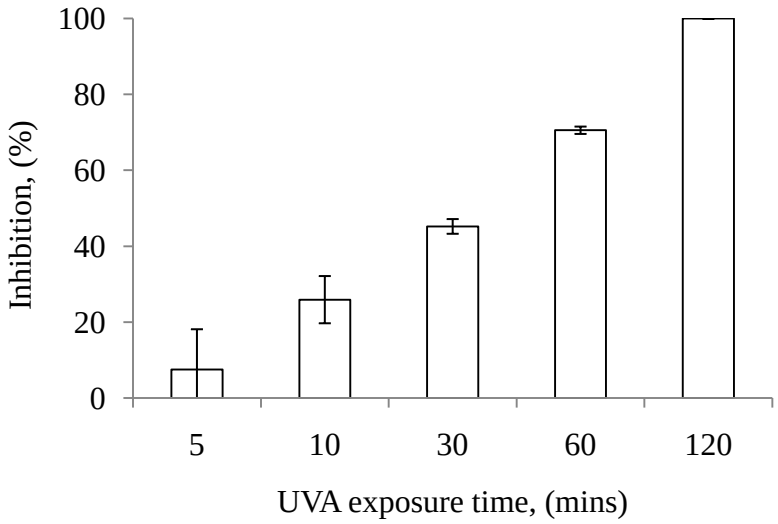

Figure 35. Nitrification inhibition by UV light.

The inhibition increased linearly with the UV exposure time. Error bars indicate one standard deviation of triplicate samples.

Reactive Oxygen Species Measurement

Intracellular ROS concentrations were measured with a fluorescence-based method using H_2DCFDA (dichlorodihydrofluorescein diacetate, Invitrogen, OR, USA), a cell-permeant indicator for ROS. After centrifuging aliquots of bacterial samples at 10,000 rpm for 15 mins, the supernatant was removed and the pellets was incubated in a loading buffer (10 μM H_2DCFDA, 20 mM MOPS, 1 mM NH_4NO_3, trace metals, and 4 mg/L K_2HPO_4) at room temperature for 30 mins. After removing the loading buffer, cells were re-suspended with prewarmed growth medium (loading buffer without H_2DCFDA) and

treated with nanoparticles. Aliquots of the culture (200 μL) were distributed in each 96-well microplate and the fluorescence was automatically measured using a microreader (VICTOR^3, PerkinElmer, CT, USA) with 485 nm excitation and 535 nm emission filters. The relative fluorescence increase (%) was calculated from the fluorescence changes after 30 min incubation. Hydrogen peroxide (H_2O_2, Fisher Scientific) was used as a standard for ROS measurements. The results of the relative fluorescence increase under different treatments were normalized in H_2O_2 concentration unit. The UVA-induced ROS was measured similarly after the bacterial samples were exposed to UV light for 30 mins outside the microreader.

5.4 Results and Discussion

Mixture Toxicity of Nanoparticles

Nitrification inhibition by metallic/oxide nanoparticles was first determined at 1 mg/L of ZnO (12 μM), CuO (13 μM), TiO_2 (13 μM), and Ag (9 μM), individually. The commercial TiO_2 nanoparticles did not show any inhibitory effect to nitrification at 1 mg/L under room light (Figure 36). The inhibition increased in the order of TiO_2 < CuO< ZnO < Ag. This result is consistent with published data (Adams et al., 2006; Heinlaan et al., 2008). Because of known antimicrobial activity of Ag nanoparticles to nitrification, the toxicity in a series of mixture containing Ag and other metallic oxide nanoparticles was determined, which was predominated by Ag nanoparticles (Figure 36). The toxicity of the mixture such as Ag + CuO, Ag + TiO_2, Ag + CuO + TiO_2 was roughly the same (within one standard deviation) as the sum of the toxicity of individual nanoparticles (t-

test, $\alpha = 0.05$). For the mixture of Ag and ZnO, the toxicity of the mixture was lower than predicted by concentration addition. The reason of having such an antagonistic effect between Ag and ZnO is unknown, which may be related to possible complexation between Ag^{+} and $Zn(OH)_4^{2-}$ after nanoparticle dissolution.

Since nanotoxicity is often size dependent (Jiang et al., 2008), the true sizes of commercial nanoparticles were measured. The size of commercial nanoparticles in water suspension was much bigger than the claimed size (Table 7), consistent with the findings published recently (Adams et al., 2006; Heinlaan et al., 2008). The true sizes of commercial nanoparticles were all well above 100 nm. When the commercial nanoparticles in powder form was added in deionized water, they aggregated rapidly because metal oxide particles within the particle size range of 1 nm to 10 μm tend to have high aggregation coefficient ($s > 1$) (Zhang et al., 2008). Many commercial nanoparticles are modified with surfactants or polymers, which may behave differently from the bulk or aggregate form in terms of their dissolution and suspension in water. However, particle size may change substantially during dry periods. In this study, the metallic oxide nanoparticles (ZnO, TiO_2, and CuO) were all in powder form and used as manufactured, without any modifications. There was no relationship between the toxicity and the average size of commercial nanoparticles resuspended in water.

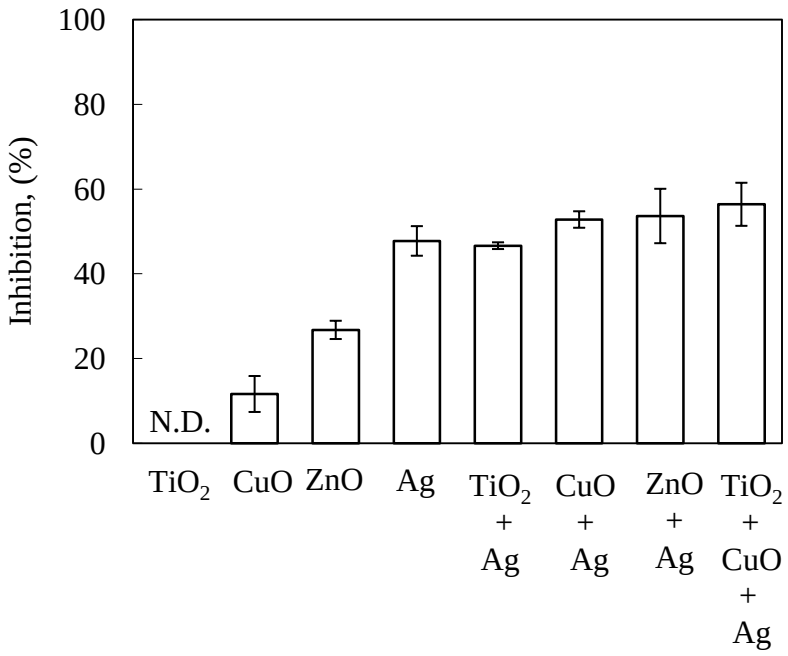

Figure 36. Individual and mixture toxicity of metal/metal oxide nanoparticles.

Nitrification inhibition by individual metallic/oxide nanoparticles or a mixture of nanoparticles in the absence of UV irradiation. The concentration of each metallic/oxide nanoparticles was 1 mg/L. N.D. means not detected.

UV Effect on Toxicity of Nanoparticles

TiO_2 nanoparticles did not inhibit nitrification in the absence of UV exposure (Figure 37a). However, nitrification was almost completely inhibited in the bacterial samples treated with 2 mg/L nano-TiO_2 and exposed to UVA radiation for 30 mins (Figure 37a). The inhibition caused by UVA radiation was only 45.2 % (± 1.9) (Figure 35). The combined treatment with nano-TiO_2 and UVA increased the toxicity because the mixture inhibition (~100%) was much higher than the sum of inhibition by UVA and nano-TiO_2 separately (mixture inhibition > 45.2 % + 0 %). For comparison, the bulk TiO_2 had the same behavior as commercial TiO_2 nanoparticles with slightly lower inhibition (Figure

37a). Previous work has shown similar results that nanoparticles are more toxic than the bulk counterpart (Heinlaan et al., 2008; Lok et al., 2006). One may expect that photolysis (chemical decomposition of organic molecules by photon energy provided) under UV exposure causes partly the toxicity. In the presence of semiconducting materials such as TiO_2, photocatalytic reactions may produce additional toxicity. Although TiO_2 itself is not toxic to nitrifying bacteria, the toxicity of TiO_2 nanoparticles dramatically increased under UV exposure.

In contrast, Ag nanoparticles were highly toxic to nitrifying bacteria regardless of UV exposure (Figure 37b). This is not unexpected since nano-Ag is not a semiconductive (photocatalytic) nanomaterial. Although photocatalytic ROS might change rapidly under the light, photocatalytic ROS concentrations were not a good predictor of nitrification inhibition by Ag nanoparticles (Chapter 3). Therefore, the toxicity of Ag nanoparticles under UV exposure was simply the sum of individual inhibition by UVA and nano-Ag at specific concentrations (Figure 37b).

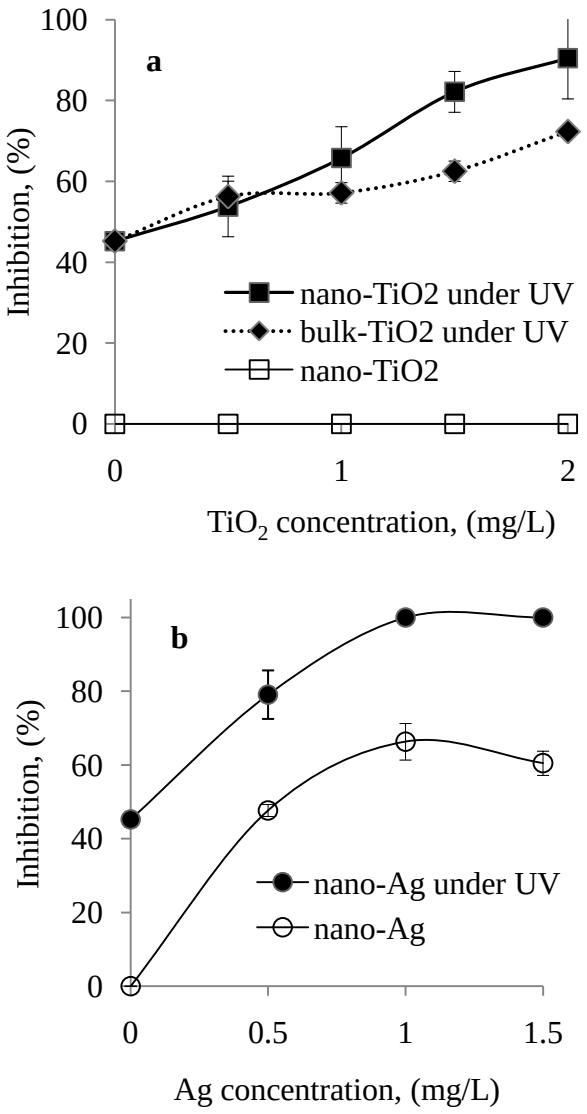

Figure 37. Nitrification inhibition by Ag NPs and TiO_2 nanoparticles with/without UVA.

Nitrification inhibition by nano-TiO_2 (a) and nano-Ag (b) in the presence (■, •) and absence (□, ○) of 30 min UVA exposure. No inhibition by nano-TiO_2 in the absence of UVA (□) was detected. For comparison, in the presence of UV exposure, the inhibition by the bulk TiO_2 (♦) was slightly less than that by nano-TiO_2 (■). Error bars indicate one standard deviation of triplicate samples.

ROS Generation and Correlation with Toxicity

Without UV exposure, no reactive oxygen species were detected in the nitrifying culture treated with nano-TiO_2 (Figure 38). However, intracellular ROS were produced in the bacterial samples after 30 min of UVA exposure and the ROS concentration was linearly increased with nano-TiO_2 concentration. The ROS concentrations corresponded to 100 ~ 310 μM H_2O_2 at 0 ~ 2 mg/L nano-TiO_2 under UVA exposure. These values were ten times higher than the ROS concentrations measured in similar nitrifying culture treated with nano-Ag (1 ~ 20 μM H_2O_2) (described in Chapter 3).

A linear relationship (R^2 = 0.98) between intracellular ROS concentration and nano-TiO_2 inhibition was observed (Figure 38). At the same TiO_2 concentrations, there was no statistical difference of intracellular ROS concentration between the bulk and commercial nano-TiO_2 (ANOVA, $P< 0.05$, Figure 38). This was not unexpected because the particle sizes of the bulk (500nm) and nano TiO_2 (~370nm) are close and comparable. However, TiO_2 nanoparticles were more toxic to nitrifying bacteria than the bulk TiO_2 (Figure 37a). At the same ROS concentration, nano-TiO_2 inhibited more than bulk TiO_2 (ANOVA, $P< 0.05$) (Figure 39). These results suggest that other cytotoxic mechanisms of nano-TiO_2 are present in addition to intracellular ROS accumulation. The toxicity (nitrification inhibition) of TiO_2 under UV exposure may be related to multiple factors including the particle size itself, photolysis under UV (chemical decomposition of organics by photon energy provided), ROS from TiO_2/UV, and chemical purity of the products.

Compared to nano-TiO_2, silver nanoparticles generated much less intracellular ROS in the bacterial cells. The intracellular ROS in the presence of Ag nanoparticles was more than an order of magnitude less than that in the presence of TiO_2 under UV exposure (Figure 39). However, an order of magnitude less inhibition than TiO_2 was not observed. Instead, silver nanoparticles show higher degree of inhibition than the nano-TiO_2 under UV exposure, which indicate that the toxicity (nitrification inhibition) mechanisms of the nanoparticles are completely different, depending on the nanoparticles.

Each nanoparticle has different toxicity mechanisms such as release of toxic dissolved metal species (ions), particle invasion, cell function destructions, ROS attack, and surface chemistry of membrane damage. The toxicity of metallic/oxide nanoparticles to bacteria depends on many physico-chemical properties of the particles, such as a) particle size, b) particle stability (e.g., dissolution and aggregation), and c) the binding affinity of original metal to cells. It is well known that TiO_2 itself is not soluble and thus has little or no toxicity (Figure 36). But, under UV radiation, it produces ROS such as hydroxyl radicals, which readily attack organic molecules and disinfect microorganisms. Ag nanoparticles are not semiconducting nanoparticles. Possible mechanisms of nitrification inhibition by nanosilver include particle attachment to cell membranes or directly entering the cell (Morones et al., 2005), causing the changes of membrane permeability and redox cycle in the cytosol, strong interference with the cellular S-containing compounds, intracellular radical accumulation, and dissipation of the proton motive force for ATP (Nel et al., 2006; Sondi and Salopek-Sondi, 2004). Therefore, intracellular ROS generation is just one of the reasons of the nitrification inhibition.

While there is abundant evidence showing that the toxicity of nanoparticles is related to the ROS accumulation in the cells (Adams et al., 2006), there is not direct proof that ROS causes inhibition. In this study, nano-Ag induced much less intracellular ROS than nano-TiO_2 under UVA under the same degree of inhibition (Figure 39). The ROS accumulation was more prominent in nano-TiO_2 than in nano-Ag presumably due to the photocatalytic properties of TiO_2. Even with the same chemical, although the intracellular ROS concentrations in both bulk and nano-TiO_2 were similar, the commercial nano-TiO_2 appeared to be more toxic (Figure 39). Therefore, the intracellular ROS may be related to toxicity of nanoparticles, but it cannot be an indicator showing the degree of inhibition by nanoparticles. In other words, ROS cannot be served as a chemical marker for toxicity determination.

In studies of nanotoxicity, the information of particle size is essential. We have shown the positive relationship between the fractions of nanosilver particles less than 5 nm and nitrification inhibition (Chapter 3). Several papers report that small size particles (< 10 nm) interact with cell membranes to inhibit cell growth (Elechiguerra et al., 2005; Morones et al., 2005). The toxicity of nanosilver was explained by cellular internalization of nano-Ag as well as Ag^+ release (Morones et al., 2005; Navarro et al., 2008). Furthermore, the fraction of small size nanoparticles is more important to determine the toxicity than the average particle size since smaller particles have a higher capability of entering the cells. The commercially available nanomaterials tend to have larger particle sizes than their reported values and should be characterized before use.

The stability of metallic/oxide nanoparticles involving dissolution and aggregation is a factor in differentiating the cytotoxicity mechanisms. Nanosilver gradually released silver

ions to produce toxicity (Navarro et al., 2008). ZnO and CuO nanoparticles also slowly released Zn^{2+} or Cu^{2+} to inhibit microbial growth (Heinlaan et al., 2008). Dissolved Fe^{2+} from Fe nanoparticles contributed to *E. coli* inactivation (Lee et al., 2008). The fact that dissolved metal ions contribute to the toxicity of nanoparticles suggests the toxicity may be different according to metal ion affinity to cell functional groups (e.g., -SH). Cell membranes also function as a ligand for the metal because membranes consist of various negative charged functional groups, such as carboxyl or phosphate groups (Campbell et al., 2002). The binding affinity to interaction sites of the cells is different with each metal ion (Niyogi and Wood, 2004). Silver has generally the high stability constant to form metal complexes (Stumm and Morgan, 1996). If the same amount of free ions is present from different metallic/oxide nanoparticles, metals (e.g., Ag) with the higher binding affinity to sites of action will likely inhibit bacterial growth more effectively.

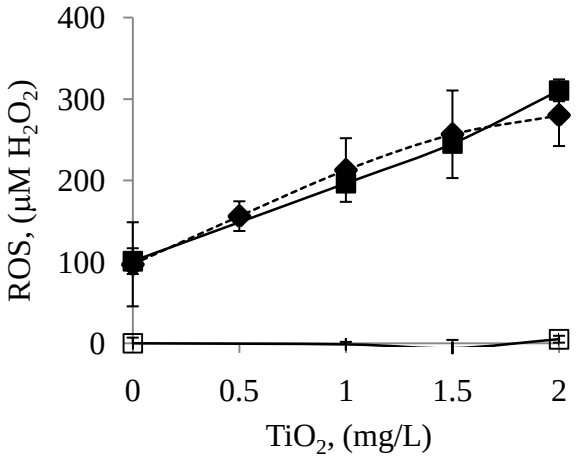

Figure 38. ROS concentration increases as a result of bacterial exposure to nano TiO_2.

Intracellular reactive oxygen species (ROS) generation in cells treated with TiO_2 nanoparticles (■) and bulk TiO_2 (♦) under UVA exposure. Without UV exposure, TiO_2 nanoparticles did not induce intracellular ROS (□). Error bars indicate on standard deviation of five replicates.

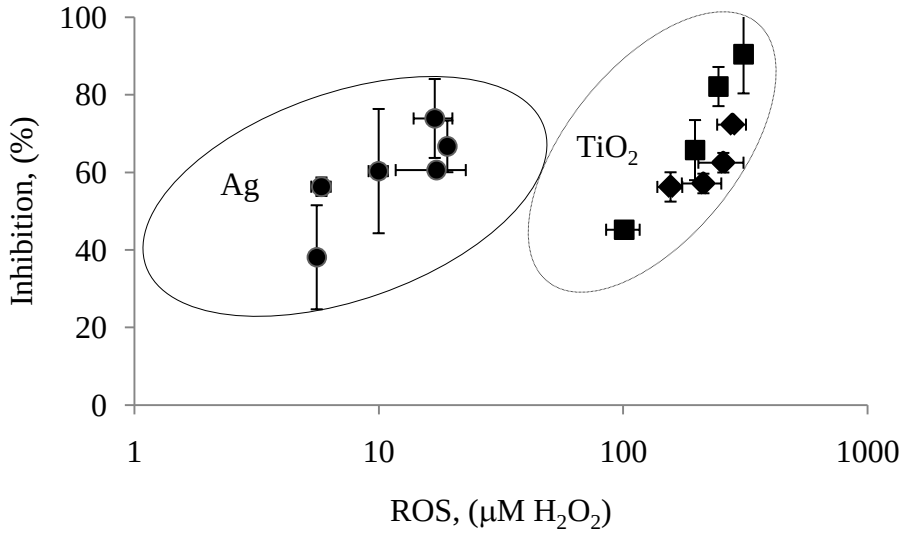

Figure 39. Comparision of induced ROS concentrations induced by Ag and TiO_2 nanoparticle exposure.

The relationship between the inhibition and ROS concentration. The inhibition was plotted as a function of ROS from samples treated with TiO_2 nanoparticles (■), TiO_2 bulk suspension (♦) under UV exposure and Ag nanoparticles (●). Note: the log-scale in X-axis.

6 Microbial Interactions with Nanosilver in a Bacterial Biofilm[5]

6.1 Abstract

Biofilms are often more resistant to toxic chemicals such as heavy metals and antimicrobial agents than planktonic cells. Nanosilver has a broad range of applications with strong antimicrobial activity. However, biofilm susceptibility to nanosilver toxicity is not well understood. Here we reported the number of active cells in planktonic or biofilm cultures after nanosilver exposure using oxygen quenching fluorescence-based microrespirometry, which is less time-consuming and offers a reliable alternative to **traditional** microbiological techniques. We also determined the aggregation behavior and the spatial distribution of nanosilver in biofilms using *E. coli* expressing green fluorescent protein and the indigenous red fluorescent nanosilver. At the same bacterial concentrations (3×10^8 CFU/mL), biofilms were four times more resistant to nanosilver inhibition than planktonic cells. Nanosilver was aggregated in the presence of planktonic or biofilm cells resulting in an increase of average particle size by a factor of 15 and 40, respectively. While nanosilver particles were distributed relatively evenly in a thin (10 μm) biofilm in aggregate form, they were able to penetrate to approximately 40 μm in a thick biofilm after 1 hour exposure. These findings suggested that biofilm resistance to nanosilver might be at least partially attributed to nanoparticle aggregation and retarded silver ion/particle diffusion.

[5] *Environmental Science and Technology*, **2009**, in review.

6.2 Objectives

Biofilms are ubiquitous in the environment. Here we investigated the biofilm resistance to nanosilver and compared the efficiency of nanosilver as an antimicrobial agent to that of silver ion. Cells of *Escherichia coli* were cultivated using either batch or continuous flow systems (drip-flow reactors, figure 40) to grow thin or thick biofilms, respectively. To test the toxicity of nanoparticles, we used fluorescence-based oxygen microrespirometry in time-resolved fluorescence mode and measured microbial oxygen consumption of biofilms that were treated with or without Ag NPs. To understand how nanoparticles are transported and spatially distributed in biofilms, we took advantage of the fluorescence properties of nanosilver and green fluorescence protein of *E. coli.*

6.3 Materials and Methods

Nanoparticles preparation

Silver nanoparticles were prepared by borohydride reduction of silver (see detail information in chapter 3). The freshly prepared nanoparticle suspensions contained roughly 50/50 of Ag+ and AgNPs and almost complete AgNPs by adding NaBH4 at the concentrations of 0.14 and 0.7 mM, respectively. The nanosilver suspensions having an average particle size of 15 to 21 nm (via TEM analysis) were well characterized as described earlier (chapter 3). The results of nanoparticle distribution analysis by the TEM were generally consistent with those by dynamic light scanning (DLS) (Figure 40).

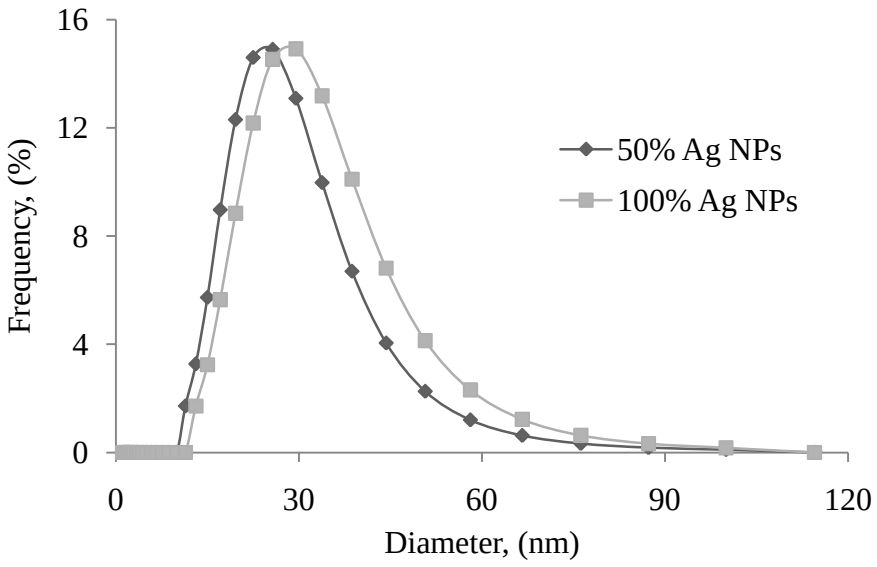

Figure 40. Dynamic light scattering size analysis of two type's nanosilver composition.

The freshly prepared nanoparticle suspensions contained roughly 50/50 of $Ag^{+}$and AgNPs (50 % Ag NPs, ♦) and almost complete AgNPs (100 % AgNPs, ■) by adding $NaBH_4$ at the concentrations of 0.14 and 0.7 mM into silver nitrate (0.7 mM) in PVA solution. The size of particles was shifted toward to a high value and the mean of size was increased to 29 nm at 100 % Ag NPs from 25 nm at 50% Ag NPs.

Biofilm and Planktonic Culture Preparation

To compare toxicity of AgNPs between biofilm and planktonic cells at the same bacterial concentrations, biofilm and planktonic cells were prepared before the oxygen fluorescence based microrespirometry was applied for microbial activity/toxicity determination. For biofilm preparation, a 96-well microplate (sterilized, Thermo Scientific) was inoculated with aliquots of overnight culture (O.D. = 0.5 at 600 nm) of *E. coli* PHL628 (a gift from Dr. Anthony Hay at Cornell University) and filled with 200 μL of nutrient broth (BBL™, Gelysate™ peptone, 5 g/L, beef extracts, 3 g/L). After covering with a lid, the microplate containing *E. coli* cells was incubated without mixing at 37 ^{o}C for 24 hours. We observed that biofilms were established only at the air–liquid

interface using crystal violet staining. The microplate prepared this way was used to determine the total cell numbers in biofilms so that the same amount of the cells was used in planktonic cell study. To this end, the biofilm cells in the microwell were rinsed three times with 300 μL of saline solution (0.9 %, NaCl) and finally filled with 200 μL of nutrient broth. The biofilm was disrupted by sonication (Sonic Dismembrator, Fisher Scientific, Pittsburgh, PA) in a water bath at 7~8 power for 20 mins. The cell numbers were then determined using standard cell cultivation methods (Madigon and Martinko, 2006).

The stock of planktonic *E. coli* PHL628 cells was prepared in a 250 mL conical flask with 150 rpm shaking at 37 ^{o}C. Samples of the planktonic cells with the same range of O.D. as that of biofilms (i.e., at the same bacterial concentration) in a challenge plate (see Microrespirometric Assay) were prepared for silver toxicity comparison between planktonic and biofilm cells.

Microrespirometric Assay

The prepared biofilms were rinsed and cleaned three times with fresh media before exposed to nanosilver (or silver ions for comparison purposes). The test samples containing AgNPs were prepared by two times serial dilution on a challenge plate. Briefly, an aliquot (125 μL) of nanosilver stock solution (0.7 mM total Ag) was added into 125 μL nutrient broth in the first well of the microplate. After pipette mixing, 125 μL of the mixed liquid was transferred to the next well. An aliquot (125 μL) of nutrient broth was filled to each well containing the biofilm to make a final volume of 250 μL. This was

followed by adding aliquots of oxygen probe (Redlight, Luxcel Biosciences) (10 μL/well; final concentration, 150 nM) on nanosilver treated planktonic and biofilm cultures (total volume = 260 μL) and finally sealing the top of each sample with a drop of heavy mineral oil supplied by the manufacturer. The heavy oil prevents transfer of ambient oxygen and liquid evaporation during experiments. The fluorescence of the cells from each well grown statically was measured every 15 minutes by a microreader (VICTOR^3, PerkinElmer) with 340 nm excitation and 642 nm emission filters in time-resolved fluorescence mode.

By measuring the time required to reach a threshold level (defined as half of the maximum oxygen probe signal) that is directly proportional to cell number based on an established calibration curve (O'Mahony and Papkovsky, 2006), we were able to calculate the numbers of metabolically active bacterial cells in biofilms (Figure 4).

Crystal Violet Biofilm Assay

For comparison purposes, biofilm formation and bacterial resistance to nanosilver or silver ions were also quantified in 96-well flat-bottomed polystyrene microtiter plates using a crystal violet biofilm assay (Flemming et al., 2009; Kim et al., 2009) with slight modification. Briefly, overnight *E. coli* PHL 628 cultures were diluted in nutrient broth to a turbidity of 0.05 at 600 nm. Diluted cultures were inoculated into the plates and were grown statically at 37°C. After 24 h, the wells were washed three times with saline solution (0.9% NaCl) to remove planktonic cells. The washed biofilms were subjected to treatment with Ag NPs or silver ions at different concentrations and were sampled at

predetermined time. Total biofilm cells (as indicated by absorbance at 600 nm) were measured by using 0.1% crystal violet staining. Absorbance data from six replicate wells were averaged to obtain each data point.

The time-dependent biofilm growth in the 96-microwells was simulated using an exponential growth model and the parameters of the specific biofilm growth rate, μ, were determined via least-squares error analysis. Three independent cultures were used to calculate the mean and standard deviation of μ.

Biofilm Cultivation for Nanosilver Distribution Study in Biofilms

Thin Biofilms. For thin biofilm samples, we cultivated *E. coli* (PHL628-gfp, kanamycin resistance gene encoded (Junker et al., 2006)) on a glass-bottom microwell dish (MatTek, MA) under batch conditions. The microwell dish was inoculated with 3 mL of six times diluted overnight culture. Cells of the *E. coli* were grown in LB-kanamycin medium and incubated statically at room temperature (25 ± 2 ^{o}C). After one day of incubation, the microwell dishes were rinsed with fresh LB medium before use.

Thick Biofims. For thick biofilms (> 50 μm), we used Drip Flow Reactor (Biosurface Technologes Co., MT, Figure 41) in a continuous flow system fed with LB (flow rate = 0.4 mL/min). Filter-sterilized kanamycin (50 mg/L, Acros Organics) was added into LB to prevent microbial contamination. Each channel has two small pegs to hold the glass coupon in place, a shallow trough that mitigates blockage of the effluent port during sloughing events and aids in coupon removal, and an effluent port which allows the continuous flow media to exit. The flow of media is the only acting shear force on the biofilm.

After 5-6 days of growth, the biofilm on the glass slide was rinsed with fresh LB medium and exposed to 3 mL (100 μL for thin biofilm) of nanosilver (700 μM, or silver ion) for one hour. Residual nanosilver was removed by washing with LB medium twice.

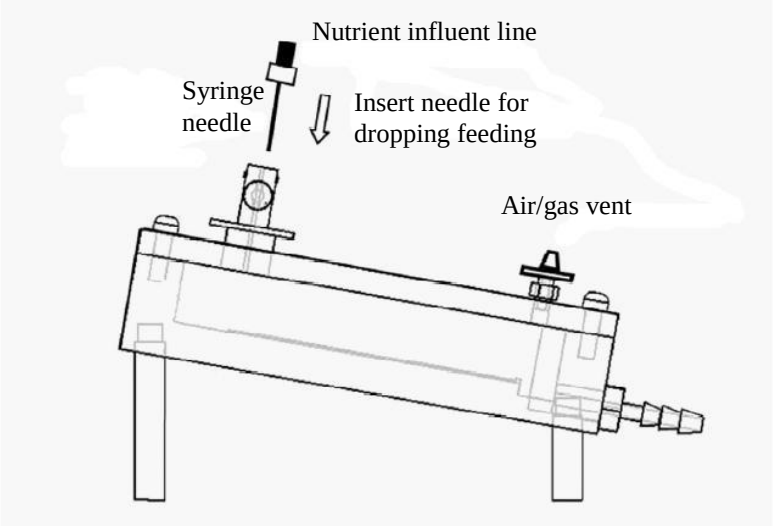

Figure 41. A schematic of Drip Flow Biofilm Reactor.

Biofilms are grown under low shear conditions. Dropping feed helps the growth of thick biofilms on the glass with ample air and nutrient supply.

Determination of Spatial Distribution of Nanosilver in Biofilms

We used a two-photon laser-scanning confocal microscope (Zeiss LSM 510 META NLO system mounted on an Axiovert 200M inverted microscope) for nanosilver/biofim fluorescence imaging. The microscope was equipped with a C-Apochromat 40×/1.2 water-immersion objective (working distance 280 μm), a femtosecond NIR laser (Coherent Chameleon XR) and non-descanned detectors for two-photon imaging, and a focus drive motor for depth imaging along the Z axis. GFP was excited at either 488 nm (thin biofilms) or 830 nm (two-photon, thick biofilms) and fluorescence emission was detected through a 500-550 nm band-pass filter. Nanosilver was excited at 750-770 nm (two-photon) and fluorescence emission was detected through a 565-615 nm band-pass filter.

6.4 Results

Biofilm resistance

Minimum bactericidal concentration (MBC) is defined as the lowest concentration of an antimicrobial agent that prevents microbial growth. Conventionally, it is the concentration that kills at least 99.9% of a planktonic (MBC_P) or biofilm (MBC_b) bacterial population (Harrison et al., 2007). As determined by microrespirometry at the same bacterial concentrations, the MBC_b and MBC_P values of the nanosilver suspension containing almost all of AgNPs were about 38 mg/L and 10 mg/L total Ag, respectively (Figure 42a). The MBC_b and MBC_P values of the Ag^+/nanosilver mixture (50/50 Ag^+ and AgNPs) were 9.5 mg/L and 2.4 mg/L total Ag, respectively (Figure 42b). Similar results were observed for Ag^+ treated planktonic/biofilm samples except higher Ag^+ toxicity against *E. coli* bacteria compared to AgNPs (Figure 42c). Hence, MBC_b was about 4-fold higher than MBC_P for nanosilver, suggesting that biofilm cells are less susceptible to nanosilver inhibition than planktonic cells.

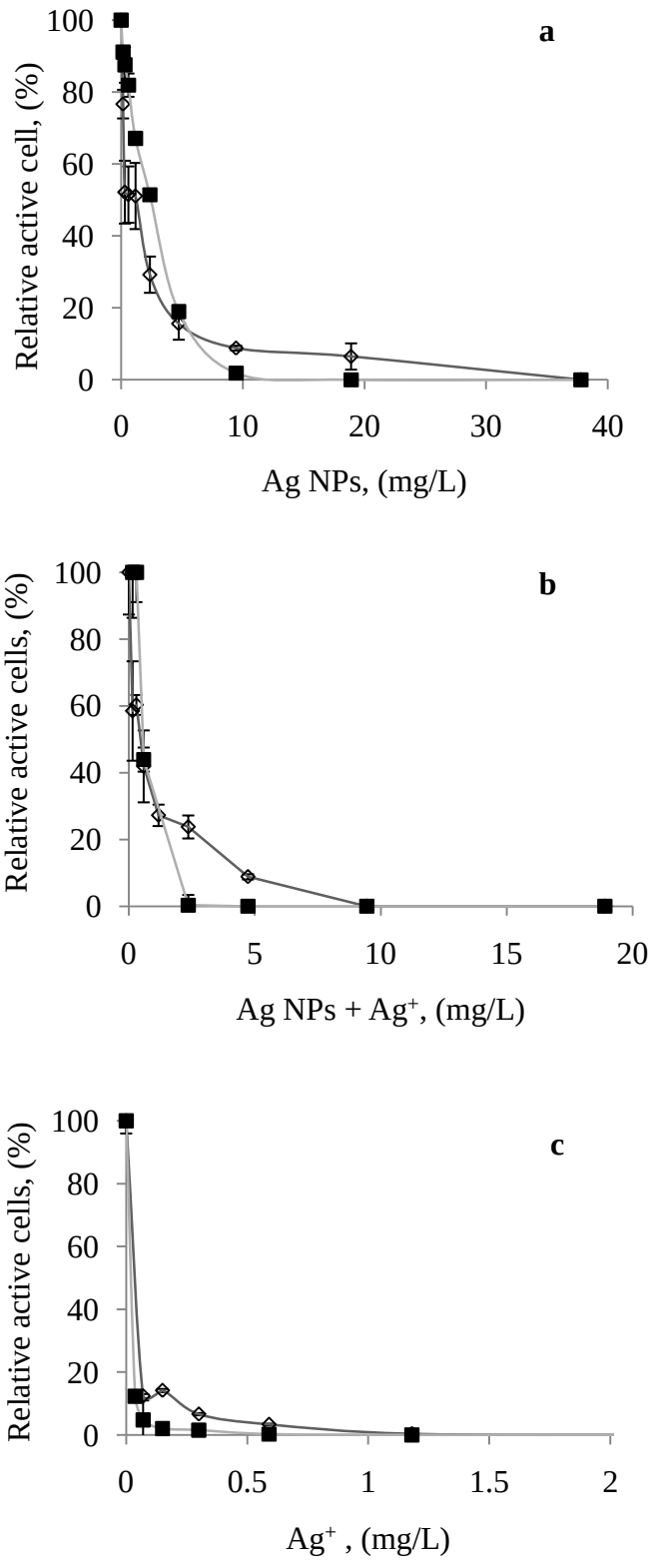

Figure 42. Biofilm resistance to silver nanoparticles and silver ions.

Biofilm (◊) and planktonic cell (■) resistance to AgNPs (a), 50/50 $Ag^+$and AgNPs (b) and Ag^+ (c) inferred from the bacterial growth data. Relative active cells (live cells treated with silver/live cells without silver) of *E. coli* after silver treatment were derived from the microrespirometric measurements of eight replicates for each treatment.

There was a concern that the use of oil in microrespirometric study might reduce both the effective nanoparticles and silver ion concentration in the water, thus provoking an underestimation of the nanosilver toxicity. Indeed, the use of oil to seal microwells shifted the nanosilver particle size distribution slightly toward the higher values (Figure 43), demonstrating the positive effect of water-oil interface on particle aggregation. However, since both planktonic and biofilm cells were exposed to Ag^+/nanosilver in the oil-sealed microwells, the difference of MBC values between planktonic and biofilm cells was unlikely attributed to the oil effect.

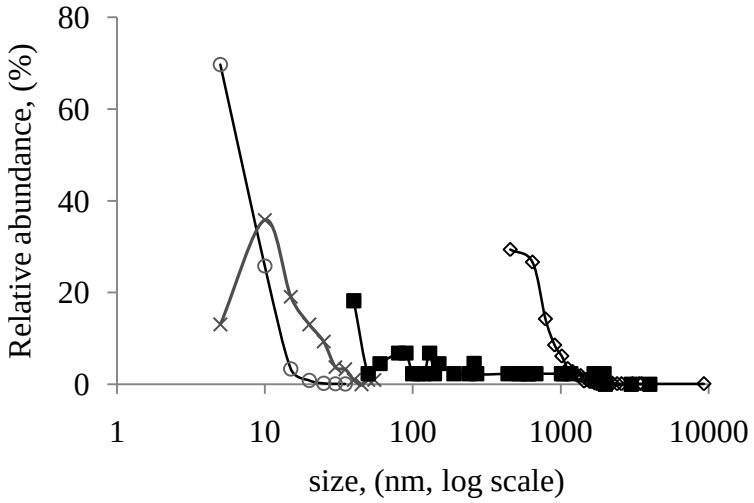

Figure 43. Nanosilver particle size changes in the presence of oil (used in microrespirometry) or planktonic/biofilm cells.

The size of silver nanoparticles initially synthesized using PVA as a capping agent (o) was shifted toward a higher value when the nanosilver suspension was covered by heavy oil (×). Silver nanoparticles were aggregated in the presence of planktonic cells (■) or biofilms (◊). The particle size distribution was determined from TEM images except that

of AgNPs in the presence of biofilms, which was determined based on the fluorescence images (Figure 45e).

Instead, the difference was thought to be caused by nanoparticle aggregation in biofilms due to changes in ionic strength (Chen and Stewart, 2002) and interaction with various complexing agents (Choi et al., 2009; Zhang et al., 2003) such as extracellular polymetric substances released by the bacteria. Once nanoparticles aggregate, their toxicity may be reduced due to particle size increase (Carlson et al., 2008; Choi and Hu, 2008). In this study, nanoparticle aggregation was observed in both planktonic and biofilm cultures (Figure 43 and 44). TEM analysis clearly demonstrated that the interactions of planktonic cells with nanosilver resulted in particle aggregation and a particle/cluster size increase from an average of 20 nm to about 300 nm (or by a factor of 15). Laser-scanning confocal microscopic observations further indicated that the interactions of biofilm cells with nanosilver resulted in particle aggregation even more significantly with a final average aggregate size of about 800 nm (an increase by a factor of 40), although these nanosilver clusters were well distributed in a thin (10 μm) biofilm (Figure 45e and f). These results suggest that nanotoxicity in biofilms may be controlled by several important factors such as particle aggregation along with retarded silver ion/particle diffusion, as described below.

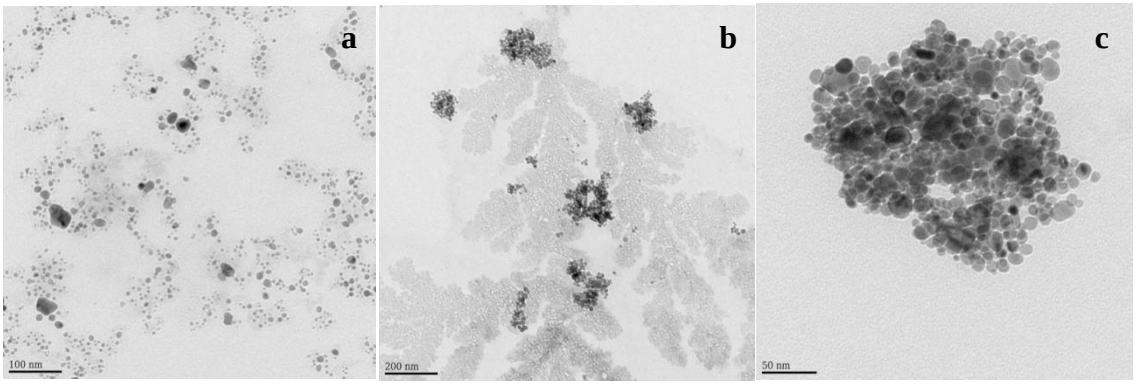

Figure 44. Silver nanoparticle aggregation in the presence of planktonic bacteria using TEM

Silver nanoparticle suspension initially made in the lab (average size = 15 to 21 nm, scale bar = 100 nm) (a); aggregated silver nanoparticles after mixing with *E. coli* culture (sized increased to about 300 nm, scale bar = 200 nm) (b); high magnified image of silver nanoparticles in *E. coli* culture from TEM image (b) (scale bar = 50 nm) (c).

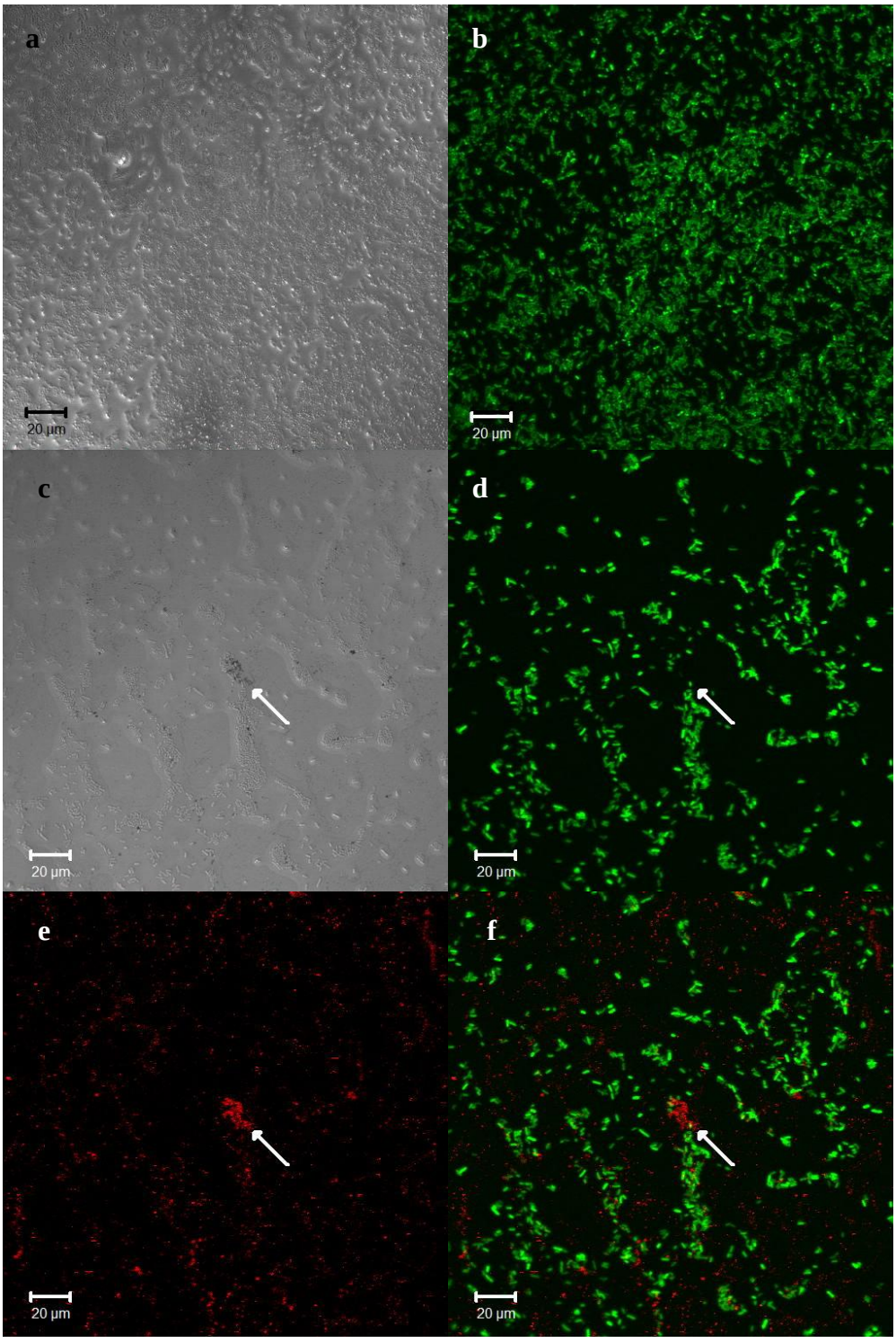

Figure 45. Nanosilver distribution in a thin biofilm:

Negative control biofilm (green) taken with differential interference contrast (DIC) microscopy (a) and confocal scanning laser microscopy (b). Nanosilver exposed biofilm

taken with DIC (c), confocal scanning laser microscopy for biofilm only (d), two-photon laser scanning microscopic images for nanosilver only (e), and a combined image of d and e (f). Scale bars indicate 20 μm.

Spatial Distribution of Nanosilver in Biofilms

The synthesized nanosilver had the surface plasmon resonance band at 400 nm (Figure 46 a), typical for noncovalently stabilized nanosilver. At this excitation wavelength nanosilver showed emission spectra in the visible range (450 - 650 nm) with peaks at 550 and 610 nm (Figure 46 b). Nanosilver in the thin biofilms of *E. coli* expressing green fluorescent protein (GFP) was imaged by confocal laser scanning microscopy. We used GFP as a biofilm reporter because it does not require pretreatment for cell labeling and its fluorescence does not interfere with that from nanosilver. Nanosilver was relatively evenly distributed in a thin biofilm although significant aggregation of the nanosilver particles (arrow) was observed (Figure 45f). In addition, *E. coli* cells appeared to lose their green fluorescent activity (Figure 45 c,d vs. Figure 45a,b) after being exposed to nanosilver possibly due to the antimicrobial action of nanosilver.

Two-photon laser scanning microscopy (2P-LSM) was used to determine the spatial distribution of nanosilver in the thick biofilms (Figure 47). 2P-LSM allows for longer imaging of biological specimens with less photobleaching than conventional confocal microscopy. *E. coli* exposed to nanosilver (red) still had GFP activity (green), as demonstrated by the overlap of the two fluorescence signals (yellow). We detected nanosilver fluorescence up to a depth of 40 μm in a biofilm treated for one hour with nanosilver. We also observed decreasing GFP fluorescence with increasing depth inside the thick biofilm, consistent with a depletion of oxygen since the GFP flurochrome

requires oxygen to develop (Hansen et al., 2001). Although GFP fluorescence at depths deeper than 50 μm (Figure 48) was not visualized, the technique using *E. coli* expressing green fluorescent protein and the indigenous red fluorescent nanosilver provided sufficient capability of determining nanoparticle distribution in biofilms without introducing the potential interference by the fluorescent markers (if applied).

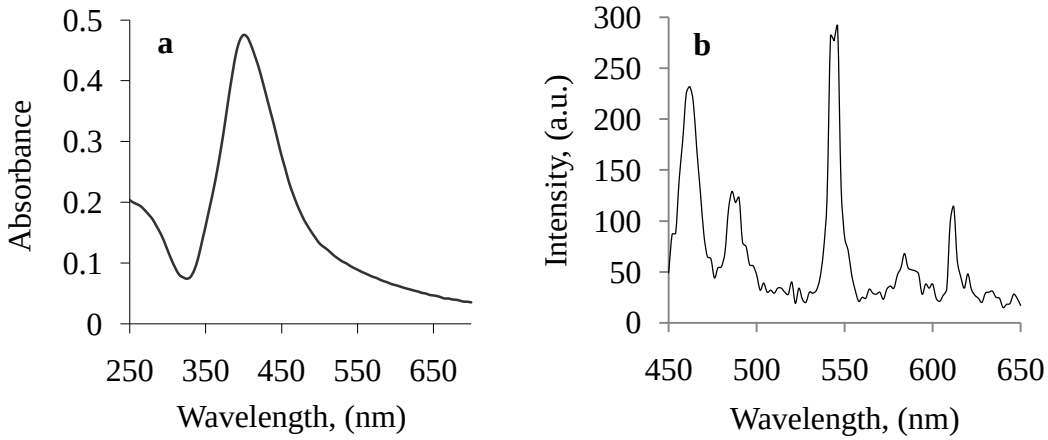

Figure 46. The absorbance and emission spectrum of nanosilver.

(a) UV-Vis absorbance spectrum of nanosilver**,** (b) fluorescence emission spectrum of nanosilver (excitation wavelength = 400 nm).

a

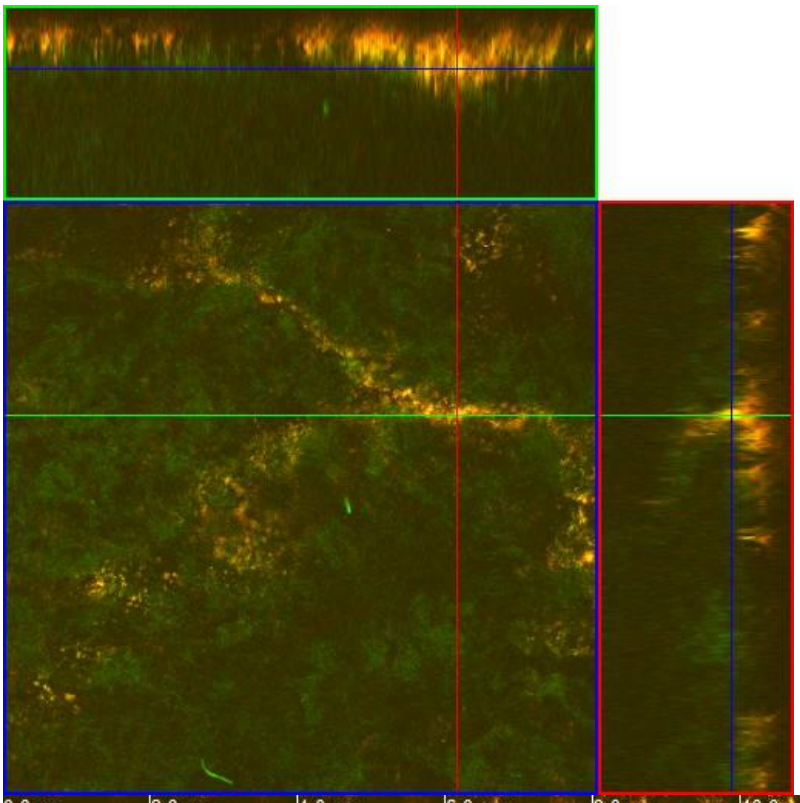

b

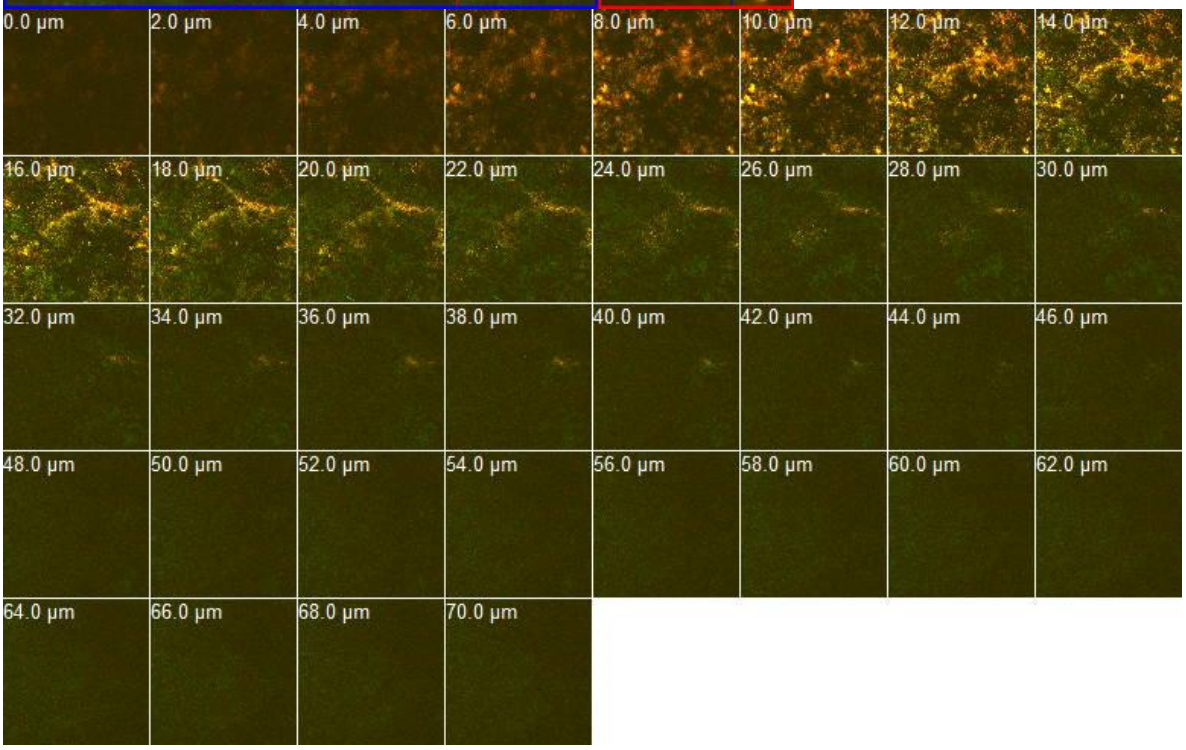

Figure 47. Nanosilver distribution in a thick biofilm using two-photon laser scanning microscopy

the combined image (at 20 μm depth, z-stack image) using the excitation wavelength of 770 nm (for nanosilver, red) and 830 nm (for gfp, green) performed individually with yellow showing overlap of nanosilver and *E. coli* (a); Z-stack image gallery through 70 μm of the biofilm (every 2 μm) while nanosilver was visualized at the biofilm depths of less than 40 μm (b).

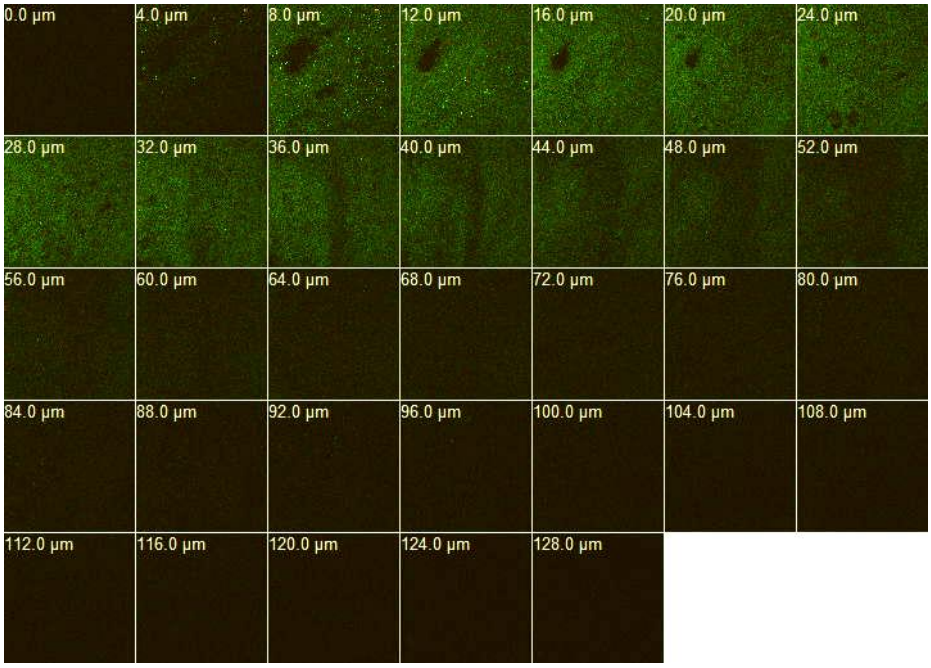

Figure 48. Z-stack images of the negative control, *E. coli*-GFP biofilm without nanosilver. GFP fluorescence gradient (lateral or vertical) was not detected within the >50 μm thick biofilm due to limited diffusive oxygen required to develop GFP.

6.5 Discussion

To our knowledge, this is the first report about local distribution of nanoparticles in biofilms. Our results show that nanosilver penetrated the same range of depths into biofilms as metal ions such as Zn^{2+} (Hu et al., 2005) and Cu^{2+} (Hu et al., 2007). Once biofilms are exposed to heavy metals, metal ions are easily accumulated and immobilized

in biofilms by EPS biosorption and chemical complexation/precipitation with anionic ligands (Hullebusch et al., 2003). Like silver ions, AgNPs are strongly adsorbed to bacterial cells (Benn and Westerhoff, 2008; Elechiguerra et al., 2005; Morones et al., 2005). Dissolution of nanosilver results in the formation of stable Ag_xS_y precipitates in the presence of sulfide (Choi et al., 2009). Interactions of nanosilver with biofilm cells resulted in significant particle aggregation and an increase of aggregate size by a factor of 40 (Figure 43), which decreased apparent particle diffusivity according to the Stokes-Einstein equation. Hence, particle aggregation coupled with retarded diffusive transport of nanosilver and Ag^+ from particle dissolution may lead to biofilms to confer resistance to Ag^+/nanosilver and therefore reduced toxicity.

Biofilms can be up to 1,000 times more resistant to toxicants than the planktonic cells (Mah et al., 2003). The mechanisms of biofilm resistance to antimicrobial agents include efflux pumps, enzyme mediated resistance, target mutations, and adaptation of the outer membrane structure (Harrison et al., 2007). Other possible protection mechanisms include slow penetration of the antimicrobial agents, development of the resistant phenotype, altered microenvironment with different level of metabolic activity within the biofilm, and interactions of the antimicrobial agents with the biofilm (Stewart and William Costerton, 2001). Further study is needed to determine other possible mechanisms of biofilm resistance to nanosilver including different metabolic activity and spatial heterogeneity of antimicrobial resistance gene expression of microbial cells within biofilms.

Nanosilver can impart toxicity in both ion and particle forms (Navarro et al., 2008). Silver ions released from nanosilver may react with the microbial membrane and inactivate cell functions while small particles may enter the cells to disrupt microbial metabolism, making nanosilver highly toxic (Carlson et al., 2008; Choi and Hu, 2008; Jiang et al., 2008). Therefore, the toxicity of nanosilver may be controlled by particle size (cell internalization), Ag^+ release rate (particle stability), and surface characteristics (e.g., surface film formation). These properties may be differentially affected by metal exposure time (i.e., short term vs. long-term) (Navarro et al., 2008) and in various types of media or microorganisms, resulting in changes in the efficacy of antimicrobial activity. While this study mainly determined the short-term nanosilver toxicity, it is possible that in a long-term nanoparticle exposure study, biofilm cells could be more impacted by nanosilver due to the longer term interactions of silver incorporated within the biofilm (e.g., physical entrapment and diffusion limitation for Ag^+ release from nanoparticle dissolution) with bacteria.

It would be desirable to use viability stains to determine the spatial distribution of living biomass within biofilms after nanosilver treatment. We have used a metabolic marker in biofilm cultures, fluorescein diacetate (FDA), which reacts with non-specific esterases in metabolically active micro-organisms to produce green fluorescence (Chavez de Paz et al., 2008). However, results were not promising due to ineffective staining. The redox fluorescence dye, 5-cyano-2,3-ditolyl tetrazolium chloride (CTC), which targets dehydrogenase activity to generate red fluorescence as well as the LIVE/DEAD

BacLight™ stains, could not be used because of the presence of indigenous red fluorescence of nanosilver aggregates.

By using oxygen fluorescence based microrespirometry, the minimum bactericidal concentration and associated number of metabolically active cells in planktonic or biofilm cultures were easily determined in parallel and real time. For comparison purposes, the crystal violet biofilm assay is more time-consuming and error-prone (Figure 49). Since microbial exposure to Ag^{+}/AgNPs likely results in a decrease of microbial activity, and since microbial activity can be precisely determined in a closed system containing biofilm or planktonic cells at the same bacterial concentration, the microresirometric assay developed in this study offers a reliable alternative to traditional microbiological techniques for ecotoxicological research.

Our results highlight the resistance of biofilms to nanosilver toxicity by using a newly developed fluorescence-based microrespirometric assay. By exploiting the indigenous red fluorescence of nanosilver, this study presents a new method to investigate the fate and transport of nanosilver in biofilms for additional research on nano-microbial interactions.

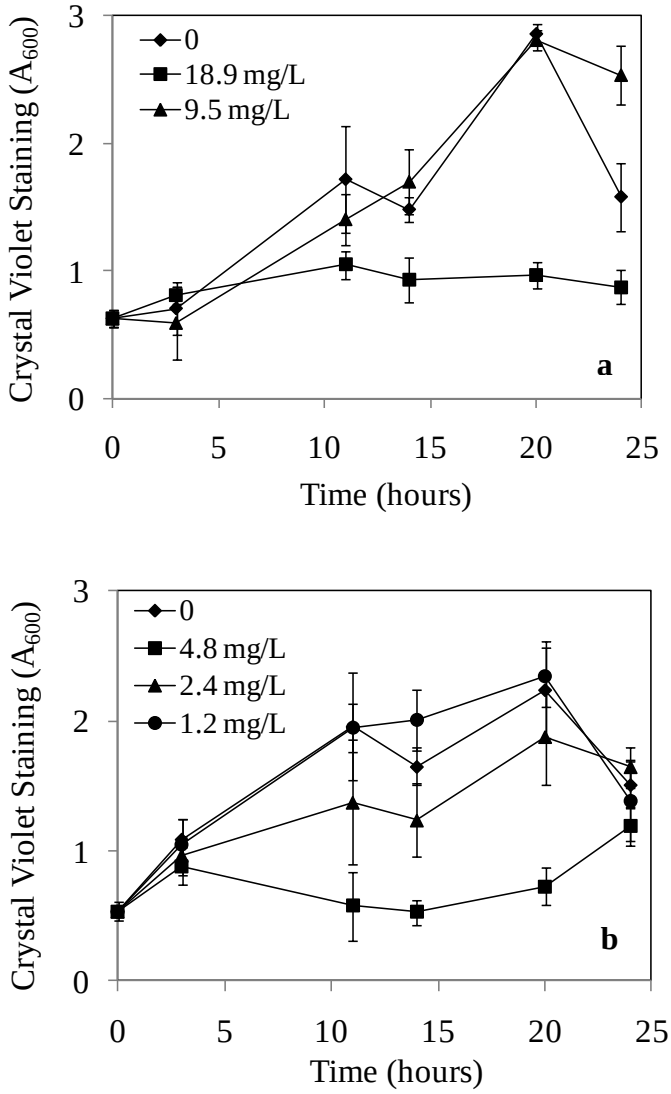

Figure 49. A crystal violet biofilm assay to determine nanosilver toxicity.

Biofilm growth of E. coli PHL628 in polystyrene microtiter wells after being exposed to different concentrations of Ag NPs (a) or Ag^+ (b). The average specific biofilm growth rate for E. coli PHL628 is 0.072 ± 0.003 h^{-1}, which is similar to the biofilm growth (0.08 ± 0.02 h^{-1}) observed in a Staphylococcus Epidermidis biofilm (Zheng and Stewart, 2004). (a) Based on the calculated specific biofilm growth rate, biofilm growth was inhibited 70 % by 18.9 mg/L Ag NPs ($p < 0.001$) but was not influenced by the concentrations less than 9.5 mg/L ($p > 0.5$). (b) No inhibition was observed at Ag^+ concentrations below 1.2 mg/L ($p > 0.5$), but the biofilm growth was reduced significantly by more than 70 % as the Ag^+ concentrations increased to 4.8 mg/L or higher ($p < 0.001$). We observed slight inhibition of biofilm growth at the Ag^+ concentration of 2.4 mg/L, but it is not statistically significant ($p = 0.07$).

7 Summary

The toxicity of silver nanoparticles to planktonic anc biofilm cells was evaluated in this research to better understand environmental implication of nanoparticles as nanotechonology enhanced products are emerging. Silver nanoparticles of known size distribution were prepared in the laboratory for toxic test and they were well distributed in an aqueous suspension. Nitrifying bacteria (a mixture of *nitrosospira, nitrobacter,* and *nitrospira*) were used as model autotrophic organisms and *E. coli* (PHL628) as a representative heterotrophic bacterium. Three kinds of microbial activity/toxicity tests (specific oxygen uptake rate measurement, GFP-tagged microbial fluorescence measurement, and time-resolved microrespirometry) were developed according to the properties of model organisms or microbial growth conditions. The biofilm of *E. coli* was cultivated such that a planktonic cells having the same biomass concentration was paired for nanosilver toxicity comparision between planktonic and biofilm cells. The spatial distribution of nanoparticles in biofilms provides additional information of the fate and transport of nanoparticles inside the biofilms.

Silver nanoparticles strongly inhibited nitrifying bacterial activity. At the same total silver concentrations, silver nanoparticles were more toxic than silver ion to nitrifying bacteria whilesilver ion appeared more toxic to *E. coli* growth than nanosilver. Based on a short-term batch respirometric assay, at 9.3 μM Ag (i.e., 1 mg/L Ag), the inhibitions on nitrifying bacterial growth by Ag NPs, Ag^+ ions and AgCl colloids were 86 ± 3%, 42 ± 7%, and 46 ± 4%, respectively. By using a prolonged microtiter assay, at 4.2 μM Ag, the

inhibitions on the growth of *E. coli* PHL628-gfp by Ag NPs, Ag^+ ions and AgCl colloids were 55 ± 8%, 100%, and 66 ± 6%, respectively.

To understand the mode of antimicrobial action of silver nanoparticles, reactive oxygen species (ROS) inside cells (intracellular) and outside cells (extracellular) were measured after bacterial exposure to nanoparticles. The toxicity of silver nanoparticles was related to intracellular ROS concentration but not extracellular ROS. For comparision purposes, the toxicity of commercially available TiO_2 nanoparticles was evaluated under UVA light because of their semiconductor property. TiO_2 nanoparticles showed much less toxicity to bacteria although they induced higher levels of intracellular ROS than silver nanoparticles. The results indicate that reactive oxygen species are not a good chemical marker to determine nanotoxicity.

Size-dependent toxicity was presented when the bacteria were exposed to silver nanoparticles. Various sizes of silver nanoparticles were prepared by changing the ratio of reducing agent (BH_4^-) / silver ion (Ag^+). The particles with larger portions of smaller size particles (< 5 nm) had higher toxicity to microorganisms, suggesting that dual modes of antimicrobial action by silver nanoparticles may exist inhibition by silver ion through oxidative nanoparticle dissolution and penetration of small size nanoparticles inside the cell, even though the pathway of nanoparticle penetration inside the bacteria is not confirmed.

To reduce nanosilver toxicity, the role of sulfide and ligand strength in controlling nanosilver toxicity to nitrifying bacteria was identified. Sulfide appeared to be the only ligand to effectively reduce nanosilver toxicity. By adding a small aliquot of sulfide that

was stoichiometrically complexed with Ag NPs, the nanosilver toxicity to nitrifying organisms was reduced by up to 80%. Scanning electron microscopy coupled with energy dispersive X-ray analysis indicated that Ag NPs were highly reactive with sulfide to form new Ag_xS_y complexes or precipitates that was stable under aerobic conditions. The results suggest that the toxicity of silver nanoparticles depends on many environmental factors including ionic strength, pH, and chemical compositions in addition to original chemical/physical properties of nanoparticles.

Biofilms were determined to be more resistant to nanosilver inhibition than planktonic cells. In addition, nanosilver was less toxic to biofilms than silver ion. Biofilm cells strongly influenced nanoparticle aggregation, suggesting that biofilms may confer resistance to nanosilver through retarded particle diffusion and particle aggregation. The spatial distribution of nanosilver in biofilms was also analyzed using *E. coli* expressing green fluorescent protein and the indigenous red fluorescence of aggregated silver particles. Nanosilver was distributed evenly in a thin (10 μm) biofilm and penetrated to approximately 40 μm in a thick biofilm after 1 hour exposure.

8 Future Research Work

Further study is needed to determine other possible mechanisms of biofilm resistance to nanosilver including spatially different bacterial activity in biofilms. Nanoparticle aggregations and transport retardation likely caused to reduced toxicity of nanoparticles to biofilm cells (chapter 6). But other factors may be involved in biofilm resistance to nanosilver. While this study mainly determined the short-term nanosilver toxicity, bacterial cells could be more impacted by nanosilver in long-term biofilm exposure studies due to slow and continuous silver ion release. More study is needed to investigate the different composition of Ag^{+}/Ag within the biofilm because of the heterogeneity property of the biofilm bacterial population. Furthermore, in the long-term toxicity study, we are interested in spatial heterogeneity of antimicrobial resistance gene expression of the bacterial cells within biofilms.

The mechanism of cell internalization of small metallic nanoparticle is still less understood in bacterial cells. Also, the fate and effect of nanoparticles inside the cells are not well determined. Although we showed intercellular reactive oxygen species were accumulated in the nanosilver exposed cells, ROS accumulation was related with the toxicity of nanosilver but it might not be used for accurately nano-toxicity prediction. While a trojan-horse type mechanism was proposed to explain high-level toxicity of nanoparticles (Limbach et al., 2007), the fate of small nanoparticles (e.g., size < 10 nm) inside the bacterial cells and the relationship to nanotoxicity are yet to be investigated.

To better understand their environmental impacts, field study of the fate of nanoparticles in different environmental media (ground water, sediments, NAPL,etc) is urgently needed. Because the toxicity of metallic nanoparticles to bacteria and ecological systems depends on nanoparticle properties such as particle size, particle stability, and the binding affinity of original metal to cells, the study of the fate of nanoparticles requires the comprehensive understanding of geo-chemical-bio interactions in the environment. For example, solutions of high ionic strength can affect particle aggregation and various ligands can form a complex with metallic nanoparticles. Based on the data about the fate and toxicity of silver nanoparticles in planktonic and biofilm systems from this study and future work, we will hopefully be able to work on a real natural or engineered system to determine nano-toxicity to wastewater treatment and the environment.

9 Reference

Adams, L.K., Lyon, D.Y. and Alvarez, P.J.J., 2006. Comparative eco-toxicity of nanoscale TiO_2, SiO_2, and ZnO water suspensions. Water Res. 40 (19), 3527-3532.

Alvarez, P.J., 2006. Nanotechnology in the environment - The good, the bad, and the ugly. J. Environ. Engin. -Asce 132, 1233-1233.

Benn, T.M. and Westerhoff, P., 2008. Nanoparticle silver released into water from commercially available sock fabrics. Environ. Sci. Technol., in press, available on line.

Benn, T.M. and Westerhoff, P., 2008. Nanoparticle silver released into water from commercially available sock fabrics. Environ. Sci. Technol. 42 (18), 7025-7026.

Bertram, B.O.B. and Playle, R.C., 2005. Effects of waterborne complexing agents on silver uptake and depuration in rainbow trout. J. Fish Biol. 66 (1), 182-197.

Bianchini, A., Rouleau, C. and Wood, C.M., 2005. Silver accumulation in Daphnia magna in the presence of reactive sulfide. Aqua. Toxicol. 72 (4), 339-349.

Blaser, S.A., Scheringer, M., MacLeod, M. and Hungerbuhler, K., 2008. Estimation of cumulative aquatic exposure and risk due to silver: Contribution of nano-functionalized plastics and textiles. Sci. Total Environ. 390 (2-3), 396-409.

Blum, D.J.W. and Speece, R.E., 1991. A database of chemical toxicity to environmental bacteria and its use in interspecies comparisons and correlations. J. Water Poll. Control. Federation 63, 198-207.

Bojinova, A., Kralchevska, R., Poulios, I. and Dushkin, C., 2007. Anatase/rutile TiO_2 composites: Influence of the mixing ratio on the photocatalytic degradation of Malachite Green and Orange II in slurry. Mater. Chem. Phys. 106 (2-3), 187-192.

Boussiba, S., Resch, C.M. and Gibson, J., 1984. Ammonia uptake and retention in some cyanobacteria. Arch. Microbiol. 138 (4), 287-292.

Burks, B. and Minnis, M., 1994. Onsite wastewater treatment systems. Hogarth House, Ltd., Madison, Wisconsin.

Bury, N.R., Shaw, J., Glover, C. and Hogstrand, C., 2002. Derivation of a toxicity-based model to predict how water chemistry influences silver toxicity to invertebrates. Comp. Biochem. Physiol. Part C: Toxicol. Pharmacol. 133 (1-2), 259-270.

Campbell, P.G., Errécalde, O., Fortin, C., Hiriart-Baer, V.P. and Vigneault, B., 2002. Metal bioavailability to phytoplankton--applicability of the biotic ligand model. Comp. Biochem. Physiol. C Toxicol. Pharmacol. 133 (1-2), 189-206.

Carlson, C., Hussain, S.M., Schrand, A.M., K. Braydich-Stolle, L., Hess, K.L., Jones, R.L. and Schlager, J.J., 2008. Unique cellular interaction of silver nanoparticles: size-dependent generation of reactive oxygen species. J. Phys. Chem. B 112 (43), 13608-13619.

Cervantes, F.J., Pavlostathis, S.G. and van Haandel, A.C., editors. 2006. Advanced Biological Treatment Processes for Industrial Wastewaters: Principles and Applications. IWA Publishing.

Chain, P., Lamerdin, J., Larimer, F., Regala, W., Lao, V., Land, M., Hauser, L., Hooper, A., Klotz, M., Norton, J., Sayavedra-Soto, L., Arciero, D., Hommes, N., Whittaker, M. and Arp, D., 2003. Complete genome sequence of the ammonia-oxidizing bacterium and obligate chemolithoautotroph *Nitrosomonas europaea*. J. Bacteriol. 185 (9), 2759-2773.

Chan, M.A., Lawless, J.L., Lam, S.K. and Lo, D., 2000. Fiber optic oxygen sensor based on phosphorescence quenching of erythrosin B trapped in silica-gel glasses. Anal. Chim. Acta 408 (1-2), 33-37.

Chandran, K. and Smets, B.F., 2000. Single-step nitrification models erroneously describe batch ammonia oxidation profiles when nitrite oxidation becomes rate limiting. Biotechnol. Bioeng. 68, 396-406.

Chavez de Paz, L.E., Hamilton, I.R. and Svensater, G., 2008. Oral bacteria in biofilms exhibit slow reactivation from nutrient deprivation. Microbiol. 154 (7), 1927-1938.

Chen, X. and Stewart, P.S., 2002. Role of electrostatic interactions in cohesion of bacterial biofilms. Appl. Micro.Biotech. 59 (6), 718-720.

Chiemchaisri, C., Jaitrong, L., Honda, R., Fukushi, K. and Yamamoto, K., 2007. Photosynthetic bacteria pond system with infra-red transmitting filter for the treatment and recovery of organic carbon from industrial wastewater. Water Sci. Technol. 56, 109-116.

Chisti, Y., 2007. Biodiesel from microalgae. Biotechnol. Adv. 25 (3), 294-306.

Cho, K.-H., Park, J.-E., Osaka, T. and Park, S.-G., 2005. The study of antimicrobial activity and preservative effects of nanosilver ingredient. Electrochim. Acta 51 (5), 956-960.

Cho, M., Chung, H., Choi, W. and Yoon, J., 2004. Linear correlation between inactivation of *E.coli* and OH radical concentration in TiO_2 photocatalytic disinfection. Water Res. 38 (4), 1069-1077.

Choi, O., Clevenger, T.E., Deng, B., Surampalli, R.Y., Louis Ross, J. and Hu, Z., 2009. Role of sulfide and ligand strength in controlling nanosilver toxicity. Water Res. 43 (7), 1879-1886

Choi, O., Deng, K.K., Kim, N.-J., Ross Jr, L., Surampalli, R.Y. and Hu, Z., 2008. The inhibitory effects of silver nanoparticles, silver ions, and silver chloride colloids on microbial growth. Water Res. 42 (12), 3066-3074.

Choi, O. and Hu, Z., 2008. Size dependent and reactive oxygen species related nanosilver toxicity to nitrifying bacteria. Environ. Sci. Technol. 42, 4583-4588.

Chou, C.S., Yang, R.Y., Weng, M.H. and Yeh, C.H., 2008. Preparation of TiO_2/dye composite particles and their applications in dye-sensitized solar cell. Powder Technol. 187 (2), 181-189.

Cole, J.R. and Halas, N.J., 2006. Optimized plasmonic nanoparticle distributions for solar spectrum harvesting. App. Phys. Lett. 89 (15).

Creighton, J.A. and Eadont, D.G., 1991. Ultraviolet-visible absorption spectra of the colloidal metallic elements. J. Chem. Soc., Faraday Trans. 87, 3881-3891.

De-Bashan, L.E., Moreno, M., Hernandez, J.-P. and Bashan, Y., 2002. Removal of ammonium and phosphorus ions from synthetic wastewater by the microalgae *Chlorella vulgaris* coimmobilized in alginate beads with the microalgae growth-promoting bacterium *Azospirillum brasilense*. Water Res. 36 (12), 2941-2948.

DunphyGuzman, K.A., Finnegan, M.P. and Banfield, J.F., 2006. Influence of surface potential on aggregation and transport of titania nanoparticles. Environ. Sci. Technol. 40 (24), 7688-7693.

Dytczak, M.A., Londry, K.L. and Oleszkiewicz, J.A., 2008. Activated sludge operational regime has significant impact on the type of nitrifying community and its nitrification rates. Water Res. 42 (8-9), 2320-2328.

Efrima, S. and Bronk, B.V., 1998. Silver colloids impregnating or coating bacteria. J. Phys. Chem. B 102, 5947-5950.

Elechiguerra, J., Burt, J., Morones, J., Camacho-Bragado, A., Gao, X., Lara, H. and Yacaman, M., 2005. Interaction of silver nanoparticles with HIV-1. J. Nanobiotechnol. 3 (1), 6-15.

Elechiguerra, J.L., Burt, J.L., Morones, J.R., Camacho-Bragado, A., Gao, X., Lara, H.H. and Yacaman, M.J., 2005. Interaction of silver nanoparticles with HIV-1. J. Nanobiotechnol. 3 (1), 6.

Elkins, J.G., Hassett, D.J., Stewart, P.S., Schweizer, H.P. and McDermott, T.R., 1999. Protective role of catalase in *Pseudomonas aeruginosa* biofilm resistance to hydrogen peroxide. Appl. Environ. Microbiol. 65 (10), 4594-4600.

Farber, J.L., 1994. Mechanisms of cell injury by activated oxygen species. Environ. Health Perspect. 102, 17-24.

Flemming, K., Klingenberg, C., Cavanagh, J.P., Sletteng, M., Stensen, W., Svendsen, J.S. and Flaegstad, T., 2009. High in vitro antimicrobial activity of synthetic antimicrobial peptidomimetics against staphylococcal biofilms. J. Antimicrob. Chemother. 63 (1), 136-145.

Ghijsen, J., Tjeng, L.H., van Elp, J., Eskes, H., Westerink, J., Sawatzky, G.A. and Czyzyk, M.T., 1988. Electronic structure of Cu_2O and CuO. Phys. Rev. B 38 (16), 11322.

Gogoi, S.K., Gopinath, P., Paul, A., Ramesh, A., Ghosh, S.S. and Chattopadhyay, A., 2006. Green fluorescent protein-expressing *Escherichia coli* as a model system for investigating the antimicrobial activities of silver nanoparticles. Langmuir 22 (22), 9322-9328.

González, C., Marciniak, J., Villaverde, S., García-Encina, P. and Muñoz, R., 2008. Microalgae-based processes for the biodegradation of pretreated piggery wastewaters. Appl. Microbiol. Biotechnol. 80 (5), 891-898.

Grady, C.P.L., Daigger, G.T. and Lim, H.C., 1999. Biological wastewater treatment. Marcel Dekker, New York.

Grassian, V.H., O'Shaughnessy, P.T., Adamcakova-Dodd, A., Pettibone, J.M. and Thorne, P.S., 2007. Inhalation exposure study of titanium dioxide nanoparticles with a primary particle size of 2 to 5 nm. Environ. Health Perspect. 115, 397-402.

Green, F.B., Bernstone, L.S., Lundquist, T.J. and Oswald, W.J., 1996. Advanced integrated wastewater pond systems for nitrogen removal. Water Sci. Technol. 33, 207-217.

Hamamoto, A., Mori, M., Takahashi, A., Nakano, M., Wakikawa, N., Akutagawa, M., Ikehara, T., Nakaya, Y. and Kinouchi, Y., 2007. New water disinfection system using UVA light-emitting diodes. J. Applied Microbiol. 103 (6), 2291-2298.

Hansen, M.C., Palmer, R.J., Jr., Udsen, C., White, D.C. and Molin, S., 2001. Assessment of GFP fluorescence in cells of Streptococcus gordonii under conditions of low pH and low oxygen concentration. Microbiology 147 (5), 1383-1391.

Harrison, J.J., Ceri, H., Roper, N.J., Badry, E.A., Sproule, K.M. and Turner, R.J., 2005. Persister cells mediate tolerance to metal oxyanions in *Escherichia coli*. Microbiol. 151 (10), 3181-3195.

Harrison, J.J., Ceri, H. and Turner, R.J., 2007. Multimetal resistance and tolerance in microbial biofilms. Nat. Rev. Micro. 5 (12), 928-938.

Harrison, J.J., Turner, R.J. and Ceri, H., 2005. Persister cells, the biofilm matrix and tolerance to metal cations in biofilm and planktonic *Pseudomonas aeruginosa*. Environ. Microbiol. 7 (7), 981-994.

Heinlaan, M., Ivask, A., Blinova, I., Dubourguier, H.-C. and Kahru, A., 2008. Toxicity of nanosized and bulk ZnO, CuO and TiO_2 to bacteria *Vibrio fischeri* and crustaceans *Daphnia magna* and *Thamnocephalus platyurus*. Chemosphere 71 (7), 1308-1316.

Henglein, A., 1998. Colloidal silver nanoparticles: Photochemical preparation and interaction with O^{-2}, CCl_4, and some metal ions. J. Mater. Chem. 10 (1), 444-450.

Ho, L., Hoefel, D., Aunkofer, W., Meyn, T., Keegan, A., Brookes, J., Saint, C. and Newcombe, G., 2006. Biological filtration for the removal of algal metabolites from drinking water. Water Sci. Technol.: Water Supply 6, 153-159.

Holt, K.B. and Bard, A.J., 2005. Interaction of silver(I) Ions with the respiratory chain of *Escherichia coli*: An electrochemical and scanning electrochemical microscopy study of the antimicrobial mechanism of micromolar Ag^{+}. Biochemistry 44 (39), 13214-13223.

Hu, Q., Westerhoff, P. and Vermaas, W., 2000. Removal of nitrate from groundwater by *Cyanobacteria*: Quantitative assessment of factors influencing nitrate uptake. Appl. Environ. Microbiol. 66 (1), 133-139.

Hu, Z., Hidalgo, G., Houston, P.L., Hay, A.G., Shuler, M.L., Abruna, H.D., Ghiorse, W.C. and Lion, L.W., 2005. Determination of spatial distributions of zinc and active biomass in microbial biofilms by two-photon laser scanning microscopy. Appl. Environ. Microbiol. 71 (7), 4014-4021.

Hu, Z., Jin, J., Abruna, H.D., Houston, P.L., Hay, A.G., Ghiorse, W.C., Shuler, M.L., Hidalgo, G. and Lion, L.W., 2007. Spatial distributions of copper in microbial biofilms by scanning electrochemical microscopy. Environ. Sci.Technol. 41 (3), 936-941.

Hu, Z.Q., Chandran, K., Grasso, D. and Smets, B.F., 2002. Effect of nickel and cadmium speciation on nitrification inhibition. Environ. Sci. Technol. 36 (14), 3074-3078.

Hu, Z.Q., Chandran, K., Grasso, D. and Smets, B.F., 2003. Impact of metal sorption and internalization on nitrification inhibition. Environ. Sci. Technol. 37 (4), 728-734.

Hullebusch, E.D.v., Zandvoort, M. and Lens, P., 2003. Metal immobilisation by biofilms: Mechanisms and analytical tools. Rev. Environ. Sci. Biotechnol. 2 (1), 9-33.

Huss, V.A.R., Frank, C., Hartmann, E.C., Hirmer, M., Kloboucek, A., Seidel, B.M., Wenzeler, P. and Kessler, E., 1999. Biochemical taxonomy and molecular phylogeny of the genus *Chlorella* sensu lato (Chlorophyta). J. Phycol. 35, 587-598.

Hussain, S.M., Hess, K.L., Gearhart, J.M., Geiss, K.T. and Schlager, J.J., 2005. In vitro toxicity of nanoparticles in BRL 3A rat liver cells. Toxicol. in Vitro 19 (7), 975-983.

Hyung, H., Fortner, J.D., Hughes, J.B. and Kim, J.-H., 2007. Natural organic matter stabilizes carbon nanotubes in the aqueous phase. Environ. Sci. Technol. 41 (1), 179-184.

Innis, M.A., Gelfand, D.H., Sninsky, J.J. and White, T.J., 1990. PCR protocols: a quide to methods and applications. Academic Press, Inc, San Diego.

Inoue, Y., Hoshino, M., Takahashi, H., Noguchi, T., Murata, T., Kanzaki, Y., Hamashima, H. and Sasatsu, M., 2002. Bactericidal activity of Ag-zeolite mediated by reactive oxygen species under aerated conditions. J. Inorg. Biochem. 92 (1), 37-42.

Janes, N. and Playle, R.C., 1995. Modeling silver binding to gills of rainbow trout (*Oncorhynchus mykiss*). Environ. Toxicol. Chem. 14 (11), 1847-1858.

Jang, J.S., Li, W., Oh, S.H. and Lee, J.S., 2006. Fabrication of CdS/TiO_2 nano-bulk composite photocatalysts for hydrogen production from aqueous H_2S solution under visible light. Chem. Phy. Lett. 425 (4-6), 278-282.

Janssen, A.J.H., Meijer, S., Bontsema, J. and Lettinga, G., 1998. Application of the redox potential for controlling a sulfide oxidizing bioreactor. Biotechnol. Bioeng. 60 (2), 147-155.

Jiang, W., KimBetty, Y.S., Rutka, J.T. and ChanWarren, C.W., 2008. Nanoparticle-mediated cellular response is size-dependent. Nat. Nano. 3 (3), 145-150.

Joye, S.B. and Hollibaugh, J.T., 1995. Influence of sulfide inhibition of nitrification on nitrogen regeneration in sediments. Science 270 (5236), 623-625.

Jung, W.K., Koo, H.C., Kim, K.W., Shin, S., Kim, S.H. and Park, Y.H., 2008. Antibacterial activity and mechanism of action of the silver ion on *Staphylococcus aureus* and *Escherichia coli*. Appl. Environ. Microbiol., Published.

Junker, L.M., Peters, J.E. and Hay, A.G., 2006. Global analysis of candidate genes important for fitness in a competitive biofilm using DNA-array-based transposon mapping. Microbiol. 152 (8), 2233-2245.

Kahraman, M., Yazici, M.M., Sahin, F., Bayrak, O.F. and Culha, M., 2007. Reproducible surface-enhanced Raman scattering spectra of bacteria on aggregated silver nanoparticles. Appl. Spectrosc. 61, 479–485.

Kallqvist, T. and Svenson, A., 2003. Assessment of ammonia toxicity in tests with the microalga, *Nephroselmis pyriformis, Chlorophyta*. Water Res. 37, 477-484.

Karunakaran, C. and Dhanalakshmi, R., 2008. Semiconductor-catalyzed degradation of phenols with sunlight. Sol. Energ. Mater. Sol. Cell. 92 (11), 1315-1321.

Kelly, K.L., Coronado, E., Zhao, L.L. and Schatz, G.C., 2003. The optical properties of metal nanoparticles: The influence of size, shape, and dielectric environment. J. Phys. Chem. B 107 (3), 668-677.

Keren, I., Kaldalu, N., Spoering, A., Wang, Y. and Lewis, K., 2004. Persister cells and tolerance to antimicrobials. FEMS Microbiol. Lett. 230 (1), 13-18.

Kim, J.S., Kuk, E., Yu, K.N., Kim, J.H., Park, S.J., Lee, H.J., Kim, S.H., Park, Y.K., Park, Y.H., Hwang, C.Y., Kim, Y.K., Lee, Y.S., Jeong, D.H. and Cho, M.H., 2007. Antimicrobial effects of silver nanoparticles. Nanomedicine 3 (1), 95-101.

Kim, Y., Wang, X., Ma, Q., Zhang, X.-S. and Wood, T.K., 2009. Toxin-antitoxin systems in *Escherichia coli* influence biofilm formation through YjgK (TabA) and Fimbriae. J. Bacteriol. 191 (4), 1258-1267.

Kloepfer, J.A., Mielke, R.E. and Nadeau, J.L., 2005. Uptake of CdSe and CdSe/ZnS quantum dots into bacteria via purine-dependent mechanisms. Appl. Environ. Microbiol. 71 (5), 2548-2557.

Kohn, T. and Nelson, K.L., 2007. Sunlight-mediated inactivation of MS2 coliphage via exogenous singlet oxygen produced by sensitizers in natural waters. Environ. Sci. Technol. 41 (1), 192-197.

Kong, H. and Jang, J., 2006. One-step fabrication of silver nanoparticle embedded polymer nanofibers by radical-mediated dispersion polymerization. Chem. Comm. (28), 3010-3012.

Kormann, C., Bahnemann, D.W. and Hoffmann, M.R., 1988. Preparation and characterization of quantum-size titanium dioxide. J. Physic. Chem. 92 (18), 5196-5201.

Kulinowski, K.M. (2008) Environmental impacts of nanosilver, An ICON Backgrounder.

Lee, C., Kim, J.Y., Lee, W.I., Nelson, K.L., Yoon, J. and Sedlak, D.L., 2008. Bactericidal effect of zero-valent iron nanoparticles on *Escherichia coli*. Environ. Sci. Technol. 42 (13), 4927-4933.

Lee, D.Y., Fortin, C. and Campbell, P.G.C., 2005. Contrasting effects of chloride on the toxicity of silver to two green algae, Pseudokirchneriella subcapitata and Chlamydomonas reinhardtii. Aqua. Toxicol. 75 (2), 127-135.

Lee, K.J., Nallathamby, P.D., Browning, L.M., Osgood, C.J. and Xu, X.-H.N., 2007. In vivo imaging of transport and biocompatibility of single silver nanoparticles in early development of Zebrafish embryos. ACS Nano 1 (2), 133-143.

Lenz, A.P., Williamson, K.S., Pitts, B., Stewart, P.S. and Franklin, M.J., 2008. Localized gene expression in *Pseudomonas aeruginosa* biofilms. Appl. Environ. Microbiol. 74 (14), 4463-4471.

Limbach, L.K., Bereiter, R., Müller, E., Krebs, R., Gälli, R. and Stark, W.J., 2008. Removal of oxide nanoparticles in a model wastewater treatment plant: influence of

agglomeration and surfactants on clearing efficiency. Environ. Sci. Technol. 42 (15), 5828-5833.

Limbach, L.K., Li, Y., Grass, R.N., Brunner, T.J., Hintermann, M.A., Muller, M., Gunther, D. and Stark, W.J., 2005. Oxide nanoparticle uptake in human lung fibroblasts: effects of particle size, agglomeration, and diffusion at low concentrations. Environ. Sci. Technol. 39 (23), 9370-9376.

Limbach, L.K., Wick, P., Manser, P., Grass, R.N., Bruinink, A. and Stark, W.J., 2007. Exposure of engineered nanoparticles to human lung epithelial cells: influence of chemical composition and catalytic activity on oxidative stress. Environ. Sci. Technol. 41 (11), 4158-4163.

Lok, C.N., Ho, C.M., Chen, R., He, Q.Y., Yu, W.Y., Sun, H., Tam, P.K.H., Chiu, J.F. and Che, C.M., 2007. Silver nanoparticles: partial oxidation and antibacterial activities. J. Biol. Inorg. Chem. 12 (4), 527-534.

Lok, C.N., Ho, C.M., Chen, R., He, Q.Y., Yu, W.Y., Sun, H.Z., Tam, P.K.H., Chiu, J.F. and Che, C.M., 2006. Proteomic analysis of the mode of antibacterial action of silver nanoparticles. J. Proteome Res. 5 (4), 916-924.

Long, T.C., Saleh, N., Tilton, R.D., Lowry, G.V. and Veronesi, B., 2006. Titanium dioxide (P25) produces reactive oxygen species in immortalized brain microglia (BV2): Implications for nanoparticle neurotoxicity. Environ. Sci.Technol. 40 (14), 4346-4352.

Madigan, M., Martinko, J.M. and Parker, J., 2000. Brock biology of microorganisms. Prentice Hall, Upper Saddle River, NJ.

Madigan, M., Martinko, J.M. and Parker, J., 2005. Brock Biology of Microorganisms. Prentice Hall, Upper Saddle River, NJ.

Madigon, M.T. and Martinko, J.M., 2006. Biology of microorganisms. Pearson Prentice Hall, Upper Saddle River, NJ.

Mah, T.-F., Pitts, B., Pellock, B., Walker, G.C., Stewart, P.S. and O'Toole, G.A., 2003. A genetic basis for *Pseudomonas aeruginosa* biofilm antibiotic resistance. Nature 426 (6964), 306-310.

Mah, T.C. and O'Toole, G.A., 2001. Mechanisms of biofilm resistance to antimicrobial agents. Trends Microbiol. 9 (1), 34-39.

Makarewicz, J.C., Boyer, G.L., Lewis, T.W., Guenther, W., Atkinson, J. and Arnold, M., 2009. Spatial and temporal distribution of the cyanotoxin microcystin-LR in the Lake Ontario ecosystem: Coastal embayments, rivers, nearshore and offshore, and upland lakes. J. Great Lakes Res. 35, 83-89.

Mandal, S. and Mallick, N., 2009. Microalga *Scenedesmus obliquus* as a potential source for biodiesel production. Appl. Micro. Biotechnol., 1-11.

Matsumura, Y., Yoshikata, K., Kunisaki, S. and Tsuchido, T., 2003. Mode of bactericidal action of silver zeolite and its comparison with that of silver nitrate. Appl. Environ. Micro. 69 (7), 4278-4281.

Maynard, A.D. and Michelson, E., 2006. The Nanotechnology Consumer Product Inventory, http://www.nanotechproject.org/44.

Mayo, A.W. and Noike, T., 1994. Effect of glucose loading on the growth behavior of Chlorella vulgaris and heterotrophic bacteria in mixed culture. Water Res. 28, 1001-1008.

McCullagh, C., Robertson, J.M.C., Bahnemann, D.W. and Robertson, P.K.J., 2007. The application of TiO_2 photocatalysis for disinfection of water contaminated with pathogenic micro-organisms: a review. Res. Chem. Intermed. 33, 359-375.

Miller, M.B. and Bassler, B.L., 2001. Quorum sensing in bacteria. Annu. Rev. Microbiol. 55 (1), 165-199.

Moore, M.N., 2006. Do nanoparticles present ecotoxicological risks for the health of the aquatic environment? Environ. Intern. 32 (8), 967-976.

Moreau, J.W., Weber, P.K., Martin, M.C., Gilbert, B., Hutcheon, I.D. and Banfield, J.F., 2007. Extracellular proteins limit the dispersal of biogenic nanoparticles. Science 316 (5831), 1600-1603.

Morones, J.R., Elechiguerra, J.L., Camacho, A., Holt, K., Kouri, J.B., Ramirez, J.T. and Yacaman, M.J., 2005. The bactericidal effect of silver nanoparticles. Nanotechnol. 16 (10), 2346-2353.

Mueller, N.C. and Nowack, B., 2008. Exposure modeling of engineered nanoparticles in the environment. Environ. Sci. Technol. 42 (12), 4447–4453.

Muñoz, R. and Guieysse, B., 2006. Algal-bacterial processes for the treatment of hazardous contaminants: A review. Water Res. 40 (15), 2799-2815.

Navarro, E., Piccapietra, F., Wagner, B., Marconi, F., Kaegi, R., Odzak, N., Sigg, L. and Behra, R., 2008. Toxicity of silver nanoparticles to *Chlamydomonas reinhardtii*. Environ. Sci. Technol. 42 (23), 8959-8964.

Navarro, E., Piccapietra, F., Wagner, B., Marconi, F., Kaegi, R., Odzak, N., Sigg, L. and Behra, R., 2008. Toxicity of silver nanoparticles to *Chlamydomonas reinhardtii*. Environ. Sci.Technol. 42 (23), 8959-8964.

Navarro, E., Piccapietra, F., Wagner, B., Marconi, F., Kaegi, R., Odzak, N., Sigg, L. and Behra, R., 2008. Toxicity of silver Nanoparticles to *Chlamydomonas reinhardtii*. Environ. Sci. Technol.

Nel, A., Xia, T., Madler, L. and Li, N., 2006. Toxic potential of materials at the nanolevel. Science 311 (5761), 622-627.

Newman, M.C. and Unger, M.A., 2003. Fundamentals of ecotoxicology CRC Press.

Nielsen, A.H., Vollertsen, J., Jensen, H.S., Madsen, H.I. and Hvitved-Jacobsen, T., 2008. Aerobic and anaerobic transformations of sulfide in a sewer system field study and model simulations. Water Environ. Res. 80, 16-25.

Niyogi, S. and Wood, C.M., 2004. Biotic ligand model, a flexible tool for developing site-specific water quality guidelines for metals. Environ. Sci. Technol. 38 (23), 6177-6192.

Noredal, T.k.I., Johansson Mats, Rosenquist Magnus, Pell Mikael, Hansson Mikael and Hallin Sara, 2007. Silver (Ag(+)) reduces denitrification and induces enrichment of novel *nirK* genotypes in soil. FEMS Micro. Lett. 270 (2), 189-194.

Nubel, U., Garcia-Pichel, F. and Muyzer, G., 1997. PCR primers to amplify 16S rRNA genes from cyanobacteria. Appl. Environ. Microbiol. 63 (8), 3327-3332.

O'Mahony, F.C., O'Donovan, C., Hynes, J., Moore, T., Davenport, J. and Papkovsky, D.B., 2005. Optical oxygen microrespirometry as a platform for environmental toxicology and animal model studies. Environ. Sci. Technol. 39 (13), 5010-5014.

O'Mahony, F.C. and Papkovsky, D.B., 2006. Rapid high-throughput assessment of aerobic bacteria in complex samples by fluorescence-based oxygen respirometry. Appl. Environ. Microbiol. 72 (2), 1279-1287.

Pal, S., Tak, Y.K. and Song, J.M., 2007. Does the antibacterial activity of silver nanoparticles depend on the shape of the nanoparticle? A study of the gram-negative bacterium *Escherichia coli*. Appl. Environ. Microbiol. 73 (6), 1712-1720.

Petit, C., Lixon, P. and Pileni, M.P., 1993. In-situ synthesis of silver nanocluster in aot reverse micelles. J. Phys. Chem. 97 (49), 12974-12983.

Polyak, K., Xia, Y., Zweier, J.L., Kinzler, K.W. and Vogelstein, B., 1997. A model for p53-induced apoptosis. Nature 389 (6648), 300-305.

Porel, S., Singh, S. and Radhakrishnan, T.P., 2005. Polygonal gold nanoplates in a polymer matrix. Chem. Commun. (18), 2387-2389.

Priester, J.H., Horst, A.M., Van De Werfhorst, L.C., Saleta, J.L., Mertes, L.A.K. and Holden, P.A., 2007. Enhanced visualization of microbial biofilms by staining and environmental scanning electron microscopy. J. Microbiol. Methods 68 (3), 577-587.

Qureshi, F.M., Badar, U. and Ahmed, N., 2001. Biosorption of copper by a bacterial biofilm on a flexible polyvinyl chloride conduit. Appl. Environ. Microbiol. 67 (9), 4349-4352.

Radniecki, T.S., Dolan, M.E. and Semprini, L., 2008. Physiological and transcriptional responses of *Nitrosomonas europaea* to toluene and benzene inhibition. Environ. Sci. Technol. 42 (11), 4093-4098.

Radniecki, T.S. and Ely, R.L., 2008. Zinc chloride inhibition of *Nitrosococcus mobilis*. Biotechnol. Bioeng. 99 (5), 1085-1095.

Rand, B.P., Peumans, P. and Forrest, S.R., 2004. Long-range absorption enhancement in organic tandem thin-film solar cells containing silver nanoclusters. J. Appl. Phys. 96, 7519-7526.

Ratte, H.T., 1999. Bioaccumulation and toxicity of silver compounds: A review. Environ. Toxicol. Chem. 18 (1), 89-108.

Redwood, P.S., Lead, J.R., Harrison, R.M., Jones, I.P. and Stoll, S., 2005. Characterization of humic substances by environmental scanning electron microscopy. Environ. Sci. Technol. 39 (7), 1962-1966.

Risgaard-Petersen, N., Nicolaisen, M.H., Revsbech, N.P. and Lomstein, B.A., 2004. Competition between ammonia-oxidizing bacteria and benthic microalgae. Appl. Environ. Microbiol. 70 (9), 5528-5537.

Rozan, T.F., Lassman, M.E., Ridge, D.P. and Luther, G.W., 2000. Evidence for iron, copper and zinc complexation as multinuclear sulphide clusters in oxic rivers. Nature 406 (6798), 879-882.

Sabatini, C.A., Pereira, R.V. and Gehlen, M.H., 2007. Fluorescence modulation of acridine and coumarin dyes by silver nanoparticles. J. Fluores. 17 (4), 377-382.

Sambhy, V., MacBride, M.M., Peterson, B.R. and Sen, A., 2006. Silver bromide nanoparticle/polymer composites: Dual action tunable antimicrobial materials. J. Am. Chem. Soc. 128 (30), 9798-9808.

Savage, N. and Diallo, M.S., 2005. Nanomaterials and water purification: Opportunities and challenges. J. Nano. Res. 7 (4-5), 331-342.

Sayes, C.M., Gobin, A.M., Ausman, K.D., Mendez, J., West, J.L. and Colvin, V.L., 2005. Nano-C_{60} cytotoxicity is due to lipid peroxidation. Biomaterials 26 (36), 7587-7595.

Schecher, W.D. and McAvoy, D.C., 2001. A chemical equilibrium modeling system, Version 4.6 for Windows. Environmental Research Software.

Shafer, M.M., Overdier, J.T. and Armstong, D.E., 1998. Removal, partitioning, and fate of silver and other metals in wastewater treatment plants and effluent-receiving streams. Environ. Toxicol. Chem. 17 (4), 630-641.

Siripong, S. and Rittmann, B.E., 2007. Diversity study of nitrifying bacteria in full-scale municipal wastewater treatment plants. Water Res. 41 (5), 1110-1120.

Sondi, I. and Salopek-Sondi, B., 2004. Silver nanoparticles as antimicrobial agent: a case study on *E. coli* as a model for Gram-negative bacteria. J. Colloid Interface Sci. 275 (1), 177-182.

Srikant, V. and Clarke, D.R., 1998. On the optical band gap of zinc oxide. J. Appl. Phys. 83 (10), 5447-5451.

Stewart, P.S. and Franklin, M.J., 2008. Physiological heterogeneity in biofilms. Nat. Rev. Micro. 6 (3), 199-210.

Stewart, P.S. and William Costerton, J., 2001. Antibiotic resistance of bacteria in biofilms. Lancet 358 (9276), 135-138.

Strik, D.P.B.T.B., Terlouw, H., Hamelers, H.V.M. and Buisman, C.J.N., 2008. Renewable sustainable biocatalyzed electricity production in a photosynthetic algal microbial fuel cell (PAMFC). Appl. Micro. Biotechnol. 81 (4), 659-668.

Stumm, W. and Morgan, J.J., 1996. Aquatic chemistry:Chemical equilibria and rates in natural waters. John Wiley & Sons, Inc., New York.

Tchobanoglous, G., Burton, F.L. and Stensel, H.D., 2003. Wastewater engineering treatment, disposal, and reuse. McGraw-Hill, New York.

Teitzel, G.M. and Parsek, M.R., 2003. Heavy metal resistance of biofilm and planktonic *Pseudomonas aeruginosa*. Appl. Environ. Microbiol. 69 (4), 2313-2320.

Tsuneda, S., Aikawa, H., Hayashi, H., Yuasa, A. and Hirata, A., 2003. Extracellular polymeric substances responsible for bacterial adhesion onto solid surface. FEMS Microbiol. Lett. 223 (2), 287-292.

Verma, A., Uzun, O., Hu, Y., Hu, Y., Han, H.-S., Watson, N., Chen, S., Irvine, D.J. and Stellacci, F., 2008. Surface-structure-regulated cell-membrane penetration by monolayer-protected nanoparticles. Nat Mater 7 (7), 588-595.

Wang, H. and Joseph, J.A., 1999. Quantifying cellular oxidative stress by dichlorofluorescein assay using microplate reader. Adv. Free Radic. Biol. Med. 27 (5-6), 612-616.

Wang, J.M., 2003. Interactions of silver with wastewater constituents. Water Res. 37 (18), 4444-4452.

Wang, Q., Garrity, G.M., Tiedje, J.M. and Cole, J.R., 2007. Naive bayesian classifier for rapid assignment of rRNA sequences into the new bacterial taxonomy. Appl. Environ. Microbiol. 73 (16), 5261-5267.

Wang, Y., Wu, M. and Zhang, W.F., 2008. Preparation and electrochemical characterization of TiO_2 nanowires as an electrode material for lithium-ion batteries. Electrochim. Acta 53 (27), 7863-7868.

Wei, C., Lin, W.Y., Zainal, Z., Williams, N.E., Zhu, K., Kruzic, A.P., Smith, R.L. and Rajeshwar, K., 1994. Bactericidal activity of TiO_2 photocatalyst in aqueous-media - toward a solar-assisted water disinfection system. Environ. Sci.Technol. 28 (5), 934-938.

Wenseleers, W., Stellacci, F., Meyer-Friedrichsen, T., Mangel, T., Bauer, C.A., Pond, S.J.K., Marder, S.R. and Perry, J.W., 2002. Five orders-of-magnitude enhancement of two-photon absorption for dyes on silver nanoparticle fractal clusters. J. Phys. Chem. B 106 (27), 6853-6863.

White, D., 2000. The physiology and biochemistry of prokaryotes. Oxford University Press, Inc, New York.

Wiesner, M.R., Lowry, G.V., Alvarez, P., Dionysiou, D. and Biswas, P., 2006. Assessing the risks of manufactured nanomaterials. Environ. Sci. Technol. 40 (14), 4336-4345.

Wu, H.L., Hseu, R.S. and Lin, L.P., 2001. Identification of *Chlorella* spp. isolates using ribosomal DNA sequences. Bot. Bull. Acad. Sin. 42 (2), 115-121.

Yamaguchi, H., Matsuda, K. and Irie, M., 2007. Excited-state behavior of a fluorescent and photochromic diarylethene on silver nonoparticles. J. Phys. Chem. C 111 (10), 3853-3862.

Yamamoto, S. and Watarai, H., 2006. Surface-enhanced Raman spectroscopy of dodecanethiol-bound silver nanoparticles at the liquid/liquid interface. Langmuir 22, 6562-6569.

Yamanaka, M., Hara, K. and Kudo, J., 2005. Bactericidal actions of a silver ion solution on *Escherichia coli*, studied by energy-filtering transmission electron microscopy and proteomic analysis. Appl. Environ. Microbiol. 71 (11), 7589-7593.

Yoshida, M., Yoshida, T., Kashima, A., Takashima, Y., Hosoda, N., Nagasaki, K. and Hiroishi, S., 2008. Ecological dynamics of the toxic bloom-forming cyanobacterium Microcystis aeruginosa and its cyanophages in freshwater. Appl. Environ. Microbiol. 74, 3269-3273.

Zhai, H.J., Sun, D.W. and Wang, H.S., 2006. Catalytic properties of silica/silver nanocomposites. J. Nanosci. Nanotechnol. 6, 1968-1972.

Zhang, H., Gilbert, B., Huang, F. and Banfield, J.F., 2003. Water-driven structure transformation in nanoparticles at room temperature. Nature 424 (6952), 1025-1029.

Zhang, Y., Chen, Y., Westerhoff, P., Hristovski, K. and Crittenden, J.C., 2008. Stability of commercial metal oxide nanoparticles in water. Water Res. 42 (8-9), 2204-2212.

Zheng, Z. and Stewart, P.S., 2004. Growth limitation of *Staphylococcus epidermidis* in biofilms contributes to rifampin tolerance. Biofilms 1 (01), 31-35.

Zhou, B., Nichols, J., Playle, R.C. and Wood, C.M., 2005. An in vitro biotic ligand model (BLM) for silver binding to cultured gill epithelia of freshwater rainbow trout (*Oncorhynchus mykiss*). Toxicol. Appl. Pharmacol. 202 (1), 25-37.

10 APPENDIX A: Nitrification Performance Data Collected from the Continous Flow Autotrophic Bioreactor

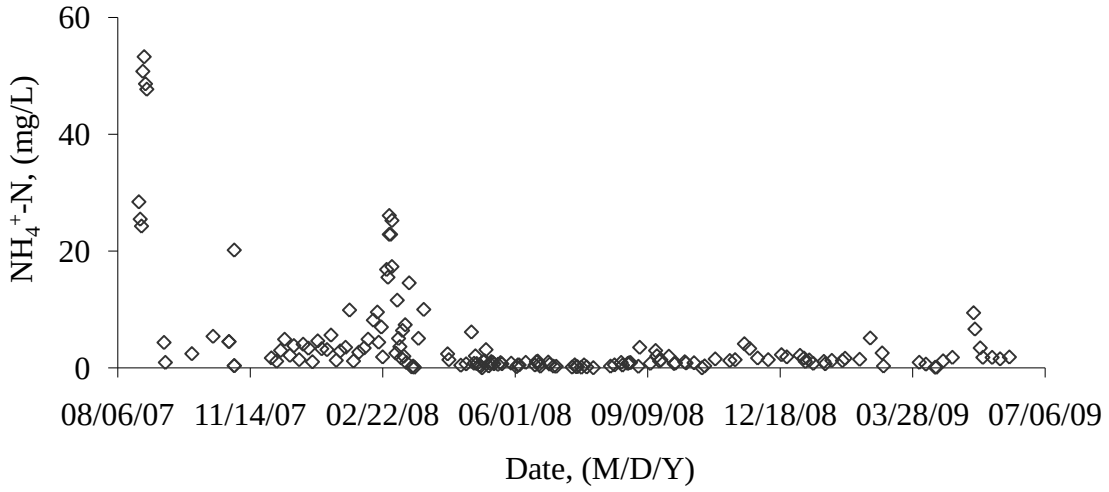

Figure 50. Effluent aNH_4^+-N concentrations during the period of study.

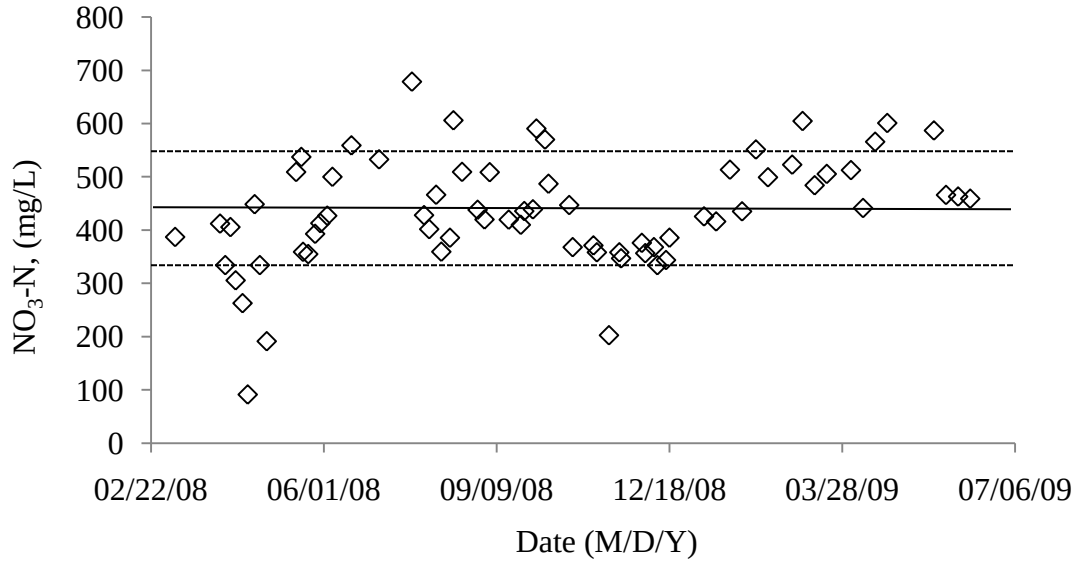

Figure 51. Effluent NO_3^--N concentrations during the period of study.

Horizontal lines indicated average of nitrate-N, (437±104) mg/L.

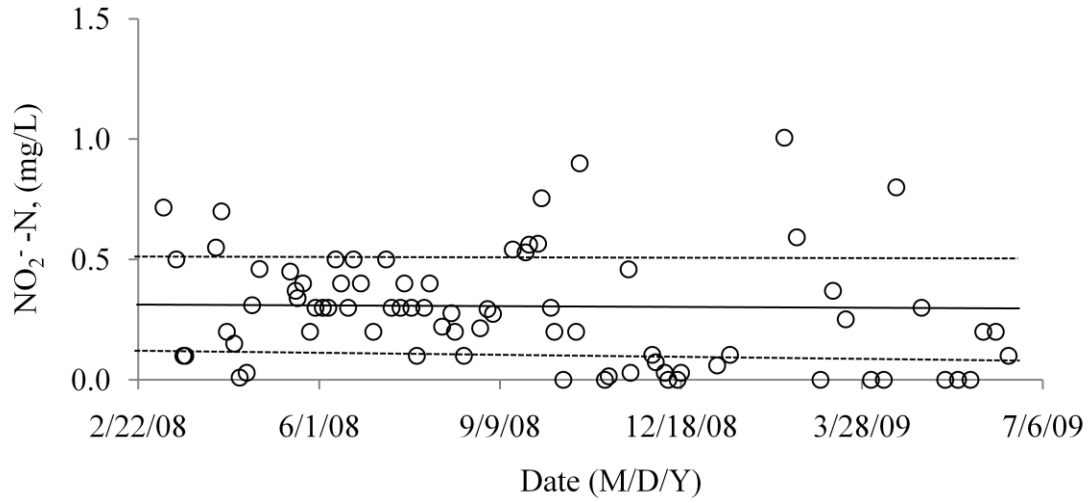

Figure 52. Effluent NO_2^--N concentrations during the period of study.

Horizontal lines indicated average of nitrite-N, (0.3±0.2) mg/L.

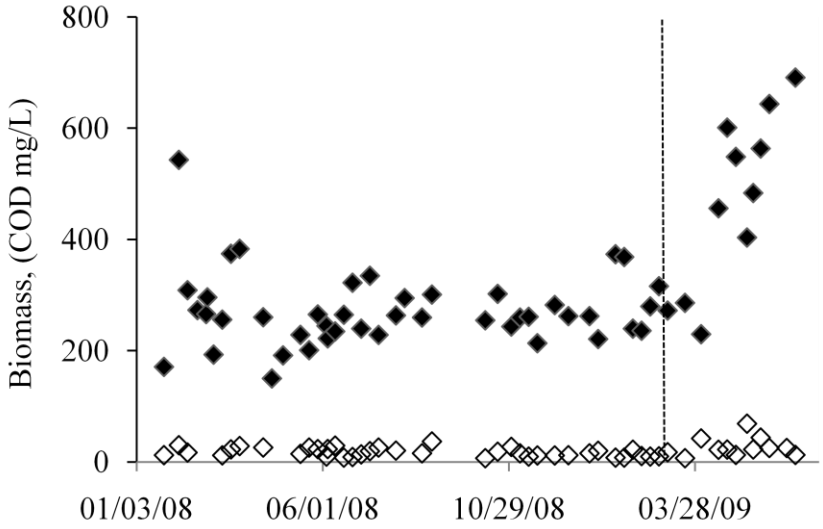

Figure 53. Biomass COD concentrations in the nitrification bioreactor.

A vertical line shows agal contaminations started.

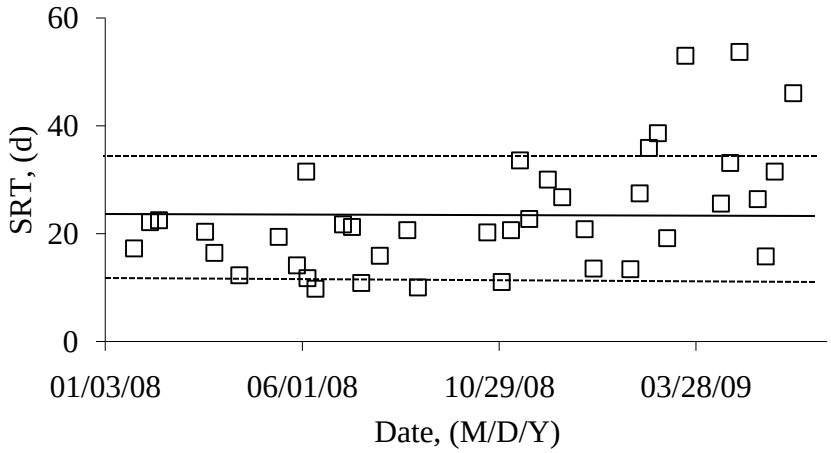

Figure 54. Solids retention time of the nitrification bioreactor.

The average SRT (bold line) was 23.5±11.0 (dash line). The target STR was 20 d. After agal contamination (March, 2009), algae increased SRT of the tank.

11 APPENDIX B: The fragment analysis based on T-RFLP patterns presented in the nitrifying bioreactor

Nitrosospira lineage (AOB)

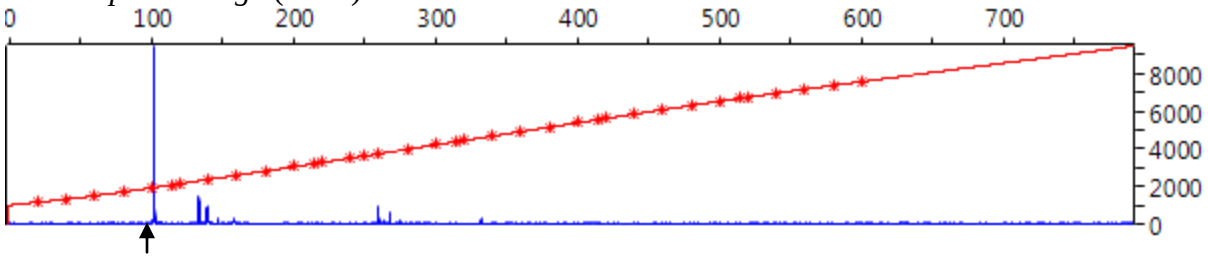

102 bp

Nitrobacter species (NOB)

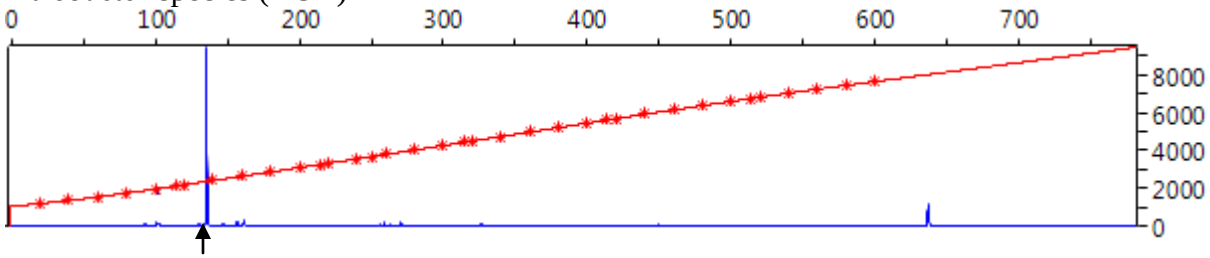

136 bp

Nitrospira species (NOB)

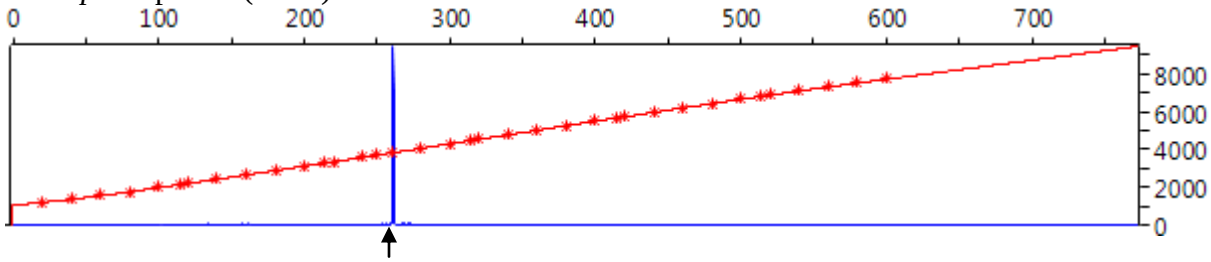

261 bp

12 APPENDIX C: Nitrifying Bacterial Growth Inhibition in the Presence of Algal Species[6]

Abstract

Nitrifying bacteria and microalgae are important microorganisms in open pond wastewater treatment systems. Nitrification involving the sequential oxidation of ammonia to nitrite and nitrate, mainly due to autotrophic nitrifying bacteria, is essential to biological nitrogen removal in wastewater and global nitrogen cycling. When a continuous flow autotrophic bioreactor, initially designed for nitrifying bacterial growth was contaminated by microalgae, we monitored both the microalgal and nitrifying bacterial activity by measuring specific oxygen production rate (SOPR) for microalgae and specific oxygen uptake rate (SOUR) for nitrifying bacteria to better understand algal-bacterial interactions. The growth of microalgae inhibited the maximum nitrification rate by a factor of 4 although the ammonium nitrogen fed to the reactor was almost completely removed. Terminal restriction fragment length polymorphism (T-RFLP) analysis indicated that the community structures of nitrifying bacteria remained unchanged, containing the dominant *Nitrosospira*, *Nitrospira* and *Nitrobacter* species. PCR amplification coupled with cloning and sequencing analysis resulted in identifying *Chlorella emersonii* and an uncultured cyanobacterium as the dominant species in the autotrophic bioreactor. Notwithstanding the fast growth rate of the microalgae and the algal toxicity to nitrifiers, algae were more easily lost in effluent than nitrifying bacteria

[6] *Environmental Science and Technology*, **2009**, in review.

because of their poor settling characteristics. Both microorganisms grew together in the bioreactor with constant individual biomass fractions because of the uncoupled solids retention times for algae and nitrifiers. The results indicate that compared to conventional wastewater treatment systems, even longer minimal SRTs (e.g., by a factor of 4) should be considered in phototrophic bioreactors for complete nitrification and nitrogen removal.

Introduction

Nitrifying bacteria are mainly composed of ammonia-oxidizing bacteria (AOB) such as *Nitrosospira* and *Nitrosomonas* and nitrite-oxidizing bacteria (NOB) such as *Nitrospira* and *Nitrobacter*. Nitrifying bacteria play an important role in wastewater nutrient removal and nitrogen cycling in the environment. The autotrophic nitrification process by nitrifying bacteria is generally the rate-determining step in biological nitrogen removal because of their slow growth rate and their sensitivity to environmental changes (Blum and Speece, 1991).

Microalgae (single celled algae) such as cyanobacteria and *Chlorella* have been used in wastewater treatment (Boussiba et al., 1984; Chiemchaisri et al., 2007; De-Bashan et al., 2002; González et al., 2008; Hu et al., 2000; Muñoz and Guieysse, 2006) partially because of their nutrient uptake potential and oxygen production to facilitate aeration in wastewater treatment (Muñoz and Guieysse, 2006). As renewable energy draws much attention, they become an attractive source recently for biodiesel production (Chisti, 2007; Mandal and Mallick, 2009; Muñoz and Guieysse, 2006). Moreover, a naturally selected alga has been applied to a photosynthetic algal microbial fuel cell powered with solar

energy to generate biocatalyzed electricity (Strik et al., 2008), demonstrating diverse applications of algae in the environment.

Understanding the algal-bacterial interactions in the environment is essential to explore algae-based wastewater treatment processes. Several studies of the interaction between algae and bacteria have been reported (De-Bashan et al., 2002; Muñoz and Guieysse, 2006; Risgaard-Petersen et al., 2004). Algae deliver oxygen for bacterial respiration but may inhibit bacterial growth by increasing the pH (pH could be increased to 10.6 as a result of algal respiration) (Green et al., 1996) or by producing substances toxic to bacteria (Muñoz and Guieysse, 2006). In sediments, where ammonia-oxidizing bacteria and benthic microalgae contend for the available nitrogen, algae out-compete the former due to their fast growth rate and N uptake capacity (Risgaard-Petersen et al., 2004). However, no significant negative effect of pH on the growth of *Chlorella vulgaris* and heterotrophic bacteria has been reported at influent glucose concentrations between 25 and 700 mg/L in laboratory bioreactors (Mayo and Noike, 1994). Bacteria can remove the toxic compounds released from algae (Ho et al., 2006), while nitrifying organisms remove high concentrations of ammonia that may be inhibitory to algal growth (Kallqvist and Svenson, 2003).

The objective of this research was to determine the impact of algal growth on autotrophic nitrifying activity that is essential in biological nitrogen removal. In this study, we measured algal and nitrifying bacterial activities through the measurements of specific oxygen production rate (SOPR) and specific oxygen uptake rate (SOUR), respectively, after separating the biomass of algae from nitrifiers by natural sedimentation. The microbial community structures in the co-culture autotrophic system were determined by

terminal restriction fragment length polymorphism (T-RFLP), cloning and sequencing analysis after polymerase chain reaction (PCR) amplification. The major finding was that the growth of microalgae inhibited the maximum nitrification rate by a factor of 4 although the performance of the reactor was not apparently affected.

Materials and Methods

Bioreactor

A lab-scale autotrophic nitrifying bioreactor seeded with activated sludge from the Columbia Wastewater Treatment Plant in Missouri was operated for more than two years (see chapter 2). All nitrogen species including ammonium, nitrate, and nitrite along with nitrifying bacterial growth inferred from SOUR measurements described below were routinely measured. After 670 days of operation (beginning in March 2009), a significant mixed liquor color change from brown to green indicated algal contamination, which was attributed to the algae possibly present in tap water that was used for feed preparation. The bioreactor was operated under the normal fluorescent light in the laboratory. The average SRT values were determined based on the amount of daily wasted biomass from the reactor and biomass loss in effluent (Grady et al., 1999).

Microscopic observations

An aliquot of microbial suspension from the autotrophic bioreactor was put on slide glass and covered with a cover slip. The upright Olympus Vanox AHBT3 (Center Valley, PA)

was used and images were taken by Leica DFC295 CMOS camera (color digital camera) (Bannockburn, IL).

Specific oxygen uptake rate and specific oxygen production rate measurements

The algal and nitrifying bacterial activities were determined from the specific oxygen production or uptake rate measurements using extant respirometry (Figure 55). Before each respirometric test of SOUR or SOPR, natural sedimentation was used to separate the nitrifying bacteria from algae. Biomass separation by gravity was fast and successful because nitrifying bacteria easily formed flocs and quickly settled down at the bottom whereas algae were largely suspended in the upper layer of the mixed liquor. To separate nitrifiers from microalage, an aliquot (100 mL) of mixed liquor from the parent bioreactor was filled in a graduated cylinder. After 5 min sedimentation, the upper layer of the mixed liquid (about 97% of the total liquid volume) was collected as algal biomass before use. The remaining portion of the mixed liquid containing nitrifying bacteria was rinsed twice with distilled water to remove the residual algae and resuspended in the feed solution without ammonia or the supernatant of effluent after 1 hour settlement to prevent nutrient limitation. The concentration of each biomass fraction was measured in chemical oxygen demand (COD) units using commercially available reagents (HACH COD vials, Loveland, CO).

Oxygen uptake rate (OUR, corrected with endogenous respiration) due to ammonia oxidation was determined after injecting an aliquot of ammonium to the separated nitrifying bacterial culture in a closed respirometric bottle (see 1.3.1). SOUR was

calculated by dividing the oxygen uptake rate by the nitrifying biomass concentration. For SOPR (ratio of OPR to algal biomass COD) measurement, algal biomass suspension was filled in the closed respirometric system where the amount of dissolved oxygen (DO) increase due to photosynthesis was automatically recorded in the lab with fluorescent light tubes and ordinary bulbs. Because the algal biomass suspension contained sufficient inorganic carbon due to the addition of sodium carbonate in the parent reactor, there was no additional CO_2 required for algal growth. The change of DO in the respirometric bottle was measured by a DO probe (YSI model 5300A, Yellow Springs, OH) and continuously monitored at 4 Hz by an interfaced computer. All samples were prepared and tested at least in duplicate.

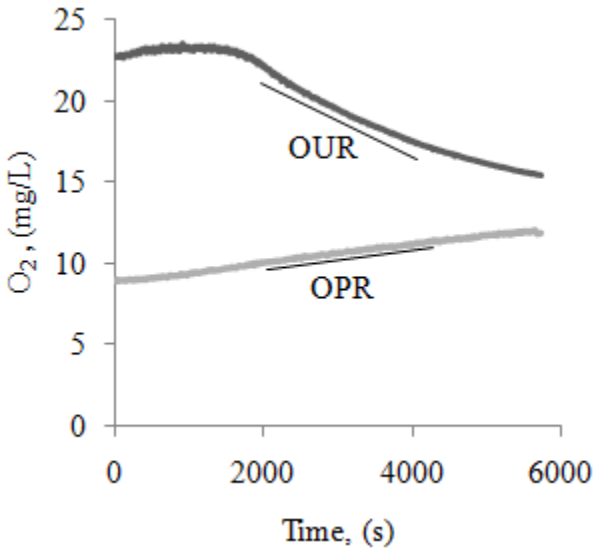

Figure 55. Nitrification and algal photosynthesis inferred from SOUR and SOPR measurements.

The changes of dissolved oxygen concentration due to nitrifying bacterial growth (oxygen consumption after adding NH_4^+-N at 1700s top curve) or microalgae growth (oxygen production, bottom line).

Nitrifying bacterial community analysis

T-RFLP was used to analyze nitrifying bacterial community in the bioreactor based on the 16S rRNA gene for ammonia-oxidizing bacteria and nitrite-oxidizing bacteria as described in a previous study (Siripong and Rittmann, 2007). We extracted DNA from 2 mL of mixed liquor from the bioreactor using Ultraclean Soil DNA Isolation Kit (Carlsbad, CA). All primers were synthesized by Intergrated DNA Technologies (Coralville, IA). A fluorescent dye, 6-FAM, was incorporated into the DNA fragment in fluorescence-labeled primers. Considering the low concentration of DNA from the nitrifiers, we amplified DNA from the 16S rRNA gene of AOB and NOB by a nested PCR, using the universal primers 11f and 1492r to produce an initial increase in template concentration. This was followed by the specific amplification of the nitrifier genes (Siripong and Rittmann, 2007). The imformation of PCR amplification, digestion, and fragment analysis are written in 5.3.

PCR amplification of cyanobacterial 16s rRNA gene and C*hlorella* 18s rRNA gene

Cyanobacterial 16S rRNA gene (420 bps) was amplified from extracted DNA using primers Cya359F and Cya781R(a) (Nubel et al., 1997) (Table10). NS1 and NS2 amplify nuclear encoded-18S small-subunit rRNA gene region (Wu et al., 2001) of fungi, protists, and red and green algae (Innis et al., 1990). Each 50 μL PCR reaction mixture contained 2×Taq Master Mix (Qiagen, Valencia, CA, 3mM $MgCl_2$, 200 μM dNTP and 2.5 U Taq polymerase in final concentrations), 20 pmol of each primer, and 1 μL of DNA template. The thermal profile used for the cyanobacteria-specific amplification was: 5 mins at 94 ˚C; 35 cycles of 1 min at 94 ˚C, 1min at 60 ˚C, and 1min at 72 ˚C; and a final elongation

for 5 min at 72 ˚C. The thermal profile used for the NS1-NS2 amplification was: 5 mins at 94 ˚C; 35 cycles of 45 s at 94 ˚C, 45 s at 58 ˚C, and 1min at 72 ˚C; and a final elongation for 5 min at 72 ˚C. PCR was performed in a MJ Mini^{TM} personal thermal cycler (Bio-Rad, Hercules, CA).

Table 10. Specific primers for *Chlorella* and cyanobacteria to identify microalgae in the nitrification bioreactor.

Primers	Sequences (5' to 3')	Target
NS1	GTA GTC ATA TGC TTG TCT C	550-bp fragment of SSU 18S rDNA of wide variety of fungi, protists, and algae
NS2	GGC TGC TGG CAC CAG ACT TGC	
CYA106F	CGG ACG GGT GAG TAA CGC GTG A	675-bp fragment of SSU 16S rDNA of cyanobacteria
CYA781R(a)	GAC TAC TGG GGT ATC TAA TCC CAT T	

Cloning and sequencing algae DNA

Amplified DNA gene of algae from the reactor was cloned into pCR4 vector with the TOPO-TA cloning kit according to the manufacturer's protocols (Invitrogen, San Diego, CA). Approximately 1,000 ng templates was used for sequencing reaction using Big Dye Terminator cycle sequencing kit (Applied Biosystems, Foster City, CA) with M13F to obtain sequence from one strand of the insert. DNA sequencing was performed on the Applied Biosystems 3730XL 96-capillary DNA Analyzer at the DNA Core Facility. The sequencing chemistry used in this work was Applied Biosystems BigDye Terminator

version 3.1. The unincorporated primers and nucleotides were removed from the reactions using the BD XTerminator kit (Applied Biosystems).

Phylogenetic analysis

Sequences were initially analyzed for phylogenetic affiliation using the BLAST program (http://blast.ncbi.nlm.nih.gov/Blast.cgi). For phylogenetic tree construction, each sequence was subjected to a BLAST analysis. The two sequences with the highest similarities indicated by BLAST were selected. We used 106–805 *E. coli* positions of the 16S rRNA gene, corresponding to cynobacteria bases (Nubel et al., 1997). Cytobacterial DNA sequences were also analyzed using the online software Classifier of the Ribosomal Database Project (http://rdp.cme.msu.edu/classifier/classifier.jsp) (Wang et al., 2007). The reference species for *Chlorella* were selected based on the known molecular phylogeny of the genus *Chlorella* from a previous study (Huss et al., 1999). Reference sequences were obtained form Genbank, and aligned using ClustalX. Calculation of the phylogenetic tree was based on the neighbor-joining method using bootstrapping. The rooted bootstrapped phylogenic tree was rendered in the TreeView software using *Phyllosiphon arisari* for cyanobacterium and *Gloeotilopsis planctonica* for *Chrollea* as the outgroup.

Results

Co-growth of nitrifiers and microalgae in bioreactor

Green microalgae accidentally contaminated the nitrifying bioreactor after about two years of operation, indicated by a color change of the mixed liquor from brown (before contamination) to green (after algal intrusion) (Figure 57). Almost complete nitrification was achieved before and after contamination, as indicated by weekly measurements of ammonium, nitrite, and nitrate concentrations in reactor effluent. Before day 670, the average concentrations of NH_4^+-N, NO_2^--N and NO_3^--N were 1.1, 0.4, and 419 mg/L, respectively. The corresponding nitrogen species concentrations were 2.0, 0.3, and 437 mg/L after contamination. The effluent COD increased from 17.1 ± 7.8 to 26.6 ± 18.3 mg/L, which was attributed to the loss of planktonic (free-swimming) microalgae (5~10 μm size). Correspondingly, the total biomass in the reactor was increased from 272 ± 66 mg/L to 598 ± 170 mg/L because of algal growth (Figure 58). After day 670, the ratio of nitrifying biomass (C_n) to microalgae (C_a) in the reactor was relatively constant (C_n/C_a = 2.2). Because of the planktonic growth of algae with poor settling properties and the loss of algal cells in the effluent, the average solids retention times of the two autotrophic organisms were uncoupled, resulting in an average value of 27.9 d and 8.5 d for nitrifying bacteria and algae, respectively.

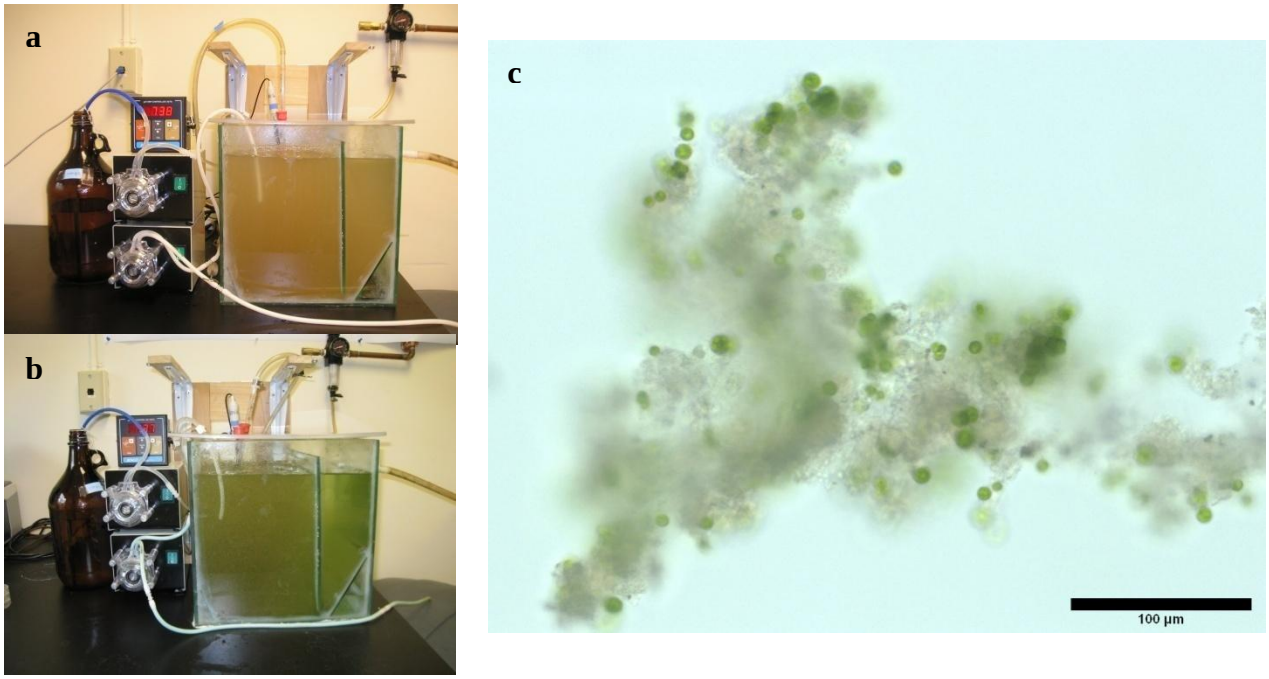

Figure 56. Co-growth of nitrifying bacteria and microalgae in the continuous flow autotrophic bioreactor.

(A) nitrifying bacteria enrichment cultures (having a brown color, picture taken in August 2007). (B) co-cultures of algal and nitrifying bacterial cells after algal contamination (picture taken in March, 2009). (C) Microscopic image of the co-cultures. Nitrifiers aggregated and formed flocs while green microalgae cells attached to the nitrifer flocs. The size of microalgae ranged from 5 to10 μm (scale bar = 100 μm).

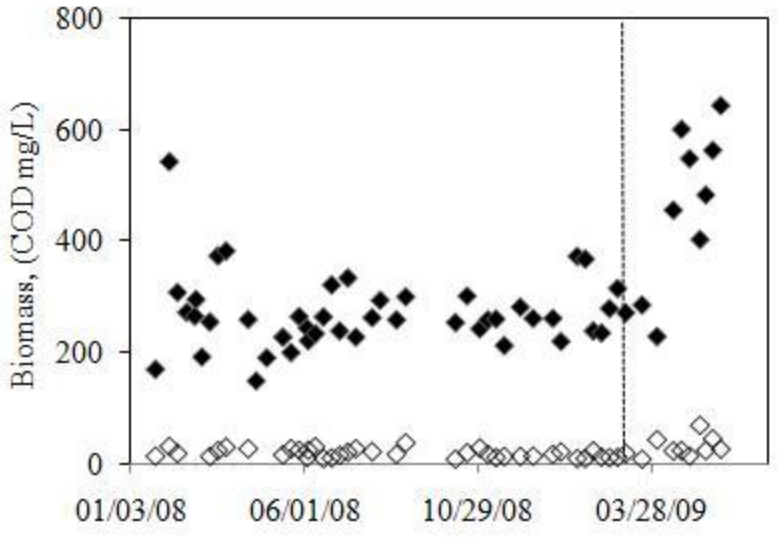

Figure 57. Biomass concentrations in the autotrophic reactor and in the reactor effluent.

The vertical line shows the start of algal growth in the bioreactor at 670 days after operation. Filled diamonds indicate biomass concentration in the autotrophic reactor and empty ones show the biomass in effluents. Increased biomass is due to algae contamination in the autotrophic reactor.

Community structure of nitrifying bacteria

T-RFLP analysis (see more detail information in 5.3) indicated that the nitrifying bacterial community structure remained the same before and after algal contamination. *Nitrosospira* was the dominant genus of ammonia-oxidizing bacteria in the reactor while *Nitrospira* and *Nitrobacter* species were dominant among nitrite-oxidizing bacterial populations. These results are consistent with recent studies suggesting, *Nitrosospira* and *Nitrospira* have relatively higher substrate affinity and competitive advantage over *Nitrosomonas* and *Nitrobacter*, respectively, under low NH_4^+ or NO_2^- concentration conditions (Dytczak et al., 2008).

Microbial growth rates inferred from SOUR and SOPR

Nitrifiers and microalgae collected from the autotrophic bioreactor were easily separated by gravity separation (Figure 59). The maximum specific oxygen uptake rate of ammonia oxidation was decreased from (2.2 ± 0.8) to (0.5 ± 0.3) mg O_2/mg COD-nitrifying biomass·day after algal contamination. Hence, algal growth resulted in nitrification inhibition by approximately 77%. Meanwhile, the SOPR of microalgae in the bioreactor remained at a constant value of 0.1 ± 0.01 mg O_2/mg COD-algal biomass·day.

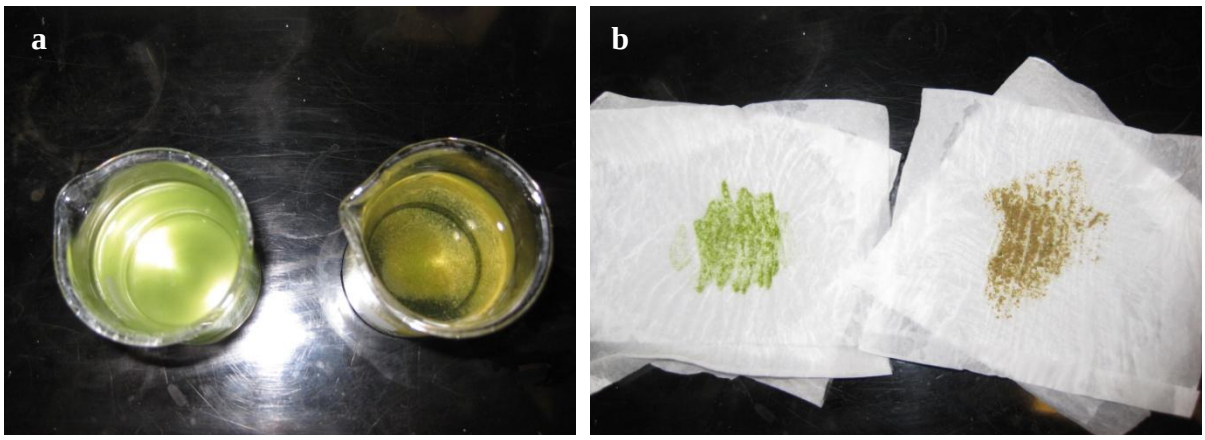

Figure 58. Separation of microalgae from nitrifying bacteria by gravity separation.

(A) Separation of microalgae (in left beaker) and nitrifying bacteria (in right beaker) from the co-culture taken from the parent bioreactor. (B) Upon air-drying, the collected biomass showed a typical green or brown color for algae and nitrifying bacteria, respectively.

Microalgae identification

Microalgae were identified by cloning and sequence analysis. The primers NS1 and NS2 used to identify algae are universal primers which amplify 18S rRNA genes of a wide variety of fungi and algae (Innis et al., 1990). Since all sequenced clones had the same sequence as the Alg_clone1, this clone was considered to be the dominant alga in the bioreactor. The analysis of 18S rRNA gene sequences (~550 bp) of the Alg_clone1 revealed that the sequence had high affiliation to a known *Chlorella* species and has 100% homology to the partial sequence of 18S rRNA gene of *Chlorella emersonii* NIES 690 (Accession no. AJ242761 in GenBank) (Figure 60). Our microscopic observation clearly indicated the dominant algae as green, spherical cells having a size of 10 µm (Figure 57c), which were consistent with the features of *Chlorella*. Therefore, the microscopic results support the phylogenetic analysis and suggest the dominant algal species in the genus of the green single-celled microalgae is *Chlorella*.

The primers CYA 106F and CYA 781R (a) used to identify cyanobacteria are specific primers which amplify 16S rRNA gene of cyanobacteria (Nubel et al., 1997). All clones from CYA-PCR products had the same sequences as the Cya clone1, which was considered to be the dominant cyanobacteria species in the autotrophic bioreactor. The analysis of 16S rRNA gene sequence (~670 bp) of the Cya clone1 by RDP II classifier (http://rdp.cme.msu.edu/classifier/classifier.jsp) showed 91% homology with a chloroplast gene sequence of an unclassified cyanobacterial species founded in river or lake (Figure 61).

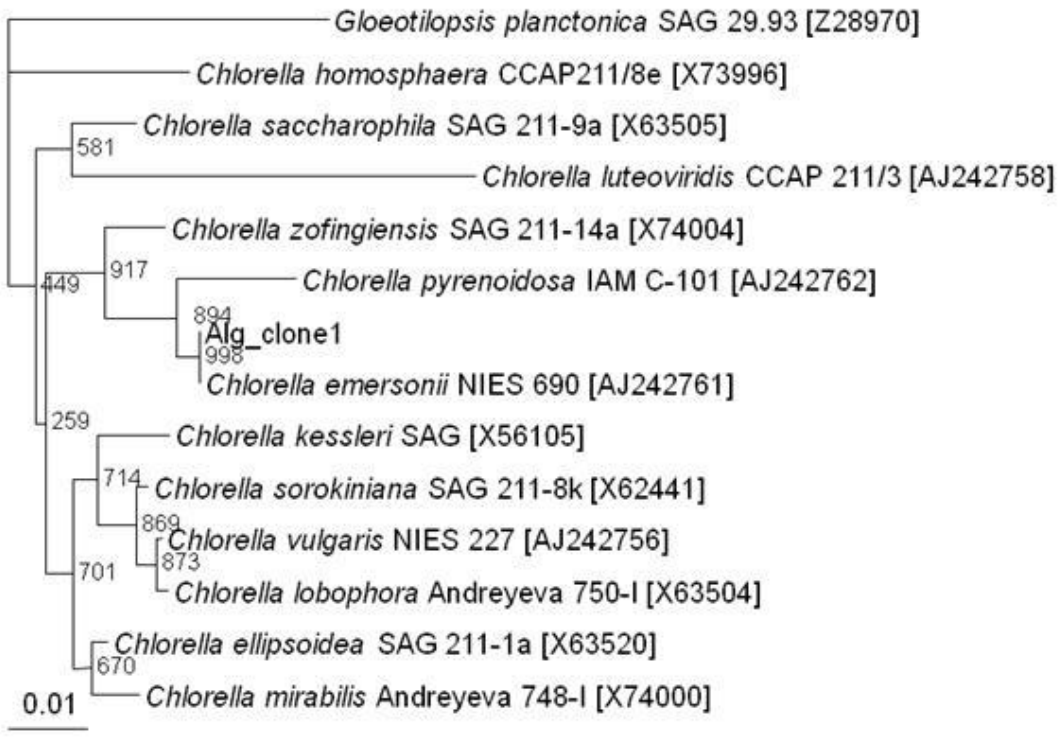

Figure 59. Phylogenetic analysis of the cloned *Chlorella* 18S rRNA gene (Alg_clone1) from the autotrophic bioreactor.

Calculation of the phylogenetic tree was based on the neighbor-joining method using bootstrapping. The tree was rooted with the 18S rRNA gene sequence of the *Gloeotilopsis planctonica* as the outgroup. Values near the branch points are based on 1000 bootstrap replications. The scale bar corresponds to 1 substitution per 100 nucleotide positions.

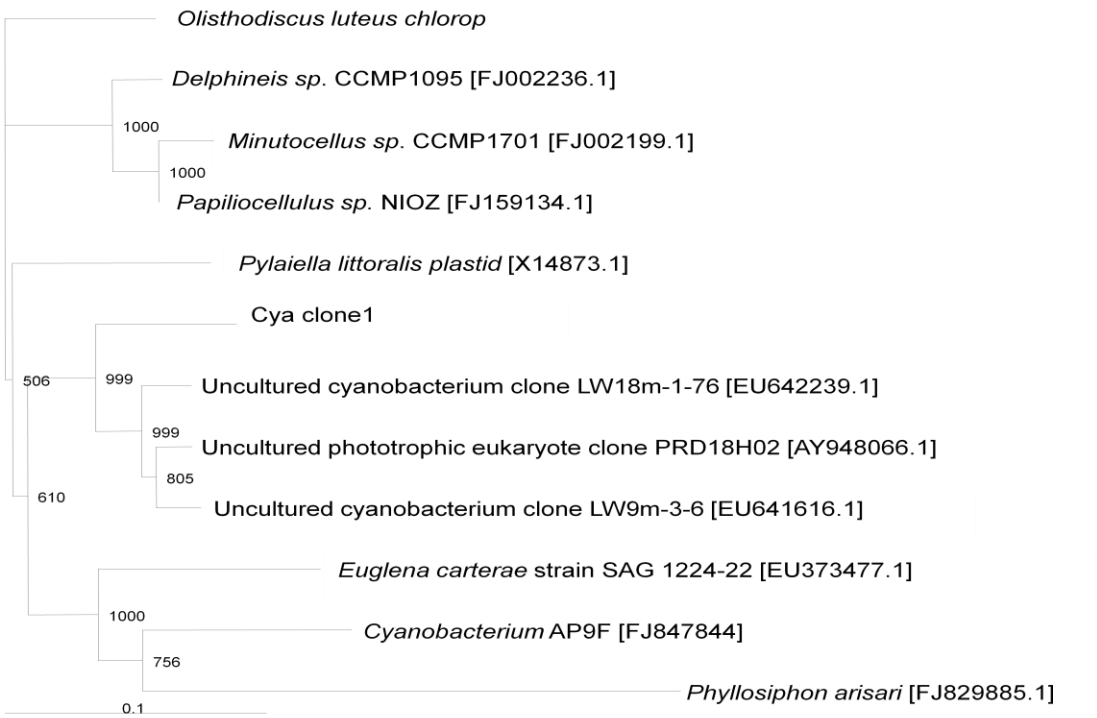

Figure 60. Phylogenetic analysis of the cloned cyanobacterial 16S rRNA gene (Cya clone1) from the autotrophic bioreactor.

Calculation of the phylogenetic tree was based on the neighbor-joining method using bootstrapping. The tree was rooted with the 16S rRNA gene sequence of the *Phyllosiphon arisari* as the outgroup. Values near the branch points are based on 1000 bootstrap replications. The scale bar corresponds to 10 substitutions per 100 nucleotide positions.

Discussion

The contamination of the autotrophic nitrifying bioreactor was evident upon visualization and microscopic analysis. Using T-RFLP and cloning analysis after PCR amplification, we confirmed two dominant microalgal species that were identified as *Chlorella emersonii* and an uncultured cyanobacterium in the reactor. The presence of these organisms caused significant nitrification inhibition, resulting in reduction of nitrifying bacterial growth by a factor of 4, although T-RFLP results indicated that a relatively constant nitrifying bacterial community structure was maintained and the nitrifying bioreactor effluent remained containing low NH_4^+ and NO_2^- concentrations.

Nitrification inhibition in the presence of algae was attributed to cynotoxins released by the uncultured cyanobacterium. Toxic compounds might be released by the algae, especially cyanobacteria (Makarewicz et al., 2009; Yoshida et al., 2008). However, detection of these chemical toxins and determination of their composition is beyond the scope of this study.

Specific growth rate of nitrifiers (μ_A) is related to SOUR as described in equation 8 (Grady et al., 1999).

$$\mu_A = \frac{Y_A}{1-Y_A} \cdot \frac{r_{SO}}{X_B} = \frac{Y_A}{1-Y_A} \cdot SOUR \qquad \text{Equation 8}$$

where Y_A is true growth yield for nitrifiers on COD basis, r_{SO} is reaction rate for dissolved oxygen, and X_B is active biomass of nitrifiers. Similarly, for microalgal growth, the specific growth rate of algae can be derived as follows:

The reaction of microalgal photosynthesis can be represented by the following molar-based equation:

$$6CO_2 + HCO_3^- + NH_4^+ + 27H^+ + 27e^- = C_6H_{10}O_2N + CH_2O + 10H_2O + O_2$$

Equation 9

Based on an empirical formula of algae $C_6H_{10}O_2N$ (Cervantes et al., editors. 2006; Green et al., 1996), the COD equivalent of algae biomass is approximately 1.57g COD/g$C_6H_{10}O_2N$.

Therefore, specific growth rate coefficient (μ_{ma}) of microalgae could be calculated from SOPR using equation 10 correct in equation as well

$$\mu_{ma} = \frac{1\ mol\ C_6H_{10}O_2N}{1\ mol\ O_2} \times \frac{128\ g\ C_6H_{10}O_2N/mol\ C_6H_{10}O_2N}{32\ g\ O_2/\ mol\ O_2} \times \frac{1.57\ g\ biomass\ COD}{g\ C_6H_{10}O_2N} \cdot \left(\frac{g\ O_2}{g\ biomass\ COD \cdot t}\right) = 6.28 \cdot (SOPR)$$

Equation 10

The calculated maximum growth rates of nitrifiers and microalgae in the co-culture system were 0.16 ± 0.1 d^{-1} and 0.62 ± 0.07 d^{-1} respectively. The reported growth rate of microalgae is from 0.31-1.08 d^{-1}, which is slower than that of heterotrophic bacteria because of the larger algal cell size (Muñoz and Guieysse, 2006). This rate is comparable

with that of nitrifiers under normal growth conditions (~1 d^{-1}) (Grady et al., 1999). Due to the algal growth, microalgae inhibited the growth of nitrifying bacteria and reduced their growth rate by a factor of 4 (i.e., from 0.7 ± 0.3 d^{-1} to 0.16 ± 0.1 d^{-1}). Although in the coculture autotrophic growth system microalgae grew 4-times faster than nitrifiers, the relative constant of the ratio of nitrifier biomass to algae and the low algal biomass in the tank was maintained largely because of the higher loss of algal cells in the reactor effluent (i.e., a shorter SRT of algae than that of nitrifiers).

Due to the long SRT of nitrifying bacteria in the tank, the ammonium was almost completely oxidized to nitrate by nitrifying bacteria even though nitrification was inhibited by microalgae. The effluent nitrogen concentrations of ammonium, nitrite, and nitrate were relatively constant before and after algal contamination. Except a slight increase of effluent COD due to the loss of algal cells, the effluent water quality was not changed upon microalgae contamination in the algal-bacterial co-growth system. Although microalgae prefer ammonium to nitrate as their nitrogen source (Green et al., 1996), uptake of ammonium by the algal species appeared to be insignificant as indicated by the effluent nitrate concentrations.

13 VITA

Okkyoung Choi was born in Seoul, Republic of Korea. She previously studied in the Department of Botany and Microbiology, University of Oklahoma, USA. She earned her B.S. and M.S. Degrees in environmental engineering from Korea in 2000 and 2002, respectively. Ms. Choi worked as a Research Associate, Research Institute of Biological and Environmental Technology, Biosaint Co., Seoul for one year before coming to the U.S. to pursue her Ph.D. degree. She has published several papers related to silver nanoparticle research in *Journal of Environmental Engineering, Water Research*, and *Environmental Science & Technology*.